PHILOSOPHICAL TRANSACTIONS OF THE ROYAL SOCIETY A MATHEMATICAL, PHYSICAL & ENGINEERING SCIENCES

Large Magnetic Reynolds Number Dynamo Action in a Spatially Periodic Flow with Mean Motion

A. M. Soward and S. Childress

Phil. Trans. R. Soc. Lond. A 1990 **331**, 649-733
doi: 10.1098/rsta.1990.0097

Phil. Trans. R. Soc. Lond. A **331**, 649–733 (1990) [649]
Printed in Great Britain

LARGE MAGNETIC REYNOLDS NUMBER DYNAMO ACTION IN A SPATIALLY PERIODIC FLOW WITH MEAN MOTION

By A. M. SOWARD[1] and S. CHILDRESS[2]

[1] *Department of Mathematics and Statistics, The University, Newcastle upon Tyne, NE1 7RU, U.K.*
[2] *The Courant Institute of Mathematical Sciences, 251 Mercer Street, New York 10012, U.S.A.*

(*Communicated by P. H. Roberts, F.R.S. – Received 31 May 1989 – Revised 21 December 1989*)

CONTENTS

 [Published 30 June 1990

We consider a problem of advection and diffusion of passive scalar and vector fields in a particular family of steady fluid flows. These flows are obtained by adding a small uniform velocity to a spatially periodic array of spiral eddies. The uniform flow, $\bar{\boldsymbol{u}}_{\mathrm{H}}$, is taken to have the discrete form

$$\bar{\boldsymbol{u}}_{\mathrm{H}} = \epsilon(M, N, 0)/(M^2+N^2)^{\frac{1}{2}}, \quad \epsilon \ll 1,$$

where M, N are relatively prime integers. The spatially periodic part, $\boldsymbol{u}'$, may be expressed in terms of a streamfunction ψ',

$$\boldsymbol{u}' = (\partial\psi'/\partial y, -\partial\psi'/\partial x, K\psi'), \quad \psi' = \sin x \sin y,$$

where K is a constant. The flow we study is therefore $\boldsymbol{u} = \bar{\boldsymbol{u}}_{\mathrm{H}} + \boldsymbol{u}'$.

Our work is motivated by applications of dynamo theory and to classical diffusion of passive scalars. The above family of flows was chosen as typical of spatially periodic flow with non-zero mean velocity, $\bar{\boldsymbol{u}}_{\mathrm{H}}$. The flows are comparatively simple because they are independent of z. Nevertheless the projection of the streamline pattern onto the plane $z = 0$ can be surprisingly complex, owing to the structure of $\boldsymbol{u}$ modulo the cell of periodicity of $\boldsymbol{u}'$.

This structure accounts for our special form of $\bar{\boldsymbol{u}}_{\mathrm{H}}$ above, which makes the tangent of the angle of inclination of the uniform current a rational number. This uniform component breaks up the eddy pattern into closed eddies whose bounding streamlines begin and end at X-type stagnation points. The set of all such streamlines define the boundaries of the open channels, which fill the regions between the closed eddies and lie near the separatrices of $\boldsymbol{u}'$. Then, for example, when $L = M+N$ is even the channel structure repeats under a shift $(M\pi, N\pi)$ in the xy plane, leading to a periodicity in channel length of order L. Analogous results apply to the case L odd. This geometry raises interesting questions regarding the advection and diffusion of fields in the irrational limit, i.e. when $M, N \to \infty$, $M/N \to$ irrational. A basic result of this paper will be formal asymptotic expressions, for average physical quantities of interest, in the irrational limit.

An asymptotic theory of advection–diffusion is exploited, based upon a separation into closed eddies, channels, and separatrix boundary layers. The fundamental assumption is that the dimensionless parameter R (a magnetic Reynolds number in the dynamo problem, a Péclet number in diffusion problems) is large, meaning that transport by molecular diffusion is nominally small compared with transport by advection. For large R, the X-type stagnation points trigger boundary layers, which for given M, N extend a distance of order L before repeating the structure. This leads to channel boundary layers of width $L^{\frac{1}{2}}R^{-\frac{1}{2}}$, compared with eddy boundary layer of width $R^{-\frac{1}{2}}$ and channel widths of order ϵL^{-1}, the eddies being separated by gaps of widths order ϵ. In this setting the irrational limit is taken after the above asymptotic structure is isolated by the limit $R \to \infty$.

Our results consist of numerical studies for $\beta = \epsilon R^{\frac{1}{2}}$ of order unity, and analytic asymptotic expressions derived under the condition $\beta \gg L^{\frac{3}{2}}$. In the former, the eddy separation width is comparable with the eddy boundary layer width, so that we study the transition from transport dominated by boundary layers to transport dominated by channels. In the asymptotic theory for large β, the boundary-layer contributions may be neglected and the problem reduces to the analysis of channel geometry. Even here, the condition $\beta \gg L^{\frac{3}{2}}$ restricts us to a countable set of mean flow orientations. The relation between solutions for these special orientations, and their immediate neighbours with irrational tangents, is discussed. Representative results for effective diffusion of a passive scalar field, and for mean induced electromotive force in an electrically conducting fluid (the α-effect) are presented. We also discuss the present examples in relation to the more complex problem of advection–diffusion by flows with chaotic lagrangian paths.

1. Introduction

The analysis presented in the present paper is motivated primarily by the theory of kinematic dynamo action by the movement of an electrically conducting fluid in the presence of an electromagnetic field (see, for example, Moffatt 1978). That theory has been extensively developed for the case where magnetic diffusion plays a dominant role, in the sense that the magnetic Reynolds number (R = velocity × length/magnetic diffusivity) is very small for the eddies of the flow. In such a limit the induced magnetic field may be assumed to be dominated by a component that varies on the large length scale, that is, a scale large compared with the size of the eddies of the flow. The details of the structure of the flow field are thus largely bypassed by the theory, or rather are evaluated only through averages over the smaller scale components of the fields. In this way an average electromotive force, the α-effect, can be calculated.

When, on the other hand, the magnetic Reynolds number is large, so that advection dominates diffusion, the situation is very different and the flow structure must be considered in detail. The large-R theory is characterized by the presence of magnetic boundary layers, of thickness $O(R^{-\frac{1}{2}})$, which thread through space and separate regions of relatively low molecular diffusion. Typically this structure is created by a process of flux expulsion, leading to magnetic voids and flux concentration into sheets and ropes (Weiss 1966; Galloway *et al.* 1978). In spite of this change in magnetic structure, the magnitude of the resulting concentration of flux is still controlled by the size of the average magnetic field threading the flow, so that for certain calculations mean-field or averaging methods can again be used. For simple steady flows, the magnitude of the resulting α-effect was first considered by Childress (1979) (hereafter referred to as paper 1).

When restricted to steady kinematic dynamo theory, the nature of the large-R theory is determined by the complexity of the streamline pattern of the flow. In spatially periodic systems, investigations have focused on the ABC family of helical flows,

$$\boldsymbol{u} = (A\sin z + C\cos y, B\sin x + A\cos z, C\sin y + B\cos x) \tag{1.1}$$

in which A, B, C are constants. These are Beltrami flows, with $\nabla \times \boldsymbol{u} = \boldsymbol{u}$. They have maximal mean helicity for given mean kinetic energy, this being an important ingredient in many examples of dynamo action (Moffatt 1978). The case $A = B, C = 0$ was studied in detail by Roberts (1972). His numerical method used a modal expansion, which took advantage of the simple form of the flow velocity (1.1). The large-R properties of this special case were later discussed as the two-dimensional case of paper 1. The case $A \neq B, C = 0$ has been treated in the dynamo context by Childress & Soward (1989) (hereafter referred to as paper 2). The geometry of the streamlines of (1.1) in the general case was discussed first by Hénon (1966) and more recently by Dombre *et al.* (1986).

These studies have illustrated the way in which boundary layers can be set up for various streamline configurations. When $C = 0$ the flow (1.1) is invariant in z and the projection of streamlines onto the xy plane yields a pattern of closed eddies separated (if $A \neq B$) by channels carrying net fluid flux. When also $C \neq 0$, however, the flow exhibits regions of lagrangian chaos. Then, if streamlines are plotted modulo 2π in x, y, z, a single line can be dense in a three-dimensional region, and it is difficult to introduce a consistent boundary-layer limit.

The present work is devoted to a variant of (1.1), which falls between the single integrable cases and those exhibiting lagrangian chaos. We first introduce the velocity field

$$\boldsymbol{u} = \bar{\boldsymbol{u}}_{\mathrm{H}} + \boldsymbol{u}'(x, y), \tag{1.2a}$$

where

$$\boldsymbol{u}' = (\partial\psi'/\partial y, -\partial\psi'/\partial x, K\psi') \quad (\psi' = \sin x \sin y + \delta \cos x \cos y), \tag{1.2b}$$

$$\bar{\boldsymbol{u}}_{\mathrm{H}} = \epsilon(\sin(lz), \cos(lz), 0), \tag{1.2c}$$

and K, ϵ, δ and l are constants. Here we refer to the xy plane as the horizontal and the z-axis as the vertical. In the special case $K = l = 2^{\frac{1}{2}}$ the motion (1.2) reduces to the Beltrami flow (1.1). The correspondence is made by a rotation of 45° about the vertical z-axis, a horizontal translation and a reduction of the length scale by a factor $2^{-\frac{1}{2}}$. The case $\epsilon = \delta = 0$ was the two-dimensional case of paper 1, while $\epsilon = 0, \delta \neq 0$ was the subject of paper 2. The present study is concerned with the limit

$$\delta = 0, \quad \epsilon \neq 0, \quad l \ll 1, \quad lz \to \theta_0 = \text{const.} \tag{1.2d}$$

The principle new feature of the flow is thus the existence of a non-zero mean velocity $\epsilon(\sin\theta_0, \cos\theta_0, 0)$. Our goal is to assess the influence of this mean motion on the boundary-layer structure, and thence on the transport of scalar field and the resulting α-effect. We are particularly interested in the role that mean motion might play in the construction of fast dynamos. Fast dynamos have the property that the growth rate $p(R)$ associated with dynamo action at given R, has a positive supremum limit for large R. Thus fast dynamo action should reflect the geometry of streamlines and their effect on the stretching and folding of field, apart from the molecular diffusion that accompanies these distortions.

For the special case of two-dimensional flows (1.2) with lz replaced by θ_0, magnetic modes can be sought in the form

$$\boldsymbol{B}(\boldsymbol{x}, t) = \mathrm{Re}\,[\mathrm{e}^{pt+\mathrm{i}qz}\hat{\boldsymbol{B}}(x, y)], \tag{1.3a}$$

of given vertical wavenumber q. The horizontal average of the induction equation yields in dimensionless units the identity

$$(p + R^{-1}q^2)(\bar{B}_x, \bar{B}_y) = \mathrm{i}Kq(-\bar{E}_y, \bar{E}_x), \tag{1.3b}$$

where $\bar{\boldsymbol{B}}_{\mathrm{H}}$ and $K\bar{\boldsymbol{E}}_{\mathrm{H}}$ are the horizontal averages $\hat{\boldsymbol{B}}$ and $(\boldsymbol{u}\times\hat{\boldsymbol{B}})_{\mathrm{H}}$ respectively. This means that the horizontal mean electromotive force is related linearly to the mean magnetic field in the form

$$K\bar{\boldsymbol{E}}_{\mathrm{H}} = \boldsymbol{\alpha}\cdot\bar{\boldsymbol{B}}_{\mathrm{H}}, \tag{1.3c}$$

where $\boldsymbol{\alpha}$ is a 2×2 matrix. Because this $\boldsymbol{\alpha}$ depends on the nature of the mean field through its dependence on the wavenumber and ultimately the complete solution, we refer to it as a generalized α-effect. The classical α-effect of mean field theory corresponds to the limiting value of the α-matrix in the long wavelength limit $q \to 0$, and can be derived directly independent of the mean field equation (1.3b).

The nature of our new dynamo with mean motion should be contrasted with the previous models. In the Roberts case $\delta = \epsilon = 0$ the horizontal motion is confined to closed eddies, which fill the squares

$$\Pi_{m,n} = [m\pi, (m+1)\pi] \times [n\pi, (n+1)\pi], \tag{1.4}$$

where m and n are integers. The circulation in neighbouring eddies is opposite in sign, while the local helicity $\boldsymbol{u}\cdot\boldsymbol{\nabla}\times\boldsymbol{u}$ has the same sign. The magnetic boundary layers which result are confined to the boundaries of these eddies, that is the lines $x = m\pi$ and $y = n\pi$. In paper 1 the mean electromotive force generated by a non-zero mean magnetic field in the absence of any z-variations was evaluated and shown to be concentrated in boundary layers. From this particularly symmetric flow the 2×2 α-matrix is isotropic:

$$-\boldsymbol{\alpha} = \alpha \boldsymbol{I} \quad (K^{-1}R^{\frac{1}{2}}\alpha \to \alpha_0 \text{ as } R\to\infty). \tag{1.5}$$

The value of the constant α_0 appropriate to the limit $q\to 0$ has been determined numerically by Anufriyev & Fishman (1982), Perkins & Zweibel (1987), Rosenbluth *et al.* (1987) and analytically by Soward (1987). According to the result (1.5) above of paper 1, the growth rate of a mode with small but fixed wavenumber q is proportional to $R^{-\frac{1}{2}}$. Galloway & Frisch (1986) calculated the growth rate at large magnetic Reynolds number numerically using, like Roberts before, full modal expansions. At the values of R considered, their results do not follow the $R^{-\frac{1}{2}}$-power law. Instead they agree with a modified asymptotic theory (Soward 1989) valid for intermediate values of R, which takes into account the dependence of α on both q and R.

The results of Soward (1987, 1989) depend very much on the fact that the vertical z-variation of the mean magnetic field can be as small as the boundary layer thickness of order $R^{-\frac{1}{2}}$. This freedom allows growth rates larger than $R^{-\frac{1}{2}}$, but does not produce a fast dynamo for the flow considered here. This calculation realizes the field structure predicted by Moffatt & Proctor (1985), who regard from a general point of view that steady flows, which produce fast dynamos, would tend to produce magnetic fields with length scale of order $R^{-\frac{1}{2}}$ essentially filling the excitation volume. The inclusion of the z-dependence of the mean field, while essential for a comprehensive study of possible fast dynamo activity, is, however, secondary for the analysis of the overall geometry of boundary layers and for reasonable estimates of α-effect. For this reason we shall ignore the vertical structure of the mean magnetic field in the present work. Our analysis will thus be more in the spirit of papers 1 and 2 than of Soward (1987), although the streamline geometry is far more complex with the addition of a mean motion.

Our analysis will build on the ideas developed in paper 2, where the case $\epsilon = 0$, $0 < \delta \ll 1$ of (1.2) was investigated in detail. As in the Roberts (1972) study with $\delta = 0$, motion is still z-independent and lies on stream surfaces, $\psi' = \text{const}$. Most of the motion remains in closed eddies. They form rows of cat's-eyes inclined at 45° with the x-axis and connected at their vertices which are located at diagonally opposite corners of the squares $\Pi_{m,n}$. The regions between each row form open channels, in which horizontal motion flows systematically in one direction but reverses in sign from one channel to the next. Just as in the Roberts case magnetic flux is expelled from the cat's-eyes and is concentrated at their boundaries and within the channel regions between them. When the channel width δ greatly exceeds the boundary layer width $R^{-\frac{1}{2}}$, the boundary layers triggered at the cat's-eye vertices (X-type stagnation points of the horizontal motion) are confined to the immediate vicinity of the separatrices connecting them. Elsewhere in the interior of the channels magnetic field is almost aligned to the flow.

As far as the dynamo mechanisms are concerned two particular orientations of the mean magnetic field $\bar{\boldsymbol{B}}_{\mathrm{H}}$ are significant. First, when $\bar{\boldsymbol{B}}_{\mathrm{H}}$ is aligned parallel to the rows of cat's-eyes in the direction $\boldsymbol{i}^{+} = (1,1)$, the resulting horizontal magnetic field simply aligns itself with the channel flow and there is very little inductive effect. Secondly, when $\bar{\boldsymbol{B}}_{\mathrm{H}}$ lies perpendicular to the rows of cat's-eyes, in the direction $\boldsymbol{i}^{-} = (1,-1)$, magnetic flux is stretched out and

intensified by an order of magnitude R in the channels so giving a strong inductive effect. Together the results for parallel and perpendicular magnetic fields show that the α-matrix in (1.3c) has the symmetric form

$$-K^{-1}\boldsymbol{\alpha} = \tfrac{1}{2}\alpha^{+}(\boldsymbol{i}^{+}\boldsymbol{i}^{+}) + \tfrac{1}{2}\alpha^{-}(\boldsymbol{i}^{-}\boldsymbol{i}^{-}). \tag{1.6}$$

The results of paper 2 show that the two eigenvalues $K\alpha^{+}$ and $K\alpha^{-}$ of the α-matrix, linked to the case of parallel and perpendicular fields respectively, have magnitudes

$$K\alpha^{+} = O(KR^{-\frac{3}{2}}\delta^{-2}), \quad K\alpha^{-} = O(KR\delta^{3}) \quad (R^{-\frac{1}{2}} \ll \delta \ll 1), \tag{1.7a}$$

when the boundary layer width $R^{-\frac{1}{2}}$ is small compared with the channel width δ. It is, however, the square root of the determinant of $\boldsymbol{\alpha}$ that determines the growth rate

$$p \approx (\det \boldsymbol{\alpha})^{\frac{1}{2}} = K(\alpha^{+}\alpha^{-})^{\frac{1}{2}} = O(KR^{-\frac{1}{2}}(R^{\frac{1}{2}}\delta)^{\frac{1}{2}}). \tag{1.7b}$$

Comparison of this result with (1.5) shows that increasing the scaled channel width $R^{\frac{1}{2}}\delta$ improves the inductive effect for modes of given vertical length scale. There is, however, no suggestion that this dynamo will give significantly faster maximum growth rates because a lower limit on the vertical length scale is imposed by the channel, and this limit increases with δ. Corresponding results for scalar diffusion were also obtained in paper 2 and recently related results have been reported by Crisanti *et al.* (1990).

In both the Roberts (1972) case and in the extension considered in paper 2, motion is two dimensional and confined to streamsurfaces. Most of the dynamo results reported for the fully three-dimensional Beltrami flow (1.1) with A, B, C non-zero are numerical. In addition to the early resuts of Roberts (1972) for two-dimensional flows, we mention particularly Arnold & Korkina (1983) and Galloway & Frisch (1984, 1986). It is clear from the last of these studies (Galloway & Frisch 1986) that very rapid growth rates can be obtained when the magnetic Reynolds number R is large. Whether or not they are fast dynamos is not clear. Nevertheless, the physical mechanisms that occur appear to be compatible with the asymptotic theory proposed in paper 1. Thus it was argued that, in the case $A = B = C = 1$, magnetic flux ropes would form on certain streamlines connecting stagnation points in which field lines would be twisted about them by the local swirling motion. When the flow in the rope diverges at the stagnation points onto two-dimensional manifolds, loops of flux expand by an order of magnitude and provide an order one α-effect. The main obstacle of the theory, discussed in Childress & Soward (1985), concerns the flow and magnetic induction on the two-dimensional manifold. It lies in the chaotic regions of the flow and has an extremely complex structure. Here we may reasonably suppose that as $R \to \infty$ structures of the flow on ever smaller length scales will continue to emerge and significantly alter the fine-scale structure of the magnetic field induced on $R^{-\frac{1}{2}}$ length scales. A complete asymptotic theory of such regions remains a daunting task yet to be undertaken. Be that as it may, these chaotic regions have long been regarded as likely sites of dynamo activity (see, for example Zeldovich *et al.* 1983, 1984 and more recently Vishik 1988, 1989) because, according to frozen field theory, the local straining motion stretches magnetic field lines at an exponential rate.

A promising approach to analysis of dynamo action within the chaotic regions might be based upon (1.2) in the Beltrami case $K = l = 2^{\frac{1}{2}}$, mentioned above, and $\delta = 0$ but with ϵ small and positive. The lagrangian orbits of this flow and other steady motions in two and three dimensions were discussed by Zaslavskii *et al.* (1988) and Chernikov *et al.* (1990), who noted that chaos in (1.2) is confined to a 'web' determined by the separatrices of the cells. That is, to regions where boundary layers arise where diffusion is active.

As we have indicated above, the present analysis makes no attempt to deal with the three-dimensional aspects of the flows (1.2) and will instead focus on the special case

$$\delta = 0, \quad 0 < \epsilon \ll 1 \tag{1.8}$$

with uniform mean horizontal flow in the form

$$\bar{\boldsymbol{u}}_{\mathrm{H}} = \epsilon \hat{\boldsymbol{u}}_{\mathrm{H}}, \quad \hat{\boldsymbol{u}}_{\mathrm{H}} = (\sin\theta_0, \cos\theta_0). \tag{1.9}$$

The complete horizontal motion, $\boldsymbol{u}_{\mathrm{H}} = \bar{\boldsymbol{u}} + \boldsymbol{u}'_{\mathrm{H}}$ has some interesting features. Motion is largely confined to closed eddies on each of the squares $\Pi_{m,n}$. The streamline bounding each eddy begins and ends at the same X-type stagnation point (a homoclinic orbit). The continuation of that streamline only returns to a similar stagnation point when

$$\tan\theta_0 = M/N \tag{1.10a}$$

is rational (see §2.2 below). In fact, if M and N are relatively prime non-negative integers with

$$L = M + N, \tag{1.10b}$$

the xy-shift from one stagnation point to the next is $(M\pi, N\pi)$ for even L and $(2M\pi, 2N\pi)$ for odd L (see (2.14) and (2.16) below). The point here is that a complicated streamline structure emerges which is periodic on a length scale of order L. So when $\tan\theta_0$ is irrational, the streamline pattern never repeats itself, thus mimicing an important feature of three-dimensional flows containing regions of lagrangian chaos. There and in the present irrational limit, the induced magnetic field responds indefinitely to finer and finer streamline structures as $R \to \infty$.

The underlying goal of the present paper is thus to bridge the gap between the earlier boundary-layer theories, for which a finite number of distinct boundary layers emerge as $R \to \infty$, and the case of chaotic flows, for which the number of distinct boundary layers need not be finite or even countable. With the simplification (1.9) we shall find that the streamlines of maximum complexity are 'almost periodic', in that the streamlines of $\boldsymbol{u}_{\mathrm{H}}$ can be dense in the plane. We shall find that in these cases finer and finer boundary-layer structure emerges as R increases to infinity.

The paper is organized as follows. In §2 the channel structure, whose boundaries are composed of all the streamlines through X-type stagnation points, is described in detail. An alternative approach, which emphasises different aspects, is developed in Appendix A using shift maps. In §3 the advection–diffusion problems discussed previously in paper 2 are outlined and modified as they relate to our new flow. As in paper 2 the study of the heat conduction equation (the thermal problem) is looked on as an introductory example from which we obtain an understanding of the key ideas underlying the solutions of the magnetic induction equation (the magnetic problem). In §4 numerical solutions of the boundary layer equations are given, which occur when the eddy boundary layer width of order $R^{-\frac{1}{2}}$ is comparable with the gap between eddies of order ϵ;

$$\beta = \epsilon R^{\frac{1}{2}} = O(1) \tag{1.11}$$

(see (3.17) below). In §5 analytic solutions are given, which are valid when the channel boundary layer width of order $R^{-\frac{1}{2}}L^{\frac{1}{2}}$ is small compared to the channel width $\pi\epsilon(M^2+N^2)^{-\frac{1}{2}}$;

$$\beta \gg L^{\frac{1}{2}}(M^2+N^2)^{\frac{1}{2}} = O(L^{\frac{3}{2}}) \tag{1.12}$$

(see (3.18) below). The values of β used in the numerical integrations are large compared with unity (see table 1 below) so that comparisons can be made with the asymptotic theory. In §6 the limitations of the analytic and numerical results for large β are discussed with particular reference to the asymptotic forms of the diffusion and α-matrices

$$\boldsymbol{D} \sim D_0(\hat{\boldsymbol{u}}_{\mathrm{H}}\hat{\boldsymbol{u}}_{\mathrm{H}}), \quad -\boldsymbol{\alpha} \sim \alpha_0(\boldsymbol{I}-\hat{\boldsymbol{u}}_{\mathrm{H}}\hat{\boldsymbol{u}}_{\mathrm{H}}) \tag{1.13}$$

(see (4.42), (5.37) and (4.64), (5.69) respectively). The values of D_0 and α_0 have irrational limits which are continuous functions of θ_0. The numerical results show that these limits are approached as $R\to\infty$ except for a number of strong resonances with flow orientations (M, N) satisfying (1.12). Of course, the number of strong resonances increases montonically with R confirming our earlier suggestion that finer structures are uncovered and resolved indefinitely, as $R\to\infty$. Put another way, the number of distinct boundary layers is finite for rational tangents and infinite for irrational tangents. In all cases, however, we have the basic estimate

$$\alpha_0 = O(KR\epsilon^3) \quad \text{as} \quad R\to\infty \tag{1.14}$$

(see (4.64)) similar to the expression (1.7a) for $K\alpha^{-}$. Our results thus fully characterize the asymptotic properties of magnetic induction by mean magnetic fields $\boldsymbol{B}_{\mathrm{H}}$ perpendicular to the direction $\hat{\boldsymbol{u}}_{\mathrm{H}}$ of the mean motion.

In the concluding remarks of §7, we estimate the dependence of the α-matrix on the vertical wavenumber q of the mean magnetic field. Unlike the earlier models, which lack mean flow, the magnetic field in our mean flow problem is dominated by large flux concentrations in the eddies. With z-dependence this flux is expelled when the vertical wavenumber q is large compared with $(KR)^{-1}$. This flux expulsion is unlikely to alter the order of magnitude estimate (1.14) for rational tangents. On the other hand, for irrational tangents it is the large horizontal magnetic field penetrating the eddies which is indirectly responsible for the large electromotive force. The horizontal field in the channels is relatively small and the important vertical channel field results from outward diffusion from the eddies. With magnetic flux expelled from the eddies the electromotive force (5.71) evaporates. Thus in the limit q fixed, $R\to\infty$, we expect α_0 to be at most of order unity in the irrational limit. This is consistent with our estimate, below (7.7), that the diffusion matrix constant D_0 is also of order unity in the irrational limit.

The main results of the present study have been summarized briefly by Soward & Childress (1990a). An extended summary, which outlines a different approach to the large β analytic solutions of §5, is given by Soward & Childress (1990b). The method, which is a variant on that used here, was recently developed by Soward (1990).

A brief remark is in order here concerning the extensive use of superscript, in addition to subscript, notation. Since both the heat conduction and magnetic induction equations are linear, the unknown thermal and magnetic variables all appear linearly. There is, therefore, generally no confusion between the use of a superscript as a label and a power. Occasionally there is the possibility of confusion when a streamfunction variable is raised to a power, but the insertion of brackets before the power is taken hopefully makes the meaning clear. To assist the reader a summary of the notation used is listed in Appendix B.

2. The geometry of the flow

2.1. *The overall structure*

We begin with a detailed discussion of the motion (1.2) in the limit (1.2*d*). Specifically, we determine the nature of the streamline pattern of the horizontal flow

$$\boldsymbol{u}_{\mathrm{H}} = \bar{\boldsymbol{u}}_{\mathrm{H}} + \boldsymbol{u}'_{\mathrm{H}} = (\partial\psi/\partial y, -\partial\psi/\partial x) \quad (\psi = \bar{\psi} + \psi'), \tag{2.1a}$$

in the xy plane. Here the fluctuating and mean contributions are

$$\boldsymbol{u}'_{\mathrm{H}} = (\partial\psi'/\partial y, -\partial\psi'/\partial x) \quad (\psi' = \sin x \sin y), \tag{2.1b}$$

$$\bar{\boldsymbol{u}}_{\mathrm{H}} = (\partial\bar{\psi}/\partial y, -\partial\bar{\psi}/\partial x) \quad (\bar{\psi} = y\bar{u}_x - x\bar{u}_y). \tag{2.1c}$$

In the absence of the uniform horizontal mean flow $\bar{\boldsymbol{u}}_{\mathrm{H}}$, the remaining fluctuating part $\boldsymbol{u}'_{\mathrm{H}}$ is the spatially periodic Roberts (1972) motion, for which the streamfunction ψ' exhibits the four symmetries

$$\psi'(\pi \pm x, y) = \psi'(y, \pi \pm x) = \mp\psi'(x, y). \tag{2.2}$$

All streamlines are closed and motion consists of eddies filling squares $\Pi_{m,n}$ (see (1.4)). The streamline at the boundary of the square defines a heteroclinic orbit through each of the four stagnation points, i.e. the four corners where $\boldsymbol{u}'_{\mathrm{H}} = 0$. The addition of the mean flow $\bar{\boldsymbol{u}}_{\mathrm{H}}$ breaks the symmetry of this motion and alters the topology of streamlines; it is this altered topology that concerns us.

The complete motion (2.1*a*) no longer has the four symmetries (2.2). Instead there are only two, which may be expressed in the form

$$\psi(m\pi + (-1)^l x, n\pi + (-1)^l y) = \bar{\psi}_{m,n} + (-1)^l \psi(x, y), \tag{2.3a}$$

where m, n are integers and

$$\bar{\psi}_{m,n} = \bar{\psi}(m\pi, n\pi), \quad l = m + n. \tag{2.3b, c}$$

Note, of course, that, since ψ' vanishes at the corners of the squares $\Pi_{m,n}$, the value $\bar{\psi}_{m,n}$ for the mean flow contribution is also the value of the streamfunction $\psi(m\pi, n\pi)$ for the complete flow. The symmetry property (2.3*a*) can aso be used to map the streamline pattern within

$$\Pi \equiv \Pi_{0,0}, \tag{2.4a}$$

which we will call the primary square, onto the entire horizontal plane. To understand this property we note that the pattern is independent of both the additive constant $\bar{\psi}_{m,n}$ and the factor $(-1)^l$ on the right of (2.3*a*). Nevertheless the form of (2.3*a*) shows that the nature of the mapping onto the square $\Pi_{m,n}$ depends on the sign of $(-1)^l$. Accordingly we introduce the $\pm$ superscript notation

$$\Pi^+_{m,n} \quad (l \text{ even}), \quad \Pi^-_{m,n} \quad (l \text{ odd}) \tag{2.4b}$$

to help distinguish the two types of square. On a $\Pi^+_{m,n}$-square the streamline pattern is related to that on the primary square by translation alone. For a $\Pi^-_{m,n}$-square the streamline pattern on the primary square must first be rotated by 180° about the vertical z-axis through its mid-point $(x, y) = (\frac{1}{2}\pi, \frac{1}{2}\pi)$. This is followed by translation as before. It follows that to determine the shape of the streamlines it is sufficient to restrict attention to the primary square Π.

In addition to the spatial symmetry, there are also symmetries of the flow with respect to certain rotations of the mean velocity vector $\bar{\boldsymbol{u}}_{\mathrm{H}}$. The obvious symmetry is with respect to a 90° rotation about the z-axis followed by a translation; for example

$$\psi(-\bar{u}_y, \bar{u}_x; \pi - y, x) = -\pi\bar{u}_x + \psi(\bar{u}_x, \bar{u}_y; x, y). \tag{2.5a}$$

There is an additional symmetry, which stems from reflexion about the diagonal $y = x$ (say) followed by a translation; for example

$$\psi(\bar{u}_y, \bar{u}_x; \pi + y, x) = -\pi\bar{u}_x - \psi(\bar{u}_x, \bar{u}_y; x, y). \tag{2.5b}$$

The solutions of our advection–diffusion problems exhibit similar symmetries. In view of the simple rotational symmetry (2.5a), we may without loss of generality restrict attention to

$$\bar{u}_x \geqslant 0, \quad \bar{u}_y \geqslant 0. \tag{2.6a}$$

Furthermore the additional reflexional symmetry (2.5b) allows us to restrict the presentation of our numerical results to the range

$$\bar{u}_y \geqslant \bar{u}_x (\geqslant 0). \tag{2.6b}$$

The topology of the flow is determined by the character of the stagnation points and the streamlines through them. On the primary square there are two stagnation points; one is X-type, the other is O-type. When the mean flow satisfies (2.6a), they are located at

$$(x^{\mathrm{s}}, y^{\mathrm{s}}) = \begin{cases} [\tfrac{1}{2}(\alpha - \beta), & \pi - \tfrac{1}{2}(\alpha + \beta)], \quad \text{X-type}, & (2.7a) \\ [\tfrac{1}{2}\pi - \tfrac{1}{2}(\alpha + \beta), & \tfrac{1}{2}\pi + \tfrac{1}{2}(\alpha - \beta)], \quad \text{O-type}, & (2.7b) \end{cases}$$

where the angles α and β are defined by

$$\sin\alpha = \pi^{-1}\psi^{\mathrm{c}}, \quad \sin\beta = -\pi^{-1}\psi^{\beta} \tag{2.7c}.$$

the fluid fluxes $\psi^{\mathrm{c}}, \psi^{\beta}$ being given by

$$\psi^{\mathrm{c}} = \bar{\psi}_{-1,1} = \pi(\bar{u}_x + \bar{u}_y), \quad \psi^{\beta} = \bar{\psi}_{1,1} = \pi(\bar{u}_x - \bar{u}_y). \tag{2.7d}$$

We note that these angles satisfy the inequalities

$$-\alpha \leqslant \beta \leqslant \alpha \leqslant \tfrac{1}{2}\pi \quad (\alpha \geqslant 0). \tag{2.7e}$$

Thus, when $\pi^{-1}\psi^{\mathrm{c}} > 1$, the angle α defined by (2.7c) is no longer real and so the stagnation points (2.7a, b) do not exist; their absence implies that no streamlines close and that the flow is topologically equivalent to the uniform stream $\bar{\boldsymbol{u}}_{\mathrm{H}}$.

The more interesting situation occurs when $\pi^{-1}\psi^{\mathrm{c}} < 1$. For these slower flows, closed eddies $\mathscr{D}^{\pm}_{m,n}$ emerge inside the squares $\Pi^{\pm}_{m,n}$, which contain O-type stagnation points linked under the mapping (2.3a) to (2.7b). Each $\mathscr{D}^{\pm}_{m,n}$-eddy is bounded by a $\mathscr{C}^{\pm}_{m,n}$-streamline. It forms a homoclinic orbit, which begins and ends at the X-type stagnation point with coordinates

$$(x, y) = (m\pi, n\pi) + \begin{cases} (x^{\mathrm{s}}, y^{\mathrm{s}}) & \text{on} \quad \Pi^{+}_{m,n}, & (2.8a) \\ (\pi - x^{\mathrm{s}}, \pi - y^{\mathrm{s}}) & \text{on} \quad \Pi^{-}_{m,n}. & (2.8b) \end{cases}$$

PHILOSOPHICAL TRANSACTIONS OF THE ROYAL SOCIETY A MATHEMATICAL, PHYSICAL & ENGINEERING SCIENCES

According to (2.3a) and (2.7a) the corresponding value of the streamfunction is

$$\psi = \begin{cases} \psi^{+}_{m,n} \equiv \bar{\psi}_{m,n+1} - \psi^{s} & \text{on} \quad \Pi^{+}_{m,n}, \qquad (2.9a) \\ \psi^{-}_{m,n} \equiv \bar{\psi}_{m+1,n} + \psi^{s} & \text{on} \quad \Pi^{-}_{m,n}, \qquad (2.9b) \end{cases}$$

where ψ^{s} is given by

$$2\psi^{s} = (\cos\alpha + \alpha\sin\alpha) - (\cos\beta + \beta\sin\beta) \geqslant 0. \qquad (2.9c)$$

An alternative, more compact and useful representation of (2.9a, b), which utilizes the fluid flux ψ^{c} defined by (2.7d) is

$$\psi^{\pm}_{m,n} = \bar{\psi}_{m+\frac{1}{2},n+\frac{1}{2}} \pm (\tfrac{1}{2}\psi^{c} - \psi^{s}). \qquad (2.9d)$$

Though the $\mathscr{D}^{+}_{m,n}$ and $\mathscr{D}^{-}_{m,n}$-eddies have similar shapes, they define essentially different flows, since a rotation is involved in transforming one into the other. On the other hand, because of the spatial periodicity of the fluctuating motion $\boldsymbol{u}'_{H}$, the flow $\boldsymbol{u}_{H}$ is invariant under the transformation $(x, y) \to (x + m\pi, y + n\pi)$ for integer m, n of even sum l, a property which is explained in (2.20) below (see also (2.3a) above). Consequently the $\mathscr{D}^{+}_{m,n}$ and $\mathscr{D}^{-}_{m,n}$-eddies form two distinct families of similar eddies.

The flow outside the closed $\mathscr{D}^{\pm}_{m,n}$-eddies consists of open streamlines, just like the mean motion $\bar{\boldsymbol{u}}_{H}$. Whenever $\psi = \psi^{\pm}_{m,n}$ for some m, n, that streamline is connected at an X-type stagnation point to the bounding $\mathscr{C}^{\pm}_{m,n}$-streamline of the corresponding $\mathscr{D}^{\pm}_{m,n}$-eddy. These eddies can be thought of as holes (or cavities) in the flow, and they seriously influence the path taken by neighbouring streamlines (see figure 1a). The effect is also illustrated in figure 1b, which shows the paths taken by streamlines ψ neighbouring $\psi^{\pm}_{m,n}$. When $\pm\psi < \pm\psi^{\pm}_{m,n}$, the streamline takes the long route past the stagnation point following the homoclinic orbit $\mathscr{C}^{\pm}_{m,n}$.

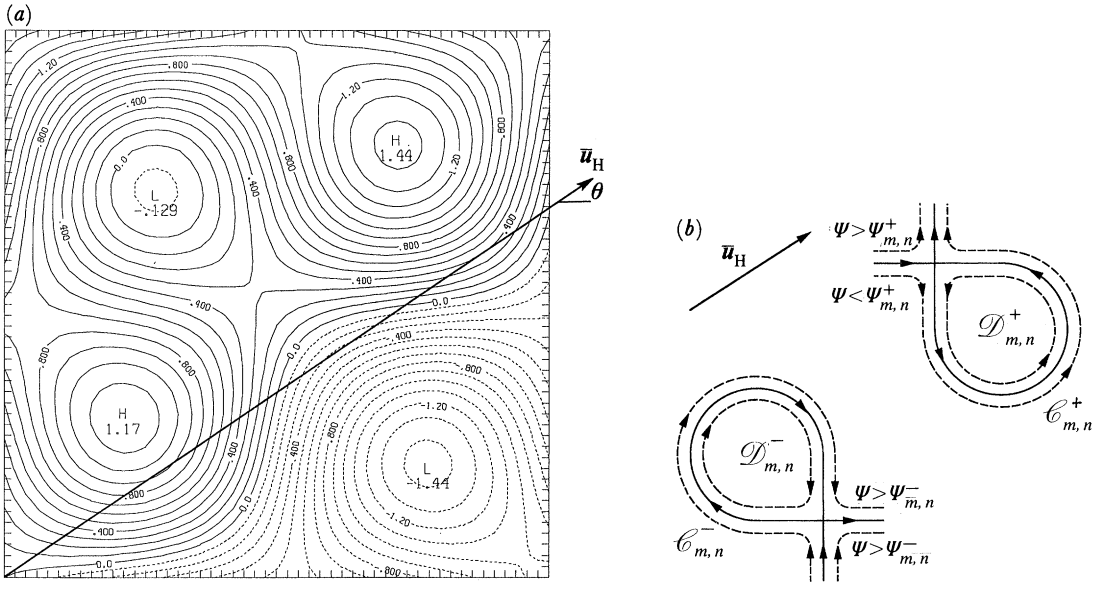

FIGURE 1. (*a*) $\epsilon = 3$, $\tan\theta = \frac{2}{3}$; streamlines of the flow (1.1). A streamline which intersects the boundary does so on a straight line parallel to the uniform components $(\bar{u}_x, \bar{u}_y)$. (*b*) The character of $\mathscr{D}^{\pm}_{m,n}$ eddies when both components of the mean flow $\bar{\boldsymbol{u}}_{H}$ are positive. The solid curves are the streamlines $\psi = \psi^{\pm}_{m,n}$, which include the eddy boundaries $\mathscr{C}^{\pm}_{m,n}$. The neighbouring streamlines are shown broken.

On the other hand, when $\pm\psi > \pm\psi^{\pm}_{m,n}$, the streamline takes the short route bypassing the eddy completely. This splitting of lagrangian history will have important consequences on the transport properties of the flow.

2.2. *Rational tangents*

When the mean flow direction $\hat{\boldsymbol{u}}_{\mathrm{H}}$ (see (1.9)) is defined by a rational tangent (see (1.10*a*)), it is convenient to represent the mean velocity (1.9) in the form

$$\bar{\boldsymbol{u}}_{\mathrm{H}} = \pi^{-1}(\Delta\psi)\,(M, N), \tag{2.10a}$$

where M, N are relatively prime integers,

$$\Delta\psi = \pi\epsilon(M^2+N^2)^{-\frac{1}{2}} \tag{2.10b}$$

and for which the stream function (2.1*c*) is

$$\bar{\psi} = \pi^{-1}(\Delta\psi)\,(yM-xN). \tag{2.10c}$$

The value of the streamfunction ψ at the X-type stagnation points given by (2.9*a–c*) then has the form

$$\psi^{\pm}_{m,n} \equiv \psi^{\pm}_{k} = k(\Delta\psi) \mp \psi^{\mathrm{s}} \quad \text{on} \quad \Pi^{\pm}_{m,n}, \tag{2.11a}$$

where, as usual, the upper and lower signs refer to $l(=m+n)$ even and odd respectively, and, in view of (2.7*d*) and (2.9*d*), the integer k is given by

$$k = (n+\tfrac{1}{2})\,M-(m+\tfrac{1}{2})\,N+(-1)^{l}\tfrac{1}{2}L \quad (L = M+N). \tag{2.11b}$$

Relative to a reference streamline $\psi^{\pm}_{m_0,n_0}(\equiv \psi^{\pm}_{k_0})$ of the same class, the fluid flux associated with an arbitrary streamline (2.11) is

$$\psi^{\pm}_{m,n} - \psi^{\pm}_{m_0,n_0} = (\Delta k)\,(\Delta\psi), \tag{2.12a}$$

where

$$\Delta k \equiv k-k_0 = (\Delta n)\,M-(\Delta m)\,N \tag{2.12b}$$

and

$$\Delta n \equiv n-n_0, \quad \Delta m \equiv m-m_0. \tag{2.12c}$$

Since $l(=m+n)$ and $l_0(=m_0+n_0)$ are either both even or both odd, it follows that

$$\Delta l = \Delta m+\Delta n \quad \text{is even.} \tag{2.12d}$$

When two distinct eddies $\mathscr{D}^{\pm}_{m,n}$ and $\mathscr{D}^{\pm}_{m_0,n_0}$ of the same class are connected by the streamline through their X-type stagnation points, the fluid flux (2.12*a*) vanishes and Δk is zero. By (2.12*b*) this condition is met when

$$\Delta m/M = \Delta n/N. \tag{2.13}$$

The smallest non-trivial solution satisfying (2.12*d*) is

$$(\Delta m, \Delta n) = (2/\tau)\,(M, N), \tag{2.14a}$$

where

$$\Delta l = (2/\tau)\,L \quad (L = M+N) \tag{2.14b}$$

and

$$\tau = \begin{cases} 2 & \text{for} \quad L \text{ even}, \\ 1 & \text{for} \quad L \text{ odd}. \end{cases} \tag{2.14c,d}$$

The result shows that there is a periodic array of $\mathscr{D}^{\pm}_{m_r, n_r}$-eddies defined by

$$(m_r, n_r) = (m_0, n_0) + (2r/\tau)\,(M, N) \tag{2.15}$$

for integer values of r, which are linked together by the single streamline, $\psi = \psi^{\pm}_k$, passing through each of their X-type stagnation points. By (2.8) these stagnation points are separated by the shift

$$(\Delta x, \Delta y) = (2\pi/\tau)\,(M, N), \tag{2.16}$$

which defines the periodicity interval for the streamlines. As already apparent in (2.14c, d), flows with L even and L odd have distinctly different characters and we refer to them subsequently as E-flows and O-flows respectively.

The fluid flux, $\Delta\Psi$, between two neighbouring streamlines $\psi^{\pm}_{m,n}$ and $\psi^{\pm}_{m_0,n_0}$ of the same class, is given by (2.12a), where Δm and Δn defined by (2.12c) are chosen to minimize Δk (see (2.12b)). According to the euclidean algorithm of number theory the minimum value of Δk for arbitrary $\Delta m, \Delta n$ is unity. With $\Delta m, \Delta n$ constrained to have even sum Δl (see (2.12d)), the minimum becomes

$$\Delta k = \tau, \tag{2.17a}$$

where τ is 2 for E-flows and 1 for O-flows (see (2.14c, d)). The corresponding fluid flux is

$$\Delta\Psi = \psi^{\pm}_{k_0+\tau} - \psi^{\pm}_{k_0} = \tau(\Delta\psi). \tag{2.17b}$$

Since streamlines of one class are equally spaced by the fluid flux $\Delta\Psi$, a streamline $\psi^{\mp}_k$ of one class generally lies in between two streamlines $\psi^{\pm}_{k_0+\tau}$ and $\psi^{\pm}_{k_0}$ of the opposite class for some value of k_0. The only exception occurs when the l-even and l-odd families are coincident. In the notation of (2.11a) and (2.12), the condition for coincidence is that

$$\psi^{+}_{m,n} - \psi^{-}_{m_0,n_0} = (\Delta k)\,(\Delta\psi) - 2\psi^{s} = 0, \tag{2.18a}$$

for some m, n of even sum l and m_0, n_0 of odd sum l_0. By (2.11b) we have

$$\Delta k = k - k_0 = (\Delta n)\,M - (\Delta m)\,N, \tag{2.18b}$$

where

$$\Delta n = n - n_0 + 1, \quad \Delta m = m - m_0 - 1 \tag{2.18c}$$

and

$$\Delta l = \Delta m + \Delta n \quad \text{is odd.} \tag{2.18d}$$

As a result, Δk is the set of all odd integers for E-flows and the set of all integers for O-flows; both sets are accommodated by the single statement

$$\Delta k = r\tau - 1 \tag{2.19a}$$

for integer r. As a result, (2.18) is met when

$$2\psi^{s} + \Delta\psi = r(\Delta\Psi) \tag{2.19b}$$

for some integer r, where $\Delta\Psi$ is defined by (2.17b).

The result (2.17b) gives physical significance to the fluid flux $\Delta\psi$ defined by (2.10b). Accordingly as M, N increase in size the fluid flux $\Delta\psi$ decreases. In particular, in the irrational limit, $(M^2 + N^2)^{\frac{1}{2}} \to \infty$, we have both $\Delta\psi$ and $\Delta\Psi$ zero. This means that the open streamlines through the X-type stagnation points are dense in the region exterior to the closed eddies for

irrational tangents, $\tan\theta_0 \neq M/N$. Furthermore, the periodicity (2.16) is lost ($(\Delta x, \Delta y) \to \infty$ as $(M^2+N^2)^{\frac{1}{2}} \to \infty$) and a streamline only passes through one distinct X-type stagnation point.

These basic structural aspects of the irrational limit can also be deduced directly from the lagrangian paths of particles in the flow. The uniform component carries a lagrangian particle from cell to cell, intercepting the separatrices of the fluctuating part (2.1 *b*) at a series of points. These points lie on a single straights line making an angle arctan (M/N) with the horizontal. Thus, modulo 2π in x, y the intercepts are those of a uniform flow on a torus (Arnold & Avez 1967). In particular, in the irrational limit the intercepts are dense on the separatices of $\boldsymbol{u}'$ and there can be no non-zero flux bounded by two adjacent separatrix streamlines of $\boldsymbol{u}_{\mathrm{H}}(=\bar{\boldsymbol{u}}_{\mathrm{H}}+\boldsymbol{u}'_{\mathrm{H}})$.

On the other hand, the meandering path which produces the intercepts requires more geometry than identification with flow on a torus. We focus on these details in the remaining paragraphs of this section, and in the following §2.3.

When we solve our advection–diffusion problems, we find it convenient, particularly for the numerical solution, to appeal to the spatial periodicity of the flow and to restrict attention to two squares of opposite type, for example the primary square $\Pi \equiv \Pi^+_{0,0}$ and its immediate neighbour $\Pi^-_{-1,0}$. Thus every point (x_m, y_n) on $\Pi^+_{m,n}$ is linked to (x, y) on $\Pi^+_{0,0}$ by the transformation

$$(x, y) = (x_m, y_n) - (m\pi, n\pi) \quad (l \text{ even}), \tag{2.20a}$$

while every point (x_m, y_n) on $\Pi^-_{m,n}$ is linked to (x, y) on $\Pi^-_{-1,0}$ by the transformation

$$(x, y) = (x_m, y_n) - ((m+1)\,\pi, n\pi) \quad (l \text{ odd}). \tag{2.20b}$$

The corresponding values of the streamfunction defining the similar streamlines through these points are given, using (2.3 *a*), by

$$\psi(x, y) = \psi(x_m, y_m) - \begin{cases} \bar{\psi}_{m,n} & (x_m, y_n) \in \Pi^+_{m,n}, \quad (2.21a) \\ \bar{\psi}_{m+1,n} & (x_m, y_n) \in \Pi^-_{m,n}, \quad (2.21b) \end{cases}$$

where, from (2.10 *c*),

$$\bar{\psi}_{m,n} = (nM - mN)\,(\Delta\psi). \tag{2.22}$$

Suppose we consider a particular open streamline $\psi = \psi_0$ through the point (x_0, y_0) on $\Pi^+_{0,0}$. Since both the x and y components of the mean velocity $\bar{\boldsymbol{u}}_{\mathrm{H}}$ are positive, the streamline passes in turn through a sequence of adjacent squares $\Pi^{\pm}_{m_r,n_r}$ $(r = 0, 1, 2, \ldots)$ with the following properties. It crosses either the side $x = (m_r+1)\,\pi$ into $\Pi^{\mp}_{m_r+1,n_r}$ or the side $y = (n_r+1)\,\pi$ into $\Pi^{\mp}_{m_r,n_r+1}$. In both cases the sum $l_r = m_r + n_r$ increases by one with r and, because $m_0 = n_0 = 0$, it takes the value $l_r = r$ after crossing the rth edge. The streamline section on each square $\Pi^{\pm}_{m_r,n_r}$ is mapped alternatively onto $\Pi^+_{0,0}$ ($l_r = r$, odd) and $\Pi^-_{-1,0}$ ($l_r = r$, even). The effect of mapping the complete streamline onto these two squares is to produce the family of streamlines

$$\psi = \psi_0 - \begin{cases} (n_r M - m_r N)\,(\Delta\psi) & (r \text{ even}) \quad \text{on} \quad \Pi^+_{0,0}, \quad (2.23a) \\ (n_r M - (m_r+1)\,N)\,(\Delta\psi) & (r \text{ odd}) \quad \text{on} \quad \Pi^-_{-1,0}, \quad (2.23b) \end{cases}$$

which are separated, as in the case of the streamlines $\psi^{\pm}_{m,n}$ of the same class discussed above, by the fluid flux $\Delta\Psi(=\tau\Delta\psi$, see (2.17 *b*)). Furthermore the periodicity section of streamline

between (x_0, y_0) on $\Pi^+_{0,0}$ and $(x_0+\Delta x, y_0+\Delta y)$ on $\Pi^+_{2M/\tau, 2N/\tau}$ (see (2.16)) is mapped one to one onto the family of streamlines (2.23) defined on $\Pi^-_{-1,0} \cup \Pi^+_{0,0}$. Note here, in particular, that under the transformation (2.20*a*) the point $(x_0+\Delta x, y_0+\Delta y)$ is mapped onto (x_0, y_0).

In the interior of the $\mathscr{D}^{\pm}_{m,n}$-eddies, we also find it convenient to identify closed streamlines

$$\mathscr{C}^{\pm\infty}_{m,n}: \quad \psi = \psi^{\pm}_{m,n} + \psi_{\pm\infty}, \tag{2.24}$$

where $\psi_\infty\,(>0)$ and $\psi_{-\infty}\,(<0)$ are constants. Then, exactly as before for the channel regions, every closed streamline $\mathscr{C}^{\infty}_{m,n}$ and $\mathscr{C}^{-\infty}_{m,n}$ can be mapped by (2.20*a*) and (2.20*b*) onto $\mathscr{C}^{\infty}_{0,0}$ and $\mathscr{C}^{-\infty}_{-1,0}$ respectively.

2.3. *Slow mean flow*

The discussion of the advection–diffusion problems in the subsequent sections is restricted to the case of slow mean flow,

$$\epsilon \ll 1. \tag{2.25}$$

With this ordering further simplifications are possible. In particular we can conveniently evaluate the circulation integral (2.31*a*) below occurring later in the analysis, and a useful result of this subsection will be an explicit formula for it based upon streamline geometry for small ϵ.

One consequence of (2.25) is that the angles α and β defined by (2.7*c*) are of order ϵ implying by (2.9*c*) that ψ^{s} is of order ϵ^2. As a result the X-type stagnation points are located close to the corners of the squares at

$$(x, y) = \begin{cases} (m\pi, (n+1)\,\pi) + O(\epsilon) & \text{on} \quad \Pi^+_{m,n}, & (2.26a) \\ ((m+1)\,\pi, n\pi) + O(\epsilon) & \text{on} \quad \Pi^-_{m,n} & (2.26b) \end{cases}$$

(see (2.8)). The corresponding values of the streamfunction are

$$\psi^{\pm}_{m,n} = \bar{\psi}_{m+\frac{1}{2}, n+\frac{1}{2}} \pm \tfrac{1}{2}\psi^{\mathrm{c}} + O(\epsilon^2) \quad \text{on} \quad \Pi^{\pm}_{m,n} \tag{2.27a}$$

(see (2.9*d*)), where now ψ^{c} defined by (2.7*d*) is

$$\psi^{\mathrm{c}} = L(\Delta\psi) \quad (L = M+N). \tag{2.27b}$$

Here both $\bar{\psi}_{m+\frac{1}{2}, n+\frac{1}{2}}$ and ψ^{c} are proportional to $\Delta\psi$, hence of order ϵ;

$$\Delta\psi = O(\epsilon). \tag{2.28}$$

It therefore follows from (2.27*a*) that the values of ψ at the X-type stagnation points are also of order ϵ. This means that the fluid flux following the open streamlines is small of order ϵ. On the other hand, since ψ is given approximately by ψ', which is of order unity in the interior of the squares $\Pi^{\pm}_{m,n}$, motion is dominated by the order one closed streamline flow inside the eddies. The mean motion filters past the eddies with an order one velocity in thin regions of width order ϵ; these regions contain the boundaries of the squares, which are the separatrices of the flow $\boldsymbol{u}'_{\mathrm{H}}$.

As far as the asymptotic analyses (cf. §3) of our advection–diffusion problems is concerned, it is only the open streamline flow and motion close to the boundaries $\mathscr{C}^{\pm}_{m,n}$ of the closed eddies up to, for example, $\mathscr{C}^{\pm\infty}_{m,n}$ (see (2.24)), where ψ is of order ϵ, that is relevant. We therefore focus

attention on that flow and ignore the order ϵ^2 corrections. Within the framework of this approximation the values of the streamfunction $\psi^{\pm}_{m,n}$ connecting the X-type stagnation points is given by (2.11) with

$$\psi^{s} = 0. \tag{2.29}$$

When L is even, both M and N are odd and, so according to (2.11 b), k is odd (even) for l even (odd). Consequently the $\psi^{\pm}_{k}$-streamlines alternate;

$$C_k : \psi = k(\Delta\psi) = \left\{ \begin{matrix} \psi^{+}_{k}\ (k \text{ odd}) \\ \psi^{-}_{k}\ (k \text{ even}) \end{matrix} \right\} \quad \text{for} \quad \text{E-flows}, \tag{2.30a}$$

and are separated one from another by a fluid flux $\Delta\psi$, whereas the fluid flux between two streamlines of the same class is $\Delta\Psi \equiv \psi^{\pm}_{k+1} - \psi^{\pm}_{k-1} = 2\Delta\psi$ (see (2.17 b)). When L is odd, on the other hand, this flux is simply $\Delta\Psi \equiv \psi^{\pm}_{k+1} - \psi^{\pm}_{k} = \Delta\psi$. Furthermore the streamline ψ^{+}_{k} and ψ^{-}_{k} are now coincident ($r = 1$ in (2.19 b)) and given by

$$C_k : \psi = k(\Delta\psi) = \psi^{\pm}_{k} \quad \text{for} \quad \text{O-flows}. \tag{2.30b}$$

For both E-flows and O-flows the streamlines C_k bound open channels

$$D_k : k(\Delta\psi) < \psi < (k+1)\,(\Delta\psi). \tag{2.30c}$$

If we focus attention to a particular channel D_k, it wanders in a complicated way about the xy plane. Fortunately the asymptotic solutions of the advection–diffusion problems, which we describe in §5 below, do not depend on the detailed description of the path taken. What is relevant, however, is the circulation integral

$$\int_{P_0}^{P_\Delta} \boldsymbol{u}_{\mathrm{H}} \cdot \mathrm{d}\boldsymbol{x} \tag{2.31a}$$

over a periodicity section, $P_0(x_0, y_0)$ to $P_\Delta(x_0 + \Delta x, y_0 + \Delta y)$, of open streamline. To evaluate it, we note that the streamline follows close to the edges of the squares $\Pi^{\pm}_{m,n}$. On the side $0 < x < \pi, y = 0$ of the primary square, for example, the flow velocity is given correct to order unity by the fluctuating velocity $u'_x(x, 0) = \sin x$. Hence the contribution to the circulation from one side is

$$\int_0^{\pi} \sin x \, \mathrm{d}x = 2. \tag{2.31b}$$

To leading order the value of

$$\int_{P_0}^{P_\Delta} \boldsymbol{u}_{\mathrm{H}} \cdot \mathrm{d}\boldsymbol{x}$$

is the same for all streamlines in one channel. If the periodicity section of the channel D_k has S_k sides, the circulation integral for that channel is

$$\Gamma_k = 2S_k. \tag{2.32}$$

In addition, we require the circulation about the homoclinic orbit bounding the closed eddies. Since each eddy has four sides, the circulation is

$$\pm\Gamma = \oint_{\mathscr{C}^{\pm}_{m,n}} \boldsymbol{u}_{\mathrm{H}} \cdot \mathrm{d}\boldsymbol{x} = \pm 8. \tag{2.33}$$

Here the minus sign for the $\mathscr{D}^{-}_{m,n}$-eddies simply reminds us that the circulation about those eddies is in the clockwise sense.

As a first step towards determining the number of sides S_k on periodicity sections, we compare the length of two neighbouring channels. Essentially, those sections of channels, which share a common boundary, have the same length. Differences arise only when one channel is diverted about four sides of a closed eddy $\mathscr{D}^{\pm}_{m,n}$, as illustrated in figure 1*b*. Consider, for example, the dividing streamline $C_0(\psi = 0)$ through the X-type stagnation point on $\mathscr{D}^{-}_{-1,0}$ at the origin $\mathrm{O}(0,0)$, as illustrated in figure 2. A periodicity section starting just downstream of O takes in one $\mathscr{D}^{-}_{m,n}$-eddy, namely $\mathscr{D}^{-}_{-1+2M/\tau,\,2N/\tau}$, before finishing at $\mathrm{O}_{\Delta}(\Delta x, \Delta y)$ (see 2.16)). In the case of E-flows (L even), the streamline C_0 is $\psi = \psi^{-}_{0}$ (see (2.30*a*)) and is only connected to $\mathscr{D}^{-}_{m,n}$-eddies. In the case of O-flows (L odd), the streamline C_0 is also of the type $\psi = \psi^{+}_{0}$ (see (2.30*b*)) and consequently is connected to $\mathscr{D}^{+}_{m,n}$-eddies. According to (2.18) the coincident streamlines are $C_0 : \psi = \psi^{-}_{-1,0} = \psi^{+}_{M,-1+N}$, for which $\Delta m = M$, $\Delta n = N$, and so the $\mathscr{D}^{-}_{m,n}$-eddy, taken in by C_0 on the periodicity section OO_{Δ}, is $\mathscr{D}^{+}_{M,-1+N}$. We now compare the paths taken by neighbouring streamlines in the channels $D_0(\psi > 0)$ and $D_{-1}(\psi < 0)$ just above and below C_0 over the periodicity section OO_{Δ}. In the case of E-flows, four extra sides are followed by the channel D_0 in passing round the eddy boundary $\mathscr{C}^{-}_{-1+2M/\tau,\,2N/\tau}$ (see figure 2*a*, $\tau = 2$). On the other hand, in the case of O-flows there are, in addition, four extra sides followed by the channel D_{-1} in passing round the eddy boundary $\mathscr{C}^{+}_{M,-1+N}$ (see figure 2*b*) and consequently the

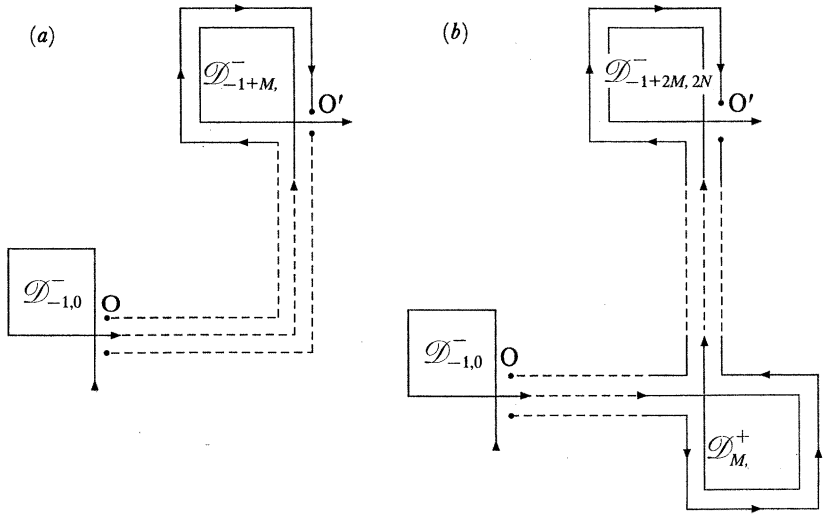

FIGURE 2. Symbolic sketches showing a periodicity section of C_0 from the origin O to O_{Δ} ($\equiv 0'$). Streamlines above ($\psi > 0$) and below ($\psi < 0$) C_0 are also shown. The paths between eddies may be very complicated. Nevertheless they are of equal length and shown broken. (*a*) E-flow with $\mathrm{O}_{\Delta}(M\pi, N\pi)$. (*b*) O-flow with $\mathrm{O}_{\Delta}(2M\pi, 2N\pi)$.

channels D_0 and D_{-1} are the same length. In summary these arguments show that the number of sides S_k of neighbouring channels are related by

$$S_k = \begin{cases} S_{k-1} + (-1)^k 4, & \text{E-flows,} \quad (2.34a) \\ S_{k-1}, & \text{O-flows.} \quad (2.34b) \end{cases}$$

Channel periodicity sections for some simple cases are illustrated in figures 3*a*, 4*a* and 5*a*.

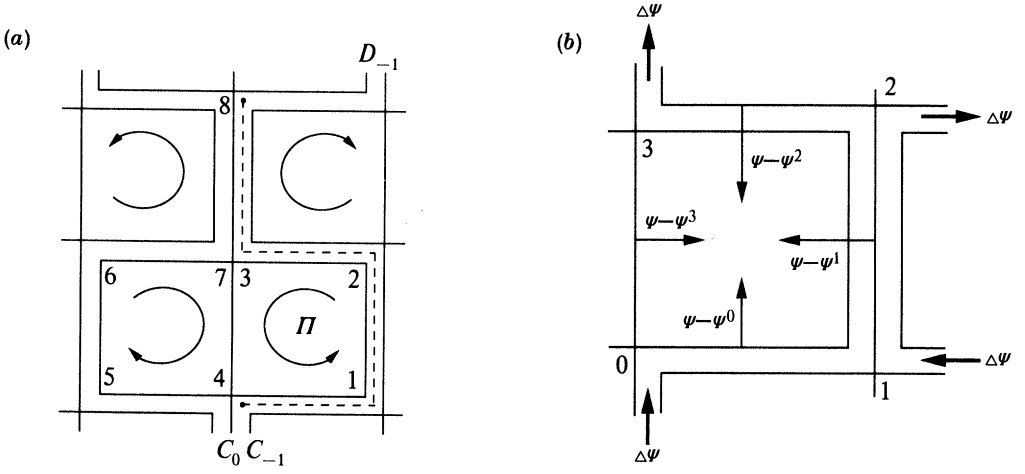

FIGURE 3. The O-flow $M = 0, N = 1$. (*a*) The eddy and channel structure. The primary eddy is labelled with Π and the sense of circulation in the eddies is indicated by the arrows. The periodicity section on D_{-1} is marked by the broken line between the dots and consists of four sides. A periodic sequence of points on the streamline C_0 at the corners of squares $\Pi^{\pm}_{m,n}$ are marked 1–8. (*b*) The channels on the four sides $\mathscr{T}^i$ of Π. The fluid flux carried on each channel is indicated and the ψ–ψ^i axis provides a measure of the fluid flux relative to the previous X-type stagnation point O^i labelled on the sketch by the superscript 'i' alone.

To make further progress we now consider the detailed channel structure near the boundary of the primary square Π. Special cases are illustrated in figures 3*b*, 4*b*, 5*b* and the general case is shown in figure 6. We label each of the X-type stagnation points at the corners of the square as

$$O^0:(0,0), \quad O^1:(\pi,0), \quad O^2:(\pi,\pi), \quad O^3:(0,\pi), \qquad (2.35)$$

which are taken in cyclic order following the sense of the circulation about $\mathscr{C}^{+\infty}_{0,0}$. We define the side $\mathscr{T}^i$ to be the edge between the corners O^i and O^{i+1}, where here and subsequently the superscript is taken modulus 4 (e.g. $O^4 \equiv O^0$ and $O^{-1} = O^3$). The value of the streamfunction

$$\psi = \psi^i = k^i(\Delta\psi) \qquad (2.36a)$$

at each of the stagnation points, given by (2.27), is in turn

$$\psi^0 = 0 \qquad (k^0 = 0) \qquad \text{at} \quad O^0 \in \mathscr{C}_{-1,0} \subset C_0, \qquad (2.36b)$$

$$\psi^1 = -\pi\bar{u}_y \qquad (k^1 = -N) \qquad \text{at} \quad O^1 \in \mathscr{C}_{1,-1} \subset C_{-N}, \qquad (2.36c)$$

$$\psi^2 = \pi(\bar{u}_x - \bar{u}_y) \qquad (k^2 = M - N) \qquad \text{at} \quad O^2 \in \mathscr{C}_{0,1} \subset C_{M-N}, \qquad (2.36d)$$

$$\psi^3 = \pi\bar{u}_x \qquad (k^3 = M) \qquad \text{at} \quad O^3 \in \mathscr{C}_{0,0} \subset C_M. \qquad (2.36e)$$

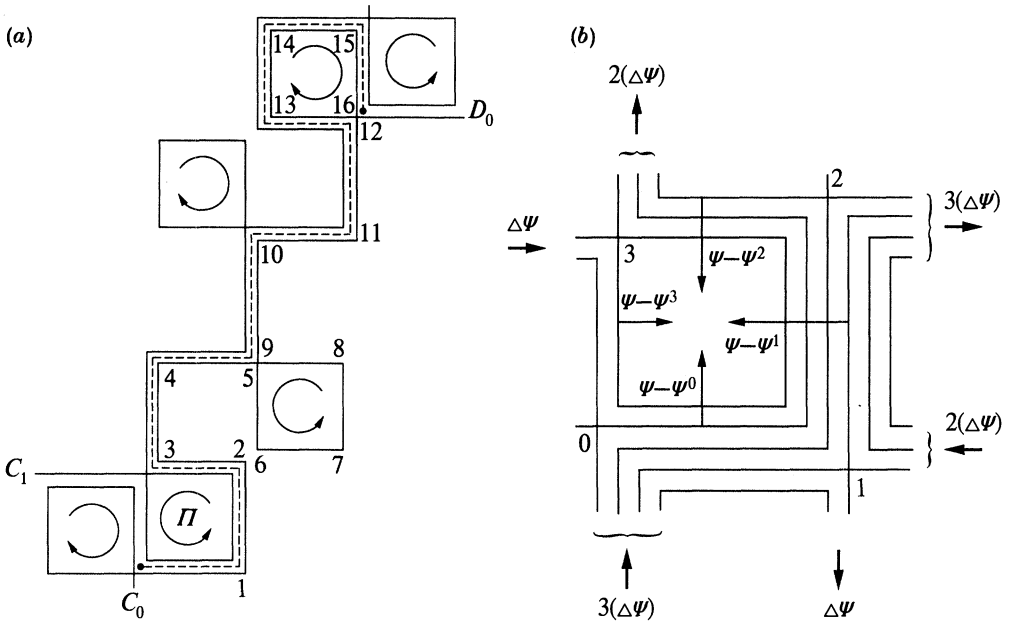

FIGURE 4. The O-flow $M = 1, N = 2$. (*a*) As in figure 3 except that now the channel D_0 is indicated. Note as in figure 2*b* that eddies of both classes are connected alternately on both C_0 and C_1. A periodic sequence of points 1–16 on C_0 is marked. (*b*) As in figure 3*b* except that only the total fluid fluxes entering and leaving the corners of Π are indicated.

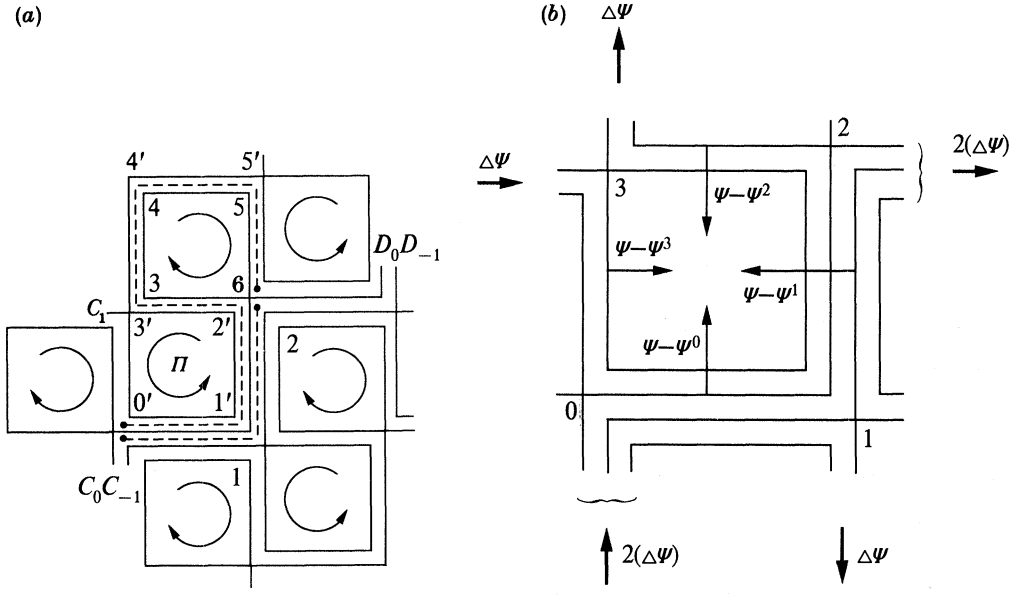

FIGURE 5. The E-flow $M = N = 1$. (*a*) As in figures 3 and 4 except that now the periodicity sections on both D_{-1} of two sides and D_0 of six sides are marked, bounded by the three streamlines C_{-1}, C_0, C_1. Note as in figure 2*a* that only eddies of like class are connected, for example $\mathscr{D}^-_{m,n}$ on C_0. Two periodic sequences of points 1–6 on C_0 and 0′ to 5′ on C_1 are marked. (*b*) As in figure 4*b*.

If we are interested in motion outside the closed streamlines $\mathscr{C}^{\pm\infty}_{m,n}$ (see (2.24)), it is appropriate to restrict attention to the ψ-range

$$(\psi^i_- + \psi_{-\infty} \equiv)\ \psi^i_{-\infty} < \psi < \psi^i_\infty (\equiv \psi^i_+ + \psi_\infty) \quad \text{on} \quad \mathscr{T}^i \tag{2.37a}$$

with

$$\psi^i_\pm = k^i_\pm(\Delta\psi). \tag{2.37b}$$

On the interior $\mathscr{C}^+_{0,0}$-edge (2.27), (2.37b) and (2.11) give

$$\psi^i_+ = \psi^+_{0,0} = \pi\bar{u}_x \quad (k^i_+ = M) \quad \text{for all } i, \tag{2.38}$$

while on the exterior $\mathscr{C}^-_{m,n}$-edges they give

$$\psi^0_- = \psi^-_{0,-1} = -\pi(\bar{u}_x + \bar{u}_y) \quad (k^0_- = -M - N), \tag{2.39a}$$

$$\psi^1_- = \psi^-_{1,0} = -2\pi\bar{u}_y \quad (k^1_- = -2N), \tag{2.39b}$$

$$\psi^2_- = \psi^-_{0,1} = \pi(\bar{u}_x - \bar{u}_y) \quad (k^2_- = M - N), \tag{2.39c}$$

$$\psi^3_- = \psi^-_{-1,0} = 0 \quad (k^3_- = 0). \tag{2.39d}$$

Furthermore the channel regions alone are defined by

$$\psi^i_- < \psi < \psi^i_+ \quad \text{on} \quad \mathscr{T}^i. \tag{2.40}$$

In that case if we wish to consider only the channel regions in $\Pi^-_{-1,0} \cup \Pi^+_{0,0}$, those on $\Pi^-_{-1,0}$ can be mapped by (2.20b) one to one on to the outer half of the side $\mathscr{T}^i$ $(i = 1, \ldots, 4)$, which lie exterior to the primary square Π. In other words, rather than map the periodicity channel sections on to $\Pi^-_{-1,0} \cup \Pi^+_{0,0}$, it is more convenient to map them directly on to the four sides, $\bigcup_{i=1}^4 \mathscr{T}^i$. From (2.38), (2.39) and (2.40) the number of channels on each side is readily calculated from the corresponding fluid flux. It is

$$\psi^i_+ - \psi^i_- = \psi^c + \Delta\psi^{i+1} \quad \text{on} \quad \mathscr{T}^i, \tag{2.41}$$

where

$$\Delta\psi^1 = -\Delta\psi^3 = M(\Delta\psi) = \pi\bar{u}_x, \tag{2.42a}$$

$$-\Delta\psi^0 = \Delta\psi^2 = N(\Delta\psi) = \pi\bar{u}_y. \tag{2.42b}$$

Here ψ^c, defined by (2.7d) and (2.27b), is the average of the fluxes carried on each of the sides circulating Π, while

$$\Delta\psi^i = \psi^{i+1} - \psi^i \tag{2.43}$$

(see (2.36)) measures the fluid flux between the streamlines through the stagnation points O^{i+1} and O^i at either end of the side $\mathscr{T}^i$. We note also that whereas the flows on $\mathscr{T}^0$ and $\mathscr{T}^1$ are directed in the positive x and y directions respectively, the flows on $\mathscr{T}^2$ and $\mathscr{T}^3$ are directed in the negative x and y directions respectively. Consequently the x and y components of the mean motion $\bar{\boldsymbol{u}}_H$ are given by

$$\bar{u}_x = \frac{1}{2\pi}(\Delta\psi^1 - \Delta\psi^3), \quad \bar{u}_y = \frac{1}{2\pi}(\Delta\psi^2 - \Delta\psi^0), \tag{2.44}$$

independent of ψ^c. Nevertheless in our advective diffusion problems, the circulating flux ψ^c plays a central role, as we shall see in §3.

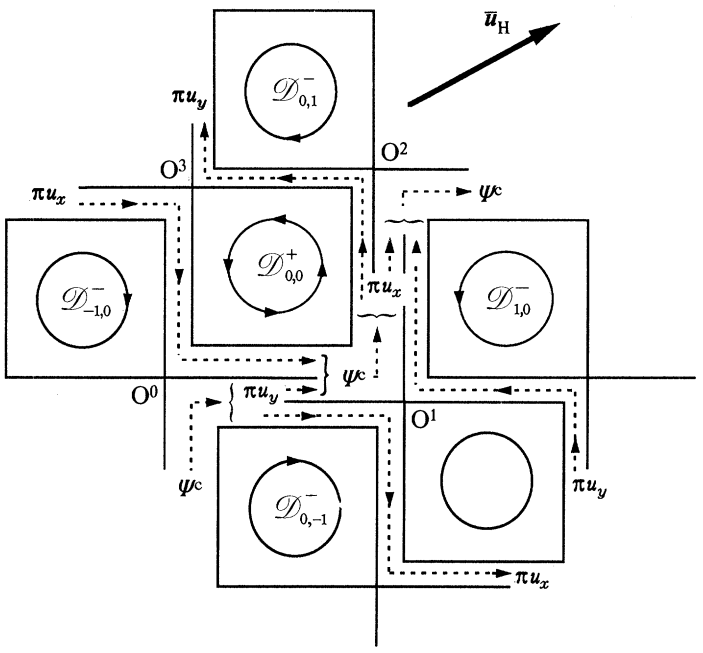

FIGURE 6. The $\mathscr{D}^+_{0,0}$ eddy on the primary square Π and its immediate neighbours $\mathscr{D}^-_{-1,0}$, $\mathscr{D}^-_{0,-1}$, $\mathscr{D}^-_{1,0}$ and $\mathscr{D}^-_{0,1}$. The fluid flux carried on each of the sides $\mathscr{T}^i$ is shown together with their partition by each of the X-type stagnation points O^i (see (2.42)). The closed eddy streamline boundaries $\mathscr{C}^+_{0,0}$ (see (2.38)) and $\mathscr{C}^-_{m,n}$ (see (2.39)) are also shown.

Before proceeding we note some other useful relations between ψ^i, $\psi^i_\pm$ and $\Delta\psi^i$ defined by (2.36) and (2.38)–(2.42). They satisfy

$$2(\psi^i_\pm - \psi^i) = \pm\psi^c + \Delta\psi^i + \Delta\psi^{i\pm1}, \tag{2.45a}$$

$$\Delta\psi^{i+1} + \Delta\psi^{i-1} = 0, \tag{2.45b}$$

$$\psi^{i+1}_- - \psi^{i-1}_- = 2(\Delta\psi^i), \tag{2.45c}$$

which imply for example that

$$(\psi^{i+1}_\pm - \psi^{i+1}) + (\psi^{i-1}_\pm - \psi^{i-1}) = \pm\psi^c, \tag{2.46a}$$

$$\psi^{i+1} + \psi^{i-1} = \psi^\beta, \tag{2.46b}$$

$$\psi^i_+ + \psi^i_- = 2\psi^i + \Delta\psi^i. \tag{2.46c}$$

We return now to the question of the number of sides S_k on the periodicity sections of channels D_k. We consider the flow between two neighbouring streamlines of the same type ψ^+_k and $\psi^+_{k+\tau}$ (say), which carries fluid flux $\Delta\Psi = \tau\,(\Delta\psi)$ (see (2.17b)). A convenient choice is the pair of channels D_{-1} and D_0 ($k = -1$ and 0, $\tau = 2$) for E-flows and the single channel D_0 ($k = 0, \tau = 1$) for O-flows. Taken over a periodicity section the total number of sides involved is $\frac{1}{2}\tau(S_{k-1} + S_k)$ for both types of flow. According to the remarks below (2.23), these sides are mapped one to one on to the rectangle $\Pi^-_{-1,0} \cup \Pi^+_{0,0}$ excluding the two eddies $\mathscr{D}^-_{-1,0}$ and $\mathscr{D}^+_{0,0}$ enclosed by them. This region is equivalent to the four sides $\bigcup_{i=1}^4 \mathscr{T}^i$ of the primary square which carry a total of $4\psi^c/(\Delta\psi) = 4L$ channel sides. This gives

$$\tfrac{1}{2}\tau(S_{k-1} + S_k) = 4L, \tag{2.47}$$

which with (2.32) and (2.34) yields the main result of this section, namely

$$\Gamma_k = 2S_k = (8/\tau)\,\Delta_k L, \tag{2.48}$$

where

$$\Delta_k = 1 + (-1)^k (\tau - 1)/L. \tag{2.49}$$

We note that Δ_k has the obvious properties

$$\tfrac{1}{2}(\Delta_k + \Delta_{k+1}) = 1, \quad \Delta_{k+1} = \Delta_{k-1} \tag{2.50}$$

and introduce for convenience later the parameter

$$\Lambda = \Delta_k \Delta_{k+1} = 1 - (\tau - 1)/L^2. \tag{2.51}$$

An alternative derivation of (2.34) and (2.48) based on the use of a shift map on channel streamfunction, is given in Appendix A.

3. The advection–diffusion problems

The flow field we have described in §2 contains features of interest in the advection and diffusion of scalar and vector fields. It shares with the flow of paper 2 the presence of islands of closed streamlines separated by channels, but now the channel connections are far more complicated and are dependent upon M, N.

In the present section we study the effect of this flow on scalar and vector fields. The scalar problem has many applications, but we shall take the view here that the scalar field is a temperature field, and so will use the terminology of heat conduction to describe it. The vector field of interest is a magnetic field, and we use the methods and terminology of dynamo theory. As we shall see, the temperature problem is in fact a prerequisite in magnetic problem, and this was our original motivation for studying it.

3.1. *The heat conduction equation*

In the thermal problem we consider the temperature field $A^*(x, y, t)$ which occurs when a steady applied temperature gradient

$$\bar{\boldsymbol{g}}_{\mathrm{H}} = \boldsymbol{\nabla}\bar{A} \quad (\bar{A} = x\bar{g}_x + y\bar{g}_y) \tag{3.1}$$

in the horizontal plane, is advected by the horizontal motion $\boldsymbol{u}_{\mathrm{H}}$ (see (2.1)). In particular the vertical components of the motion need not enter. The quantity $\bar{A}$ conveniently defines the secular or spatially growing component of A, but it is not an average of A. Indeed A is not invariant under translation, and $\bar{A}$ simply isolates this property, in a function that vanishes at the origin, the remainder of the field being spatially periodic (see (3.3) below).

A^* is also time-dependent because of the advection of $\bar{A}$ by the mean motion. The steady transport of cooler fluid by convection up the gradient causes the temperature to decrease with time. The time-dependent component may be expelled, however, by setting

$$A^* = -\bar{E}t + A(x, y), \tag{3.2a}$$

where the scalar A is steady, independent of both vertical coordinate z and time t. In terms of our dimensionless variables, A satisfies the heat conduction equation

$$\boldsymbol{u}_{\mathrm{H}} \cdot \boldsymbol{\nabla} A - \bar{E} = R^{-1}\nabla^2 A, \tag{3.2b}$$

where the constant

$$\bar{E} = \bar{\boldsymbol{u}}_{\mathrm{H}} \cdot \bar{\boldsymbol{g}}_{\mathrm{H}} \tag{3.2c}$$

represents a heat source and R is the Péclet number for the flow. Solutions of (3.2) are sought in the form

$$A = \bar{A} + A', \tag{3.3}$$

where A', like ψ' in (2.1b), is spatially periodic. Specifically, we assume that A has the transformation property

$$A(m\pi + x, n\pi + y) = \bar{A}_{m,n} + A(x, y) \quad (l \text{ even}), \tag{3.4a}$$

where m, n are integers with even sum l and

$$\bar{A}_{m,n} = \bar{A}(m\pi, n\pi). \tag{3.4b}$$

Since A' is determined only to within an arbitrary constant, its normalization remains at our discretion.

The quantity of physical interest is the heat flux $\boldsymbol{u}_{\mathrm{H}} A$. Since A increases secularly in space (see (3.1)), it is convenient to remove that secularity in the heat flux and consider the quantity

$$\boldsymbol{F}_{\mathrm{H}} = \boldsymbol{u}_{\mathrm{H}} A - \bar{\boldsymbol{u}}_{\mathrm{H}} \bar{A}, \tag{3.5}$$

instead. Our prime objective is to define and evaluate the mean heat flux $\bar{\boldsymbol{F}}_{\mathrm{H}}$, in which (3.5) is averaged over a suitable and carefully chosen domain (see (3.31) below). Since A is only determined up to an additive constant, it is clear from (3.5) that the value of $\bar{\boldsymbol{F}}_{\mathrm{H}}$ will depend upon the normalization of A'; it is determined only up to a constant multiple of $\bar{\boldsymbol{u}}_{\mathrm{H}}$. One possible normalization requires that the integral of A' over $\Pi^{-}_{-1,0} \cup \Pi^{+}_{0,0}$, like the fluctuating streamfunction ψ', vanish (see (2.1b)). On the other hand, when R is large, the value of A' in the eddies is an order of magnitude $R^{\frac{1}{3}}$ larger than its channel value. So, if we demand that A' averaged vanish, the value of A' and consequently A itself in the channel regions would be of order $R^{\frac{1}{3}}$. Since it is clearly the temperature distribution in the channel regions that is of interest, it is more natural to require that A' be of order unity in the channels, so that $\bar{A}$ correctly reflects the temperature distribution there. Thus, we choose a different normalization given by (3.27b) below. We stress, however, that other choices are possible and that the average $\bar{\boldsymbol{F}}_{\mathrm{H}}$, defined by (3.47) below, must be interpreted in the light of the chosen normalization. In any event our result is linearly related to the applied temperature gradient $\bar{\boldsymbol{g}}_{\mathrm{H}}$ and can be expressed in the form

$$\bar{\boldsymbol{F}}_{\mathrm{H}} = -\boldsymbol{D} \cdot \bar{\boldsymbol{g}}_{\mathrm{H}}. \tag{3.6}$$

The 2×2 matrix $\boldsymbol{D}$ is an effective diffusion-matrix. Again, the arbitrariness inherent in $\bar{\boldsymbol{F}}_{\mathrm{H}}$ for a flow with non-zero mean motion reflects in the non-uniqueness of $\boldsymbol{D}$. The effective diffusion term $\boldsymbol{\nabla} \cdot \bar{\boldsymbol{F}}_{\mathrm{H}}$ remains, however, uniquely determined.

3.2. *The magnetic induction equation*

In the magnetic problem we seek steady z-independent solutions of the magnetic induction equation

$$\boldsymbol{\nabla} \times (\boldsymbol{u} \times \boldsymbol{B}) + R^{-1} \boldsymbol{\nabla}^2 \boldsymbol{B} = 0 \quad (\boldsymbol{\nabla} \cdot \boldsymbol{B} = 0), \tag{3.7a}$$

where now R is the magnetic Reynolds number for the flow

$$\boldsymbol{u} = (\partial\psi/\partial y,\ -\partial\psi/\partial x,\ K\psi'). \tag{3.7b}$$

Here $\psi(=\bar{\psi}+\psi')$ is the streamfunction for the horizontal velocity (2.1), and $K\psi'$ is the vertical velocity appearing in (1.2b), where K is a constant. We express the magnetic field in the form

$$\boldsymbol{B} = (\partial A/\partial y,\ -\partial A/\partial x,\ KB), \tag{3.8}$$

where A is the magnetic vector potential for the horizontal magnetic field, and KB is the vertical magnetic field; the latter is scaled like the vertical velocity with the factor K. Solutions of (3.7a) are sought subject to the condition that the mean magnetic field is uniform and horizontal:

$$\bar{\boldsymbol{B}} = \bar{\boldsymbol{B}}_{\mathrm{H}} = (\partial\bar{A}/\partial y,\ -\partial\bar{A}/\partial x) \quad (\bar{A} = y\bar{B}_x - x\bar{B}_y). \tag{3.9}$$

Advection of the mean magnetic field $\bar{\boldsymbol{B}}_{\mathrm{H}}$ by the horizontal mean motion $\bar{\boldsymbol{u}}_{\mathrm{H}}$ leads to the well known ω-effect of dynamo theory (see, for example, Moffatt 1978). It induces the vertical z-component of the electromotive force

$$-\bar{E} = (\bar{\boldsymbol{u}}_{\mathrm{H}} \times \bar{\boldsymbol{B}}_{\mathrm{H}})_z. \tag{3.10}$$

Since the magnetic field is steady, the electric field is potential, $\boldsymbol{E} = -\nabla\phi$, and the z-component is at most a constant $\bar{E}$. Consequently the z-component of Ohm's law again yields the heat conduction equation (3.2b). The mathematical problem which emerges is exactly the same as the thermal problem if we make the identification

$$\bar{B}_x = \bar{g}_y, \quad \bar{B}_y = -\bar{g}_x \tag{3.11}$$

(see (3.1) and (3.9)). Thus, as already noted above, solution of the thermal problem is a preliminary prerequisite for the complete solution of the magnetic problem.

From the z-component of the magnetic induction equation (3.7a) we have

$$\boldsymbol{u}_{\mathrm{H}} \cdot \nabla B - R^{-1}\nabla^2 B = \boldsymbol{B}_{\mathrm{H}} \cdot \nabla\psi', \tag{3.12a}$$

where, from the definition (2.1) of the velocity,

$$\boldsymbol{B}_{\mathrm{H}} \cdot \nabla\psi' = -\boldsymbol{u}_{\mathrm{H}} \cdot \nabla A + \bar{\boldsymbol{u}}_{\mathrm{H}} \cdot \nabla A. \tag{3.12b}$$

The inhomogeneous conduction equation (3.12a) is solved subject to the condition that the mean value $K\bar{B}$ of the vertical magnetic field vanishes (see (3.9)). From the solution we can determine the mean horizontal components of the electromotive force, $K\bar{\boldsymbol{E}}_{\mathrm{H}}$, where

$$K\boldsymbol{E}_{\mathrm{H}} = (\boldsymbol{u} \times \boldsymbol{B})_{\mathrm{H}} = K[(\psi - \bar{\psi})\,\nabla A - B\nabla\psi]. \tag{3.13}$$

This is the main quantity of physical interest in the dynamo context and leads to the well known α-effect (see, for example, Moffatt 1978). In view of the linearity of the kinematic dynamo problem, the result (3.13) is linearly related to the mean magnetic field $\bar{\boldsymbol{B}}_{\mathrm{H}}$,

$$K\bar{\boldsymbol{E}}_{\mathrm{H}} = \boldsymbol{\alpha} \cdot \bar{\boldsymbol{B}}_{\mathrm{H}}, \tag{3.14}$$

where $\boldsymbol{\alpha}$ is the 2×2 α-matrix. Evidently there are similarities between the formulation of the mean heat flux (3.5), (3.6) and the mean electromotive force (3.13), (3.14). They are also reflected in the results we obtain in §§4 and 5 below.

PHILOSOPHICAL TRANSACTIONS OF THE ROYAL SOCIETY A MATHEMATICAL, PHYSICAL & ENGINEERING SCIENCES

3.3. *Asymptotics for large R*

Our analysis will ultimately be restricted to the case of large Reynolds number

$$R \gg 1. \tag{3.15}$$

In this limit and in steady flow, we generally expect diffusion to be unimportant except in thin boundary layers. These are triggered at the X-type stagnation points on the closed eddy boundaries $\mathscr{C}^{\pm}_{m,n}$. The reason for the existence of these boundary layers is easily understood. Fluid approaching the stagnation point arrives from regions in which the values of A and B are different (see figure 1*b*). Thus, when the streams merge downstream of stagnation point, the values of A and B differ and the resulting discontinuities must be smoothed out in thin boundary layers. An example is illustrated in figure 7 of the closed eddy $\mathscr{D}^{-}_{-1,0}$ bounded by $\mathscr{C}^{-}_{-1,0}$, which lies on the streamline $C_0 : \psi = 0$. Two boundary layers form. One is the recirculating eddy boundary layer on $\mathscr{C}^{-}_{-1,0}$, which has width of order $R^{-\frac{1}{2}}$. The other is the channel boundary layer on C_0 (but excluding $\mathscr{C}^{-}_{-1,0}$), whose width continues to grow downstream until it arrives at the next stagnation point. For flows with rational tangents the distance between stagnation points is of order L (see (2.48)), and so the channel boundary layer width is of order $L^{\frac{1}{2}}R^{-\frac{1}{2}}$. For flows with irrational tangents the boundary layer thickens indefinitely until neighbouring eddies overlap and join.

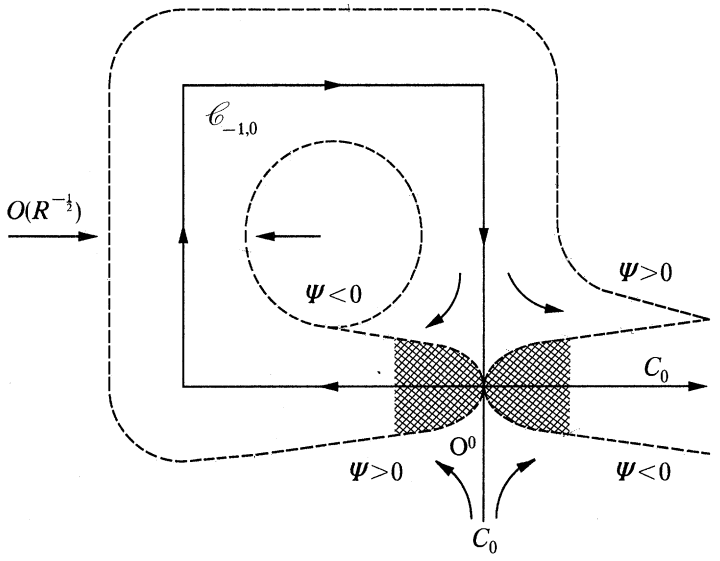

FIGURE 7. Symbolic sketch of the two boundary layers both triggered at the origin O^0, namely the eddy boundary layer on $\mathscr{C}^{-}_{-1,0}$ and the channel boundary layer on C_0 (but excluding $\mathscr{C}^{-}_{-1,0}$). The broken lines indicates their outer edges, while the hatched regions identify the regions closest to the sources at O^0.

Inside the closed eddies, diffusion is unimportant and a mainstream (or outer) solution is easily constructed (see §§3.4.1 and 3.5.1 below). For our slow mean flows

$$\epsilon \ll 1, \tag{3.16}$$

the total width of the region external to the eddies is of order ϵ (see §2.3). Hence as we indicated in the introduction the ratio of the total channel region width to boundary layer width is

$$\beta = \epsilon R^{\frac{1}{2}} \tag{3.17}$$

(see (1.11)). When β is of order unity, A and B are governed by boundary layer equations in the channel region, which we solve numerically in §4. Further mainstream solutions exist in the interior of the channels when the channel width, of order $\Delta\psi = \pi\epsilon(M^2+N^2)^{-\frac{1}{2}}$ (see (2.10b)), is large compared to the channel boundary layer width of order $L^{\frac{1}{2}}R^{-\frac{1}{2}}$, specifically

$$\beta \gg L^{\frac{1}{2}}(M^2+N^2)^{\frac{1}{2}} = O(L^{\frac{3}{2}}) \tag{3.18}$$

(see (1.12)). The leading order approximation of these mainstream solutions is obtained in §5. The mainstream solutions inside the closed eddies provide boundary conditions for both the numerical solutions of §4 and the analytic solutions of §5. They also show that the contributions to the mean heat flux $\bar{\boldsymbol{F}}_{\mathrm{H}}$ and electromotive force $K\bar{\boldsymbol{E}}_{\mathrm{H}}$ originate from the channel regions and the appropriate integral representations for them, namely (3.47) and (3.69), are derived. It is, therefore, convenient to present those eddy solutions in the following subsections before turning attention to the channel solutions in §§4 and 5.

3.4. *The thermal problem*

3.4.1. *The eddy solution*

In the slow mean flow limit (3.16), the heat source $\bar{E}$ defined by (3.2c) is small;

$$\bar{E} = O(\epsilon). \tag{3.19}$$

Consequently in the mainstream and in the eddy interiors both the diffusion term $R^{-1}\nabla^2 A$ and the heat source $\bar{E}$ in (3.2b) can be neglected at lowest order;

$$(\boldsymbol{u}_{\mathrm{H}}\cdot\nabla)\,A = 0. \tag{3.20}$$

It follows that A is constant on streamlines of the horizontal flow,

$$A = A(R^{-\frac{1}{2}};\psi). \tag{3.21}$$

Departures from this functional form are of order ϵ and R^{-1} and smaller. Moreover A is independent of R at leading order. The implied dependence on $R^{-\frac{1}{2}}$ in (3.21) reminds us that boundary layer matching may lead to corrections of order $R^{-\frac{1}{2}}$. Though those corrections were obtained in paper 2 through the use of the Wiener–Hopf method, they will not be considered here. For references to the Prandtl–Batchelor theory used in the present section, see paper 2.

The dependence of A on ψ is determined as in paper 2 by a consistency condition at higher order. We consider the closed domain $\mathscr{D}(\psi)$ bounded by the closed streamline, $\mathscr{C}(\psi):\psi =$ constant, within a $\mathscr{D}^{\pm}_{m,n}$-eddy. Integration of (3.2b) over $\mathscr{D}(\psi)$ and application of the divergence theorem yields

$$\oint_{\mathscr{C}} A\boldsymbol{u}_{\mathrm{H}}\cdot\boldsymbol{n}\,\mathrm{d}s = \bar{E}\Sigma + R^{-1}\oint_{\mathscr{C}} \boldsymbol{n}\cdot\nabla A\,\mathrm{d}s, \tag{3.22}$$

where $\boldsymbol{n}$ is the unit outward normal, s measures are length and $\Sigma(\psi)$ is the area of $\mathscr{D}(\psi)$. Now, whereas the term $\oint_{\mathscr{C}} A\boldsymbol{u}_{\mathrm{H}}\cdot\boldsymbol{n}\,\mathrm{d}s$ is in principle of order unity and dominates (3.22), we have chosen $\mathscr{C}(\psi)$ to be a streamline on which $\boldsymbol{u}_{\mathrm{H}}\cdot\boldsymbol{n}$ vanishes. Consequently, we are left with the two smaller terms on the right of (3.22). Within the framework of the approximation (3.21), the remaining integrand in (3.22) is given at leading order by

$$\boldsymbol{n}\cdot\nabla A = -R^{\frac{1}{2}}qb, \tag{3.23a}$$

where

$$R^{\frac{1}{2}}b(R^{-\frac{1}{2}};\psi) = \mathrm{d}A/\mathrm{d}\psi, \quad q = -\boldsymbol{n}\cdot\boldsymbol{\nabla}\psi. \tag{3.23 b, c}$$

Since arc length is measured counter-clockwise about $\mathscr{C}$, the element of directed arc $\mathrm{d}\boldsymbol{x}$ is related to $\mathrm{d}s$ by

$$\boldsymbol{u}_{\mathrm{H}}\cdot\mathrm{d}\boldsymbol{x} = -(\boldsymbol{n}\cdot\boldsymbol{\nabla}\psi)\,\mathrm{d}s, \tag{3.23 d}$$

and so q, defined by (3.23 c), is the velocity. Substitution of (3.23) into (3.22) yields the consistency condition

$$\gamma b = R^{\frac{1}{2}}\bar{E}\Sigma, \tag{3.24 a}$$

where

$$\gamma(\psi) = \oint_{\mathscr{C}} \boldsymbol{u}_{\mathrm{H}}\cdot\mathrm{d}\boldsymbol{x} = \oint_{\mathscr{C}} q\,\mathrm{d}s \tag{3.24 b}$$

is the circulation. We note for later use in the magnetic problem, that the ψ-derivative of (3.24 a) yields

$$\gamma\frac{\mathrm{d}b}{\mathrm{d}\psi} = R^{\frac{1}{2}}\bar{E}\left(\frac{\mathrm{d}\Sigma}{\mathrm{d}\psi} - \frac{\Sigma}{\gamma}\frac{\mathrm{d}\gamma}{\mathrm{d}\psi}\right). \tag{3.25 a}$$

From the definitions

$$\Sigma = \int_{\mathscr{D}} \mathrm{d}\Sigma \quad \text{and} \quad \gamma = \oint_{\mathscr{C}} \boldsymbol{u}_{\mathrm{H}}\cdot\mathrm{d}\boldsymbol{x},$$

it is readily established that

$$\frac{\mathrm{d}\Sigma}{\mathrm{d}\psi} = -\oint_{\mathscr{C}}\frac{1}{q}\mathrm{d}s, \quad \frac{\mathrm{d}\gamma}{\mathrm{d}\psi} = \oint_{\mathscr{C}}\frac{1}{q}\nabla^2\psi\,\mathrm{d}s. \tag{3.25 b}$$

Of particular importance are the values of A and b close to the eddy boundary. Correct to lowest order the eddies $\mathscr{D}^{\pm}_{m,n}$ are squares of area $(\Sigma =)\,\pi^2$, while the circulation about them is $(\gamma = \pm\Gamma =) \pm 8$ (see (2.33)). Thus the mainstream value of b on the eddy boundary $\mathscr{C}^{\pm}_{m,n}$ is

$$b = \pm\bar{b}, \tag{3.26 a}$$

where the $\pm$ sign relates to the sense of the circulation, and

$$\bar{b} = \tfrac{1}{8}R^{\frac{1}{2}}\pi^2\bar{E} \tag{3.26 b}$$

is of order $\beta(=\epsilon R^{\frac{1}{2}})$. Our scaling of b in (3.23 b) has been chosen so that $\bar{b}$ is of order unity when β is order one. In view of the secular behaviour of $\bar{A}$ and the result (3.21) a natural normalization of the mainstream eddy solution is

$$\bar{A} = \bar{A}_{m+\frac{1}{2},n+\frac{1}{2}} \pm A_0 \quad \text{on} \quad \mathscr{C}^{\pm}_{m,n}: \psi = \psi^{\pm}_{m,n}, \tag{3.27 a}$$

where $\bar{A}_{m+\frac{1}{2},n+\frac{1}{2}}$, defined by (3.4 b), is the mean value of $\bar{A}$ on the square $\Pi^{\pm}_{m,n}$. The additional constant A_0, as yet unknown but determined by the solution, reflects the fact the periodicity condition (3.4 a) links the solutions only on eddy boundaries of the same class. It does not relate the values of A on $\mathscr{C}^{+}_{m,n}$-boundaries to those on $\mathscr{C}^{-}_{m,n}$-boundaries. The choice of $\pm A_0$ on the $\mathscr{C}^{\pm}_{m,n}$-boundaries means that, with the secular part $\bar{A}_{m+\frac{1}{2},n+\frac{1}{2}}$ removed, the average of the value of A on two neighbouring eddy boundaries vanishes. Of course, A cannot take exactly the value

(3.27a) on $\mathscr{C}^{\pm}_{m,n}$ because of boundary layer corrections. Nevertheless, when combined with (3.26a), we can instead impose the matching condition

$$A \sim \pm[R^{\frac{1}{2}}\bar{b}(\psi-\psi^{\pm}_{m,n})+A_0]+\bar{A}_{m+\frac{1}{2},n+\frac{1}{2}} \quad \text{as} \quad \pm R^{\frac{1}{2}}(\psi-\psi^{\pm}_{m,n})\to\infty. \tag{3.27b}$$

By this device we render our solutions unique. Though, as we remarked in §3.1 above, other choices of normalization are possible.

3.4.2. *The heat flux*

We now consider the contribution to the heat flux made by the closed surface $\mathscr{D}(\psi)$ inside the eddies. Since A is a function of ψ alone, the divergence theorem implies

$$\int_{\mathscr{D}} A\nabla\psi\,\mathrm{d}\Sigma = \int_{\mathscr{D}} \nabla\left(\int A\,\mathrm{d}\psi\right)\mathrm{d}\Sigma = \left(\int A\,\mathrm{d}\psi\right)\oint_{\mathscr{C}} \boldsymbol{n}\,\mathrm{d}s, \tag{3.28a}$$

which gives

$$\int_{\mathscr{D}} A\boldsymbol{u}_{\mathrm{H}}\,\mathrm{d}\Sigma = -\left(\int A\,\mathrm{d}\psi\right)\oint_{\mathscr{C}} \mathrm{d}\boldsymbol{x} = 0. \tag{3.28b}$$

It shows that the large order $R^{\frac{1}{2}}$ values of A implied by (3.23b) do not contribute to the heat flux. Thus the transport of heat is confined entirely to the channel region and the eddy boundary layers. To compute the heat flux, we exclude the interior of the eddies by restricting attention to the region exterior to the closed streamlines $\mathscr{C}^{\pm\infty}_{m,n}$ (see (2.24)), in which

$$\pm\psi_{\pm\infty} = O(R^{-\frac{1}{2}}). \tag{3.29}$$

With the bulk of the motion excluded we are left with the narrow strips

$$\mathscr{T}_x(m+\tfrac{1}{2},n): m\pi < x < (m+1)\,\pi, \quad y = n\pi, \tag{3.30a}$$

$$\mathscr{T}_y(m,n+\tfrac{1}{2}): x = m\pi, \quad n\pi < y < (n+1)\,\pi, \tag{3.30b}$$

containing edges of the squares $\Pi^{\pm}_{m,n}$. The mid-points of the sides $\mathscr{T}_x(m+\frac{1}{2},n)$ and $\mathscr{T}_y(m,n+\frac{1}{2})$ are located at the centres $((m+\frac{1}{2})\,\pi, n\pi)$ and $(m\pi,(n+\frac{1}{2})\,\pi)$ of the displaced squares $\Pi_{m,n-\frac{1}{2}}$ and $\Pi_{m-\frac{1}{2},n}$ respectively. We now define local averages $\bar{F}^{\mathrm{loc}}_x, \bar{F}^{\mathrm{loc}}_y$ of the x and y components of the flux $\boldsymbol{F}_{\mathrm{H}}$ (see (3.5)) over each of these squares of area π^2 by

$$(\bar{F}^{\mathrm{loc}}_x(m+\tfrac{1}{2},n), \bar{F}^{\mathrm{loc}}_y(m,n+\tfrac{1}{2})) = \frac{1}{\pi^2}\left(\int_{\Pi_{m,n-\frac{1}{2}}} F_x\,\mathrm{d}\Sigma, \int_{\Pi_{m-\frac{1}{2},n}} F_y\,\mathrm{d}\Sigma\right). \tag{3.31}$$

On each of the sides $\mathscr{T}_x(m+\frac{1}{2},n)$ and $\mathscr{T}_y(m,n+\frac{1}{2})$ the flow velocity is aligned to them and given by $u_x(=\partial\psi/\partial y)$ and $u_y(=-\partial\psi/\partial x)$ respectively. The contributions made by $\boldsymbol{u}_{\mathrm{H}}A$ to the local average of $\boldsymbol{F}_{\mathrm{H}}$ is

$$\frac{1}{\pi^2}\left(\int_{\mathscr{T}_x(m+\frac{1}{2},n)} A(\partial\psi/\partial y)\,\mathrm{d}\Sigma, -\int_{\mathscr{T}_y(m,n+\frac{1}{2})} A(\partial\psi/\partial x)\,\mathrm{d}\Sigma\right), \tag{3.32a}$$

while the local average of $\bar{\boldsymbol{u}}_{\mathrm{H}}\bar{A}$ is

$$(\bar{A}_{m+\frac{1}{2},n}\,\bar{u}_x, \bar{A}_{m,n+\frac{1}{2}}\,\bar{u}_y). \tag{3.32b}$$

Together the results (3.32) yield

$$\bar{F}_x^{\mathrm{loc}}(m+\tfrac{1}{2},n)=\frac{1}{\pi^2}\int_{m\pi}^{(m+1)\pi}\left(\int_{\psi^{\mp\infty}_{m,n-1}}^{\psi^{\pm\infty}_{m,n}} A\,\mathrm{d}\psi\right)\mathrm{d}x-\bar{A}_{m+\frac{1}{2},n}\,\bar{u}_x, \tag{3.33a}$$

$$\bar{F}_y^{\mathrm{loc}}(m,n+\tfrac{1}{2})=\frac{-1}{\pi^2}\int_{n\pi}^{(n+1)\pi}\left(\int_{\psi^{\mp\infty}_{m-1,n}}^{\psi^{\pm\infty}_{m,n}} A\,\mathrm{d}\psi\right)\mathrm{d}y-\bar{A}_{m,n+\frac{1}{2}}\,\bar{u}_y. \tag{3.33b}$$

Here some care is needed over the limits of the ψ-integration. In both (3.33a, b) the upper limit is the value $\psi^{\pm\infty}_{m,n}$ on the curve $\mathscr{C}^{\pm\infty}_{m,n}$ inside the eddy $\mathscr{D}^{\pm}_{m,n}$, while in (3.33a, b) the lower limits are the values $\psi^{\mp\infty}_{m,n-1}, \psi^{\mp\infty}_{m-1,n}$ on the curves $\mathscr{C}^{\mp\infty}_{m,n-1}, \mathscr{C}^{\mp\infty}_{m-1,n}$ inside the neighbouring eddies $\mathscr{D}^{\mp}_{m,n-1}, \mathscr{D}^{\mp}_{m-1,n}$ respectively.

The assertion that $\bar{F}_x^{\mathrm{loc}}$ and $\bar{F}_y^{\mathrm{loc}}$, defined by (3.33), provide local averages hides a further complication, which is that the ψ-integrals diverge as $\pm R^{\frac{1}{2}}\psi_{\pm\infty}$ (see (2.24)) tends to infinity. Specifically, we see from (3.27b) that

$$\int^{\psi^{\pm\infty}_{m,n}} A\,\mathrm{d}\psi \sim \pi F^{\pm\infty}_{m+\frac{1}{2},n+\frac{1}{2}} \quad \text{as} \quad \pm R^{\frac{1}{2}}\psi_{\pm\infty}\to\infty, \tag{3.34a}$$

where

$$\pi F^{\pm\infty}_{m+\frac{1}{2},n+\frac{1}{2}} = \pm\left(\tfrac{1}{2}R^{\frac{1}{2}}\bar{b}[\psi_{\pm\infty}]^2+A_0\,\psi_{\pm\infty}\right)+\bar{A}_{m+\frac{1}{2},n+\frac{1}{2}}(\psi_{\pm\infty}\pm\tfrac{1}{2}\psi^{\mathrm{c}}), \tag{3.34b}$$

and the final constant $\pm\frac{1}{2}\bar{A}_{m+\frac{1}{2},n+\frac{1}{2}}\psi^{\mathrm{c}}$ (see (2.7d)) is included for convenience. The main point here is that we have already established in (3.28) that the eddy contributions to $\int \boldsymbol{u}_{\mathrm{H}}\,A\,\mathrm{d}\Sigma$ vanish. This is reflected in (3.33a), for example, by the fact that, on the eddy $\mathscr{D}^{\pm}_{m,n}$, the contribution to $\bar{F}_x^{\mathrm{loc}}(m+\frac{1}{2},n)$ comes from the upper range of integration

$$\int^{\psi^{\pm\infty}_{m,n}} A\,\mathrm{d}\psi,$$

while the contribution to $\bar{F}_x^{\mathrm{loc}}(m+\frac{1}{2},n+1)$ comes from the lower range of integration

$$\int_{\psi^{\pm\infty}_{m,n}} A\,\mathrm{d}\psi.$$

It is therefore convenient to cancel out these divergent parts, namely $F^{\pm\infty}_{m+\frac{1}{2},n+\frac{1}{2}}$ from $\bar{F}_x^{\mathrm{loc}}(m+\frac{1}{2},n)$ and $-F^{\pm\infty}_{m+\frac{1}{2},n+\frac{1}{2}}$ from $\bar{F}_x^{\mathrm{loc}}(m+\frac{1}{2},n+1)$, before evaluating (3.33). The additional constant included in (3.34b), of course, cancels when the contributions from one eddy boundary are added to the next. We have included it to eliminate any remnant spatial secular features of $\bar{F}_x^{\mathrm{loc}}$, $\bar{F}_y^{\mathrm{loc}}$. Accordingly we define the four finite parts

$$\pm\bar{F}_x^{(0)}_{(2)} = \bar{F}_x^{\mathrm{loc}}(m+\tfrac{1}{2},n)-(F^{\pm\infty}_{m+\frac{1}{2},n+\frac{1}{2}}-F^{\mp\infty}_{m+\frac{1}{2},n-\frac{1}{2}}), \tag{3.35a}$$

$$\mp\bar{F}_y^{(3)}_{(1)} = \bar{F}_y^{\mathrm{loc}}(m,n+\tfrac{1}{2})+(F^{\pm\infty}_{m+\frac{1}{2},n+\frac{1}{2}}-F^{\mp\infty}_{m-\frac{1}{2},n+\frac{1}{2}}), \tag{3.35b}$$

where $\bar{F}_x^0$, $-\bar{F}_y^3$ and $-\bar{F}_x^2$, $\bar{F}_y^1$ correspond to the upper (l even) and lower (l odd) superscripts respectively. Use of the transformation property (3.4b) and noting the channel characteristics (2.37) to (2.41) yields the result

$$\pi\bar{F}_s^i=\frac{1}{\pi}\int_0^{\pi}\left(\int_{\psi^i_{-\infty}}^{\psi^i_{\infty}} A\,\mathrm{d}\psi\right)\mathrm{d}s-\pi(F^i_{\infty}-F^i_{-\infty})-\tfrac{1}{2}(\bar{A}^i_{+}+\bar{A}^i_{-})\,(\Delta\psi^{i+1}), \tag{3.36}$$

in which s is either x or y depending on the value of i. Here we use the notation

$$\bar{A}^i_+ = \bar{A}_{\frac{1}{2},\frac{1}{2}}, \quad F^i_\infty = F^\infty_{\frac{1}{2},\frac{1}{2}} \quad (i = 0, \ldots, 3) \tag{3.37}$$

to define values on the primary $\mathscr{D}^+_{0,0}$-eddy and

$$\bar{A}^i_- = \begin{cases} \bar{A}_{\frac{1}{2},-\frac{1}{2}}, \\ \bar{A}_{\frac{3}{2},\frac{1}{2}}, \\ \bar{A}_{\frac{1}{2},\frac{3}{2}}, \\ \bar{A}_{-\frac{1}{2},\frac{1}{2}}, \end{cases} \qquad F^i_{-\infty} = \begin{cases} F^{-\infty}_{\frac{1}{2},-\frac{1}{2}}, \\ F^{-\infty}_{\frac{3}{2},\frac{1}{2}}, \\ F^{-\infty}_{\frac{1}{2},\frac{3}{2}}, \\ F^{-\infty}_{-\frac{1}{2},\frac{1}{2}}, \end{cases} \qquad i = \begin{cases} 0, & (3.38a) \\ 1, & (3.38b) \\ 2, & (3.38c) \\ 3, & (3.38d) \end{cases}$$

to define values on the neighbouring $\mathscr{D}^-_{m,n}$-eddies. Thus $\bar{F}^i_s$ takes the same value on all sides $\mathscr{T}_x(m+\frac{1}{2}, n), \mathscr{T}_y(m, n+\frac{1}{2})$ to which it refers and, in particular, defines the contribution from the side $\mathscr{T}^i$ of the primary square Π.

Inside the channel regions, A is no longer simply a function of ψ but depends on the distance s along the streamline as well. For the boundary layer formulation of the following sections we find it convenient to introduce the circulation integral

$$\sigma = \int^P \boldsymbol{u}_H \cdot \mathrm{d}\boldsymbol{x} \tag{3.39}$$

(cf. (2.31a) above). The variation of A with respect to σ continues to be relatively small, and we find it convenient to keep the notation

$$R^{\frac{1}{2}} b(\sigma, \psi) = \partial A / \partial \psi \tag{3.40}$$

introduced in (3.23b). Accordingly, an alternative form of (3.36) is obtained by integrating $\int A \, \mathrm{d}\psi$ by parts. It gives, with the help of (2.45) and (2.46),

$$\pi R^{\frac{1}{2}} \bar{F}^i_s = \mathscr{F}^i_{\infty_s} - (\mathscr{F}^i_+ - \mathscr{F}^i_-) + R^{\frac{1}{2}}(A_0 - \tfrac{1}{2}\Delta b^i)\,(\Delta\psi^i), \tag{3.41}$$

where

$$\mathscr{F}^i_{\infty_s} = -R\left\{\frac{1}{\pi}\int_0^\pi \left[\int_{\psi^i_{-\infty}}^{\psi^i_\infty} (\psi - \psi^i)\, b \, \mathrm{d}\psi\right] \mathrm{d}s\right\} + (\mathscr{F}^i_\infty - \mathscr{F}^i_{-\infty}), \tag{3.42a}$$

and

$$\mathscr{F}^i_\pm = \pm \tfrac{1}{2} R \bar{b} [\psi^i_\pm - \psi^i]^2, \tag{3.42b}$$

$$\mathscr{F}^i_{\pm\infty} = \pm \tfrac{1}{2} R \bar{b} [\psi^i_{\pm\infty} - \psi^i]^2 + R^{\frac{1}{2}} (\Delta A_{\pm\infty})\,(\psi^i_{\pm\infty} - \psi^i). \tag{3.42c}$$

The ψ-notation is defined by (2.36) to (2.42). The jumps

$$-\Delta b^i = \bar{A}^i_+ - \bar{A}^i_- \tag{3.43}$$

in $\bar{A}_{m,n}$ between neighbouring eddies are given by

$$\Delta b^1 = -\Delta b^3 = \pi \bar{g}_x (= -\pi \bar{B}_y), \tag{3.44a}$$

$$-\Delta b^0 = \Delta b^2 = \pi \bar{g}_y (= \pi \bar{B}_x). \tag{3.44b}$$

The final remainder term in (3.42c) proportional to $\Delta A_{\pm\infty}$, which denotes the difference between A and its asymptotic value (3.27b) evaluated at $\psi = \psi^i_{\pm\infty}$, vanishes when

$\pm R^{\frac{1}{2}}\psi_{\pm\infty} \to \infty$. Furthermore the term $\mathscr{F}^i_{\infty} - \mathscr{F}^i_{-\infty}$ is included in the definition (3.42*a*) of $\mathscr{F}^i_{\infty_s}$ so that it tends to a well defined limit

$$\mathscr{F}^i_s = \lim_{\pm R^{\frac{1}{2}}\psi_{\pm\infty}\to\infty} (\mathscr{F}^i_{\infty_s}), \tag{3.45}$$

when both $-R^{\frac{1}{2}}\psi_{-\infty}$ and $R^{\frac{1}{2}}\psi_{\infty}$ tend to infinity. Finally, in terms of the finite parts (3.41) we define the mean heat flux by

$$\bar{\boldsymbol{F}}_H = \lim_{\pm R^{\frac{1}{2}}\psi_{\pm\infty}\to\infty} [\tfrac{1}{2}(\bar{F}^0_x - \bar{F}^2_x), \tfrac{1}{2}(\bar{F}^1_y - \bar{F}^3_x)]. \tag{3.46}$$

Its components are

$$\bar{F}_x = \tfrac{1}{2}\pi^{-1}R^{-\frac{1}{2}}(\mathscr{F}^0_x - \mathscr{F}^2_x) - \tfrac{1}{2}R^{\frac{1}{2}}\bar{b}\psi^c\bar{u}_x - A_0\,\bar{u}_y, \tag{3.47a}$$

$$\bar{F}_y = \tfrac{1}{2}\pi^{-1}R^{-\frac{1}{2}}(\mathscr{F}^1_y - \mathscr{F}^3_y) - \tfrac{1}{2}R^{\frac{1}{2}}\bar{b}\psi^c\bar{u}_y + A_0\,\bar{u}_x. \tag{3.47b}$$

We again point out that the value of $\bar{\boldsymbol{F}}_H$ obtained in this way is dependent upon the normalization (3.27*b*). Other normalizations change $\bar{\boldsymbol{F}}_H$ by an amount proportional to $\bar{\boldsymbol{u}}_H$. So, for example, under a suitable normalization the middle terms $-\frac{1}{2}R^{\frac{1}{2}}\bar{b}\psi^c\bar{\boldsymbol{u}}_H$ in (3.47) could be removed. The advantage of the representation (3.41) over (3.36) for $\bar{F}^i_s$ is simply this: by using (3.41) we can largely ignore A in the following analysis and focus attention on the non-secular field b.

3.5. *The magnetic problem*

3.5.1. *The eddy solution*

The solution to the thermal problem resolves the horizontal part of the magnetic field $\boldsymbol{B}_H$. To complete the magnetic problem we must solve the inhomogeneous heat conduction equation (3.12) for the vertical magnetic field KB. Non-zero values of B are stimulated by the source $\boldsymbol{B}_H\cdot\nabla\psi'$ on the right of (3.12*a*). In the mainstream and, in particular, the eddy interiors two approximations can be made. First, as in the thermal problem, the diffusion term $R^{-1}\nabla^2 B$ in (3.12*a*) can be neglected. Secondly, since we have already established that to leading order A is a function of ψ alone (see (3.21)), the term $\boldsymbol{u}_H\cdot\nabla A$ in (3.12*b*) is small and dominated by the remaining term

$$\bar{\boldsymbol{u}}_H\cdot\nabla A = R^{\frac{1}{2}}b\bar{\boldsymbol{u}}_H\cdot\nabla\psi = -R^{\frac{1}{2}}b\boldsymbol{u}_H\cdot\nabla\bar{\psi}. \tag{3.48}$$

Hence to leading order (3.12) reduces to

$$\boldsymbol{u}_H\cdot\nabla\mathscr{B} = 0, \tag{3.49a}$$

where

$$\mathscr{B} = B + R^{\frac{1}{2}}\bar{\psi}b(\psi). \tag{3.49b}$$

As in (3.21) above we deduce that $\mathscr{B}$ is almost constant on streamlines and given to leading order as a function of ψ alone;

$$\mathscr{B} = \mathscr{B}(R^{-\frac{1}{2}}; \psi). \tag{3.50}$$

We proceed as in §3.4.1 to integrate (3.12*a*) over an eddy domain $\mathscr{D}(\psi)$ bounded by the closed streamline $\mathscr{C}(\psi)$. This gives, in place of (3.22), the exact result

$$0 = \int_{\mathscr{D}} \bar{\boldsymbol{u}}_H\cdot\nabla A\,\mathrm{d}\Sigma + R^{-1}\oint_{\mathscr{C}} \boldsymbol{n}\cdot\nabla B\,\mathrm{d}s, \tag{3.51}$$

where we have set all contour integrals about $\mathscr{C}$ involving $\boldsymbol{u}_{\mathrm{H}}\cdot\boldsymbol{n}$ equal to zero. We now may evaluate separately the two integrals in (3.51). Application of the divergence theorem to the first integral yields the identity

$$\int_{\mathscr{D}} \bar{\boldsymbol{u}}_{\mathrm{H}}\cdot\boldsymbol{\nabla}A\,\mathrm{d}\Sigma = -\oint_{\mathscr{C}} \bar{\psi}\boldsymbol{\nabla}A\cdot\mathrm{d}\boldsymbol{x} = -\oint_{\mathscr{C}} q^{-1}\bar{\psi}\boldsymbol{u}_{\mathrm{H}}\cdot\boldsymbol{\nabla}A\,\mathrm{d}s. \tag{3.52a}$$

Here we evaluate $\boldsymbol{u}_{\mathrm{H}}\cdot\boldsymbol{\nabla}A$ from (3.2a) using (3.21) that A is a function of ψ alone. We obtain, with (3.23),

$$\boldsymbol{u}_{\mathrm{H}}\cdot\boldsymbol{\nabla}A = \bar{E}+R^{-\frac{1}{2}}\{q^2(\mathrm{d}b/\mathrm{d}\psi)+(\nabla^2\psi)\,b\}. \tag{3.52b}$$

For the second integral in (3.51) we use the formula (3.49b) and results similar to (3.23). This yields

$$R^{-1}\oint_{\mathscr{C}}\boldsymbol{n}\cdot\boldsymbol{\nabla}B\,\mathrm{d}s = R^{-1}\oint_{\mathscr{C}}\left(-\frac{\mathrm{d}\mathscr{B}}{\mathrm{d}\psi}+R^{\frac{1}{2}}\bar{\psi}\frac{\mathrm{d}b}{\mathrm{d}\psi}\right)q\,\mathrm{d}s - R^{-\frac{1}{2}}\oint_{\mathscr{C}} b(\boldsymbol{\nabla}\bar{\psi})\cdot\boldsymbol{n}\,\mathrm{d}s, \tag{3.53}$$

in which the last integral vanishes because b and $\boldsymbol{\nabla}\bar{\psi}$ are constant on $\mathscr{C}$ and $\oint_{\mathscr{C}}\boldsymbol{n}\,\mathrm{d}s$ is zero. We now form the sum (3.51) from (3.52) and (3.53), and make use of the identities (3.24), to obtain

$$\gamma\frac{\mathrm{d}\mathscr{B}}{\mathrm{d}\psi} = -R\bar{E}\oint_{\mathscr{C}}\frac{\bar{\psi}}{q}\left\{1+\left(\frac{\Sigma}{\gamma}\right)(\nabla^2\psi)\right\}\mathrm{d}s. \tag{3.54}$$

To evaluate (3.54) we note that, when the mean velocity is slow ($\epsilon \ll 1$), motion is dominated by the spatially periodic contribution $\boldsymbol{u}'_{\mathrm{H}}$. To lowest order therefore, q and ψ have the symmetries corresponding to $|\boldsymbol{u}'_{\mathrm{H}}|$ and ψ'. It follows that (3.54) is given to leading order by

$$\gamma\frac{\mathrm{d}\mathscr{B}}{\mathrm{d}\psi} = -R\bar{E}\bar{\psi}_{m+\frac{1}{2},\,n+\frac{1}{2}}\oint_{\mathscr{C}}\frac{1}{q}\left\{1+\left(\frac{\Sigma}{\gamma}\right)(\nabla^2\psi)\right\}\mathrm{d}s, \tag{3.55}$$

where $\bar{\psi}_{m+\frac{1}{2},\,n+\frac{1}{2}}$ is the value of $\bar{\psi}$ at the centre $((m+\frac{1}{2})\,\pi, (n+\frac{1}{2})\,\pi)$ of the $\mathscr{D}^{\pm}_{m,n}$-eddy under consideration. In view of the result (3.25), this equation can be integrated giving

$$\mathscr{B} = R^{\frac{1}{2}}\bar{\psi}_{m+\frac{1}{2},\,n+\frac{1}{2}}\,b(\psi)+B^{\pm}_{m,n}, \tag{3.56a}$$

where $B^{\pm}_{m,n}$ is a constant. With (3.49b) it yields

$$B = -R^{\frac{1}{2}}(\bar{\psi}-\bar{\psi}_{m+\frac{1}{2},\,n+\frac{1}{2}})\,b(\psi)+B^{\pm}_{m,n}. \tag{3.56b}$$

Since B is spatially periodic, all $B^{+}_{m,n}$ and $B^{-}_{m,n}$ separately take the same value. In addition, since B has zero mean, it follows that

$$B^{\pm}_{m,n} = \pm B_0, \tag{3.56c}$$

where B_0 is a constant, which is determined, like A_0 in (3.27a), as part of the complete solution of the problem. Consequently (3.56b) provides the boundary condition for the channel flow, namely

$$B \sim \mp[R^{\frac{1}{2}}(\bar{\psi}-\bar{\psi}_{m+\frac{1}{2},\,n+\frac{1}{2}})\,\bar{b}-B_0] \quad \text{as} \quad R^{\frac{1}{2}}(\psi-\psi^{\pm}_{m,n})\to\infty. \tag{3.57}$$

3.5.2. *The electromotive force*

As in §3.4.2 we consider the contribution to the electromotive force made by the closed surface $\mathscr{D}(\psi)$ inside the eddies. Since, correct to leading order, A and $\mathscr{B}$ are functions of ψ, the formula (3.13) for $K\boldsymbol{E}_{\mathrm{H}}$ reduces to

$$\boldsymbol{E}_{\mathrm{H}} = \mathscr{E}\boldsymbol{\nabla}\psi, \tag{3.58a}$$

where

$$\mathscr{E} = R^{\frac{1}{2}}\psi b - \mathscr{B}. \tag{3.58b}$$

By use of the divergence theorem we thus obtain the result

$$\int_{\mathscr{D}} \boldsymbol{E}_{\mathrm{H}}\,\mathrm{d}\Sigma = \left(\int \mathscr{E}\,\mathrm{d}\psi\right)\oint_{\mathscr{C}} \boldsymbol{n}\,\mathrm{d}s = 0 \tag{3.58c}$$

(cf. (3.28) above). There is, therefore, no contribution to the mean electromotive force at this order from the eddy interiors. We may then proceed as in the case of the mean heat flux calculation to restrict attention to the region exterior to the closed streamlines $\mathscr{C}^{\pm\infty}_{m,n}$.

The boundary layer analysis of §§4 and 5 below show that B continues to have the form (3.49b) and, like A for the thermal problem, has the functional form

$$\mathscr{B}(\sigma,\psi) = B + R^{\frac{1}{2}}\bar{\psi}\bar{b}(\sigma,\psi). \tag{3.59}$$

The important point, however, is that the ψ-derivatives of $\mathscr{B}$ dominate. We can, therefore, define as before the local averages

$$(\bar{E}_x^{\mathrm{loc}}(m,n+\tfrac{1}{2}), \bar{E}_y^{\mathrm{loc}}(m+\tfrac{1}{2},n)) = \frac{1}{\pi^2}\left(\int_{\Pi_{m-\frac{1}{2},n}} E_x\,\mathrm{d}\Sigma, \int_{\Pi_{m,n-\frac{1}{2}}} E_y\,\mathrm{d}\Sigma\right) \tag{3.60}$$

on the sides $\mathscr{T}_y(m,n+\frac{1}{2}), \mathscr{T}_x(m+\frac{1}{2},n)$, where they reduce, as in (3.32), (3.33), to

$$\bar{E}_x^{\mathrm{loc}}(m,n+\tfrac{1}{2}) = \frac{1}{\pi^2}\int_{n\pi}^{(n+1)\pi}\left(\int_{\psi^{\mp\infty}_{m-1,n}}^{\psi^{\pm\infty}_{m,n}} \mathscr{E}\,\mathrm{d}\psi\right)\mathrm{d}y, \tag{3.61a}$$

$$\bar{E}_y^{\mathrm{loc}}(m+\tfrac{1}{2},n) = \frac{1}{\pi^2}\int_{m\pi}^{(m+1)\pi}\left(\int_{\psi^{\mp\infty}_{m,n-1}}^{\psi^{\pm\infty}_{m,n}} \mathscr{E}\,\mathrm{d}\psi\right)\mathrm{d}x. \tag{3.61b}$$

Substitution of (3.26a), (3.56a) into (3.58b) and use of (2.27a) shows that the asymptotic form of the integrands of (3.61) on the $\mathscr{D}^{\pm}_{m,n}$-eddy is

$$\mathscr{E} \sim \pm R^{\frac{1}{2}}[(\psi-\psi^{\pm}_{m,n}) \pm \tfrac{1}{2}\psi^{\mathrm{c}}]\,\bar{b} \mp B_0. \tag{3.62}$$

It follows that

$$\int^{\psi^{\pm\infty}_{m,n}} \mathscr{E}\,\mathrm{d}\psi \sim \pi E^{\pm\infty} \quad \text{as} \quad \pm R^{\frac{1}{2}}\psi_{\pm\infty} \to \infty, \tag{3.63a}$$

where

$$\pi E^{\pm\infty} = \pm\psi_{\pm\infty}\{\tfrac{1}{2}R^{\frac{1}{2}}\bar{b}(\psi_{\pm\infty} \pm \psi^{\mathrm{c}}) - B_0\}, \tag{3.63b}$$

which unlike (3.34) does not increase secularly with m and n. As in the thermal problem, the divergent parts of $\bar{E}_x^{\mathrm{loc}}, \bar{E}_y^{\mathrm{loc}}$ cancel between the opposite sides of eddies and so we define the finite parts

$$\pm\bar{E}_x^{(3)}_{(1)} = \bar{E}_x^{\mathrm{loc}}(m,n+\tfrac{1}{2}) \mp (E^{\infty} - E^{-\infty}), \tag{3.64a}$$

$$\pm\bar{E}_y^{(0)}_{(2)} = \bar{E}_y^{\mathrm{loc}}(m+\tfrac{1}{2},n) \mp (E^{\infty} - E^{-\infty}) \tag{3.64b}$$

similar to (3.35). Use of (3.63b) shows that their values on the four sides $\mathscr{T}^i$ of the primary square are

$$\pi R^{\frac{1}{2}}\bar{E}^i_{\mathrm{s}} = \mathscr{E}^i_{\infty_{\mathrm{s}}} + (\mathscr{E}^i_+ - \mathscr{E}^i_-), \tag{3.65}$$

where

$$\mathscr{E}^i_{\infty_{\mathrm{s}}} = R^{\frac{1}{2}}\left\{\frac{1}{\pi}\int_0^{\pi}\left[\int_{\psi^i_{-\infty}}^{\psi^i_{\infty}} \mathscr{E}\,\mathrm{d}\psi\right]\mathrm{d}s\right\} - (\mathscr{E}^i_{\infty} - \mathscr{E}^i_{-\infty}), \tag{3.66a}$$

and

$$\mathscr{E}^i_{\pm} = \pm R^{\frac{1}{2}}(\psi^i_{\pm} - \psi^i)\,\{\tfrac{1}{2}R^{\frac{1}{2}}\bar{b}[-(\psi^i_{\pm} - \psi^i) \pm \psi^c] - B_0\}, \tag{3.66b}$$

$$\mathscr{E}^i_{\pm\infty} = \pm R^{\frac{1}{2}}(\psi^i_{\pm\infty} - \psi^i)\,\{\tfrac{1}{2}R^{\frac{1}{2}}\bar{b}[(\psi^i_{\pm\infty} - \psi^i) - 2(\psi^i_{\pm} - \psi^i) \pm \psi^c] - B_0\}. \tag{3.66c}$$

Furthermore, since the integrand $\mathscr{E}$ in (3.61) is spatially periodic, the results (3.64) are independent of m and n.

Finally we let

$$\mathscr{E}^i_s = \lim_{\pm R^{\frac{1}{2}}\psi_{\pm\infty}\to\infty} (\mathscr{E}^i_{\infty_s}) \tag{3.67}$$

and define the mean electromotive force

$$\bar{\boldsymbol{E}}_{\mathrm{H}} = \lim_{\pm R^{\frac{1}{2}}\psi_{\pm\infty}\to\infty} [-\tfrac{1}{2}(\bar{E}^1_x - \bar{E}^3_x), \tfrac{1}{2}(\bar{E}^0_y - \bar{E}^2_y)]. \tag{3.68}$$

Use of (2.42)–(2.46) shows that

$$\bar{E}_x = -\tfrac{1}{2}\pi^{-1}R^{-\frac{1}{2}}(\mathscr{E}^1_x - \mathscr{E}^3_x) + B_0\,\bar{u}_x, \tag{3.69a}$$

$$\bar{E}_y = \tfrac{1}{2}\pi^{-1}R^{-\frac{1}{2}}(\mathscr{E}^0_y - \mathscr{E}^2_y) + B_0\,\bar{u}_y. \tag{3.69b}$$

The apparently clumsy formulation of the mean electromotive force in (3.66) is motivated by our development of the boundary layer problem in the following section. There we measure fluid flux from the streamline through the stagnation point at the start of each side $\mathscr{T}^i$ by the use of the coordinate $\psi - \psi^i$ (see also (A 2)). So once solutions of the thermal and magnetic problems are obtained, we proceed to evaluate $\mathscr{F}^i$ and $\mathscr{E}^i$, which are necessary to determine the mean heat flux $\bar{\boldsymbol{F}}_{\mathrm{H}}$ and the mean electromotive force $K\bar{\boldsymbol{E}}_{\mathrm{H}}$ defined by (3.47) and (3.69) respectively. Of course, the final representations, which we have obtained for $\bar{\boldsymbol{F}}_{\mathrm{H}}$ and $\bar{\boldsymbol{E}}_{\mathrm{H}}$, are intended to highlight their similarities and to emphasize the close relationship of the thermal and magnetic problems.

4. The boundary-layer problem

4.1. *The stretched coordinates*

In this section we consider the case

$$\epsilon R^{\frac{1}{2}} = \beta = O(1), \quad R \gg 1, \tag{4.1}$$

for which the total channel and boundary layer widths are comparable. This ordering implies that the mean velocity $\bar{\boldsymbol{u}}_{\mathrm{H}}$ is of order $R^{-\frac{1}{2}}$ and we therefore define

$$\pi^{-1}\boldsymbol{\eta}_{\mathrm{H}} = R^{\frac{1}{2}}\bar{\boldsymbol{u}}_{\mathrm{H}} \quad (\beta = \pi^{-1}|\boldsymbol{\eta}_{\mathrm{H}}|), \tag{4.2}$$

where $|\boldsymbol{\eta}_{\mathrm{H}}|$ is of order unity. In the channel region ψ is small of order $R^{-\frac{1}{2}}$ and so we introduce the stretched stream function

$$\zeta = R^{\frac{1}{2}}\psi, \tag{4.3}$$

and define

$$\bar{\zeta} = \pi^{-1}(y\eta_x - x\eta_y). \tag{4.4}$$

In the case of mean flows with rational tangents, we write

$$\boldsymbol{\eta}_{\mathrm{H}} = (\Delta\zeta)\,(M, N), \tag{4.5a}$$

where M, N are relatively prime integers and

$$\pi^{-1}(\Delta\zeta) = \beta(M^2+N^2)^{-\frac{1}{2}} \tag{4.5b}$$

(see (2.10) and (4.1)). The channel boundaries (2.30) are then

$$C_k : \zeta = \zeta_k = k(\Delta\zeta) \tag{4.6}$$

for integer values of k.

As we have explained in §3, it is sufficient to consider the four sides $\mathscr{T}^i$ of the primary square Π. The value of ζ at each of the X-type stagnation points O^i at the beginning of each side is

$$\zeta^i = R^{\frac{1}{2}}\psi^i \quad (\bar{\zeta} = \zeta^i \text{ at } \mathrm{O}^i). \tag{4.7a}$$

In the case of flows with rational tangents, the streamline through O^i is

$$C^i : \zeta = \zeta^i = k^i(\Delta\zeta), \tag{4.7b}$$

where the values of k^i are given by (2.36). On the side $\mathscr{T}^i$ we take O^i as the origin and introduce and stretched streamfunction

$$\xi = \zeta - \zeta^i \equiv R^{\frac{1}{2}}(\psi - \psi^i). \tag{4.8}$$

The other coordinate, namely the circulation integral σ (see (3.39)) is also measured from O^i, where it vanishes. It increases to 2 (see (2.31b)) at the next X-type stagnation point O^{i+1} at the end of the side. In terms of our new σ, ξ-coordinates each side $\mathscr{T}^i$ of the primary square Π is defined by

$$\mathscr{T}^i : 0 \leqslant \sigma \leqslant 2, \quad -\infty < \xi < \infty. \tag{4.9}$$

The side begins and ends at

$$\mathrm{O}^i : (0, 0), \quad \mathrm{O}^{i+1} : (2, \Delta\zeta^i) \tag{4.10a}$$

respectively, where

$$\zeta^{i+1} - \zeta^i = \Delta\zeta^i \equiv R^{\frac{1}{2}}(\Delta\psi^i) \tag{4.10b}$$

as in (2.43).

On each side $\mathscr{T}^i$, the ξ-coordinate of the $\mathscr{C}^{\pm}_{m,n}$-eddy boundary is

$$\xi^i_{\pm} = \zeta^i_{\pm} - \zeta^i \equiv R^{\frac{1}{2}}(\psi^i_{\pm} - \psi^i), \tag{4.11a}$$

where, from (2.36), (2.38) and (2.39),

$$\xi^0_+ = \eta_x, \qquad \xi^1_+ = \eta_x + \eta_y, \quad \xi^2_+ = \eta_y, \quad \xi^3_+ = 0, \tag{4.11b}$$

$$\xi^0_- = -\eta_x - \eta_y, \quad \xi^1_- = -\eta_y, \qquad \xi^2_- = 0, \quad \xi^3_- = -\eta_x. \tag{4.11c}$$

For completeness we note from (4.10*b*) and (2.42) that

$$\Delta\zeta^0 = -\eta_y, \quad \Delta\zeta^1 = \eta_x, \quad \Delta\zeta^2 = \eta_y, \quad \Delta\zeta^3 = -\eta_x. \tag{4.12}$$

The quantities $\xi^i_\pm$ and $\Delta\zeta^i$ satisfy several simple relations some already listed in (2.41)–(2.46). We collect together here the following:

$$\xi^i_+ + \xi^i_- = \Delta\zeta^i, \quad \xi^i_+ + \xi^{i-1}_- = 0, \tag{4.13a, b}$$

$$\xi^{i+1}_\pm + \xi^{i-1}_\pm = \pm\zeta^{\mathrm{c}} = 2\xi^i_\pm - (\Delta\zeta^i + \Delta\zeta^{i\pm1}), \tag{4.13c}$$

$$\zeta^{i+1} + \zeta^{i-1} = \zeta^\beta, \quad \Delta\zeta^{i+1} + \Delta\zeta^{i-1} = 0, \tag{4.13d, e}$$

where

$$\zeta^{\mathrm{c}} = \eta_x + \eta_y \equiv R^{\frac{1}{2}}\psi^{\mathrm{c}}, \quad \zeta^\beta = \eta_x - \eta_y \equiv R^{\frac{1}{2}}\psi^\beta. \tag{4.13f}$$

The closed streamlines $\mathscr{C}^{\pm\infty}_{m,n}$ in the interior of these $\mathscr{D}^\pm_{m,n}$-eddies have the coordinates

$$\xi^i_{\pm\infty} = \zeta^i_{\pm\infty} - \zeta^i \equiv R^{\frac{1}{2}}(\psi^i_{\pm\infty} - \psi^i), \tag{4.14a}$$

where

$$\zeta_{\pm\infty} = \zeta^i_{\pm\infty} - \zeta^i_\pm \equiv R^{\frac{1}{2}}\psi_{\pm\infty}. \tag{4.14b}$$

The flow at the end of the side $\mathscr{T}^i$ is divided by the stagnation point O^{i+1}. The flow on the primary $\mathscr{D}^+_{0,0}$-eddy side continues to the start of the next side $\mathscr{T}^{i+1}$ but the flow on the other $\mathscr{D}^-_{m,n}$-eddy side is mapped by the transformation (2.20) to the start of the side $\mathscr{T}^{i-1}$. If we consider only the flow in the channel regions up to the closed streamlines $\mathscr{C}^{\pm\infty}_{m,n}$, the mapping is

$$\sigma = 2 \quad \text{on} \quad \mathscr{T}^i \begin{Bmatrix} \xi^i_\infty > \xi > \Delta\zeta^i \\ \Delta\zeta^i > \xi > \xi^i_{-\infty} \end{Bmatrix} \quad \text{to} \quad \sigma = 0 \quad \text{on} \quad \begin{Bmatrix} \mathscr{T}^{i+1}: \zeta^{i+1}_\infty > \xi > 0 \\ \mathscr{T}^{i-1}: 0 > \xi > \xi^{i-1}_{-\infty} \end{Bmatrix} \tag{4.15}$$

(see also (A 2)), which is indicated schematically on figure 8. It is perhaps worth noting at this point that the mapping from the end $\sigma = 2$ of two opposite sides $\mathscr{T}^i, \mathscr{T}^{i+2}$ together map one to one on to the start of the pair of opposite sides $\mathscr{T}^{i-1}, \mathscr{T}^{i+1}$. The total ξ-range involved in the mapping is

$$(\xi^{i+1}_\infty - \xi^{i+1}_{-\infty}) + (\xi^{i-1}_\infty - \xi^{i-1}_{-\infty}) = 2[\zeta^{\mathrm{c}} + (\zeta_\infty - \zeta_{-\infty})], \tag{4.16}$$

independent of the value of i; a result established from (4.13), (4.14).

4.2. *The thermal problem*

4.2.1. *The solution of the heat conduction equation*

For our slow mean flows with ϵ of order $R^{-\frac{1}{2}}$ the heat source $\bar{E}$ given by (3.2*c*) is itself small and given by

$$R^{\frac{1}{2}}\bar{E} = \pi^{-1}(\boldsymbol{\eta}_{\mathrm{H}} \cdot \bar{\boldsymbol{g}}_{\mathrm{H}}) = -\pi^{-1}(\boldsymbol{\eta}_{\mathrm{H}} \times \bar{\boldsymbol{B}}_{\mathrm{H}})_z. \tag{4.17}$$

To leading order it is negligible in the heat conduction equation (3.2*b*), which in terms of the boundary layer coordinates σ, ξ (see (3.39) and (4.3)), reduces to

$$\partial A/\partial\sigma = \partial b/\partial\xi \quad (b = \partial A/\partial\zeta) \tag{4.18}$$

as in paper 2. On each side $\mathscr{T}^i$ of the primary square Π, we set

$$A(\sigma, \zeta) = A^i(\sigma, \xi), \quad b(\sigma, \zeta) = b^i(\sigma, \xi), \tag{4.19}$$

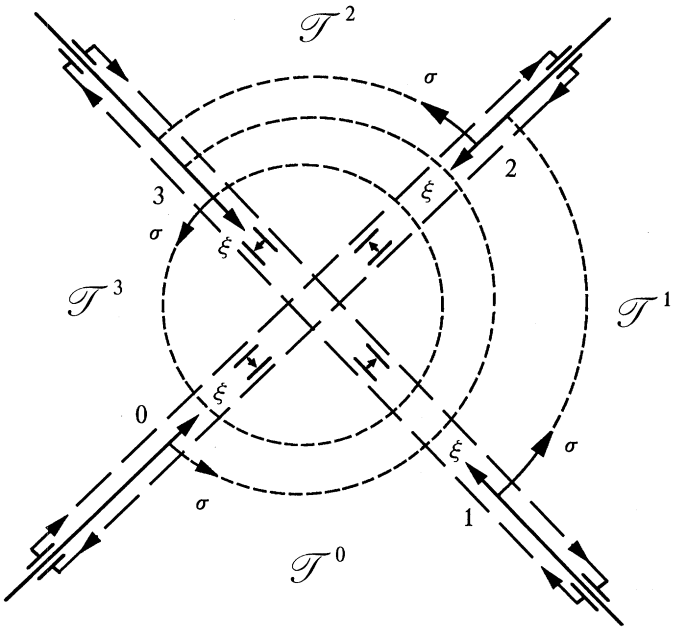

FIGURE 8. Symbolic diagram showing σ, ξ-axes for each side $\mathscr{T}^i$, $i = 0, 1, 2, 3$, of the primary eddy Π. The symbol $|\!\rightarrow\!|$ indicates that data arriving from $\mathscr{T}^{i-1}$, provides initial data for the next side $\mathscr{T}^i$ for $\xi > 0$. The diagonal connections $\ulcorner\!\!\urcorner$ indicate that data arriving from $\mathscr{T}^{i+1}$, provides initial data for the previous side $\mathscr{T}^i$ for $\xi < 0$.

where ξ is the shifted coordinate (4.8). According to (3.27b), (3.37), (3.38) and (3.43) each solution A^i satisfies the boundary conditions

$$A^i - \bar{A}_{\frac{1}{2},\frac{1}{2}} \to \begin{cases} \bar{b}(\xi - \xi^i_+) + A_0 & \text{as} \quad \xi \uparrow \infty, \quad (4.20a) \\ -\bar{b}(\xi - \xi^i_-) - A_0 + \Delta b^i & \text{as} \quad \xi \downarrow \infty, \quad (4.20b) \end{cases}$$

where, by (3.26b) and (4.17),

$$\bar{b} = \tfrac{1}{8}\pi(\boldsymbol{\eta}_{\mathrm{H}} \cdot \bar{\boldsymbol{g}}_{\mathrm{H}}) = -\tfrac{1}{8}\pi(\boldsymbol{\eta}_{\mathrm{H}} \times \bar{\boldsymbol{B}}_{\mathrm{H}})_z. \quad (4.21)$$

At each of the X-type stagnation points diffusion is negligible and A passes unaltered from the end of one side to the start of another. According to the mapping (4.15) and the transformation property (3.4), the value of A^i at the beginning ($\sigma = 0$) of the side $\mathscr{T}^i$ is related to the values of $A^{i\pm1}$ at the end ($\sigma = 2$) of the sides $\mathscr{T}^{i\pm1}$ by

$$A^i(0, \xi) = \begin{cases} A^{i-1}(2, \xi + \Delta\zeta^{i-1}) & (\xi > 0), \quad (4.22a) \\ A^{i+1}(2, \xi + \Delta\zeta^{i+1}) - \Delta b^{i+1} + \Delta b^i & (\xi < 0), \quad (4.22b) \end{cases}$$

where Δb^i is given by (3.44). If, on the other hand, we consider the derivatives b^i instead they are linked by

$$b^i(0, \xi) = Q^i \delta(\xi) + b^{i\mp1}(2, \xi + \Delta\zeta^{i\mp1}) \quad (\pm\xi > 0), \quad (4.23a)$$

where the δ-function source proportional to

$$Q^i = A^{i-1}(2, \Delta\zeta^{i-1}) - A^{i+1}(2, \Delta\zeta^{i+1}) + \Delta b^{i+1} - \Delta b^i \quad (4.23b)$$

is determined by the jump in the value of $A^i(0, \xi)$ across $\xi = 0$.

The solutions of the heat conduction equation (4.18), which we construct, involve the elementary (similarity) solutions

$$G_0(\sigma,\xi) = \tfrac{1}{2}(\partial G_1/\partial\xi) = (4\pi\sigma)^{-\frac{1}{2}}\mathrm{e}^{-\xi^2/4\sigma}, \tag{4.24a}$$

$$G_1(\sigma,\xi) = (\partial G_2/\partial\xi) = \mathrm{Erf}\,(\xi/\sqrt{4\sigma}), \tag{4.24b}$$

$$G_2(\sigma,\xi) = \xi\,\mathrm{Erf}\,(\xi/\sqrt{4\sigma}) + (4\sigma/\pi)^{\frac{1}{2}}\mathrm{e}^{-\xi^2/4\sigma}, \tag{4.24c}$$

which satisfies the initial conditions

$$G_0(0,\xi) = \delta(\xi), \quad G_1(0,\xi) = \mathrm{sgn}\,\xi, \quad G_2(0,\xi) = |\xi|. \tag{4.25}$$

The expressions (4.25) also give the asymptotic behaviour of G_0, G_1, G_2 as $\xi\to\pm\infty$. To accommodate the boundary conditions (4.20) we seek solutions of (4.18) in the form

$$b^i(\sigma,\xi) = \hat{b}^i + \tilde{b}^i, \tag{4.26a}$$

where

$$\hat{b}^i(\sigma,\xi) = \bar{b}G_1. \tag{4.26b}$$

The remaining part $\tilde{b}^i$ satisfies the heat conduction equation (4.18). Integration of (4.26a) with respect to ξ shows that the boundary conditions (4.20) are met when

$$\tilde{b}^i(\sigma,\xi)\to 0 \quad \text{as} \quad \xi\to\pm\infty \tag{4.27}$$

and, with the use of (4.13a),

$$\tilde{I}^i \equiv \int_{-\infty}^{\infty}\tilde{b}^i(\sigma,\xi)\,\mathrm{d}\xi = -\bar{b}(\Delta\zeta^i) - \Delta b^i + 2A_0. \tag{4.28a}$$

In view of (4.13e) and (3.44) these integrals have the property

$$\tilde{I}^{i+1} + \tilde{I}^{i-1} = 4A_0. \tag{4.28b}$$

The mathematical problem for $\tilde{b}^i$ is completed by linking the end values $\tilde{b}^i(2,\xi)$ with the start values $\tilde{b}^i(0,\xi)$. By (4.23) and (4.26) we have

$$\tilde{b}^i(0,\xi) = Q^i\delta(\xi) + \tilde{b}^i_{\mathrm{reg}}(0,\xi), \tag{4.29a}$$

where

$$\tilde{b}^i_{\mathrm{reg}}(0,\xi) = \tilde{b}^{i\mp1}(2,\xi+\Delta\zeta^{i\mp1}) + \bar{b}G_1^{\pm}(\xi+\Delta\zeta^{i\mp1}) \quad (\pm\xi>0) \tag{4.29b}$$

is the regular part and

$$G_1^{\pm}(\xi) = G_1(2,\xi)\mp 1. \tag{4.29c}$$

To determine Q^i we integrate (4.29a) over the complete range $-\infty<\xi<\infty$. The contribution from the last term in (4.29b) proportional to $\bar{b}$ vanishes because of the symmetry

$$G_1^-(-\xi+\Delta\zeta^{i+1}) = -G_1^+(\xi+\Delta\zeta^{i-1})$$

and we are left with

$$Q^i = \tilde{I}^i - (\tilde{I}^{i-1}_+ + \tilde{I}^{i+1}_-), \tag{4.30a}$$

where

$$\tilde{I}^i_+ = \int_{\Delta\zeta^i}^{\infty}\tilde{b}^i(2,\xi)\,\mathrm{d}\xi, \quad \tilde{I}^i_- = \int_{-\infty}^{\Delta\zeta^i}\tilde{b}^i(2,\xi)\,\mathrm{d}\xi \tag{4.30b}$$

and
$$\tilde{I}^i_+ + \tilde{I}^i_- = \tilde{I}^i. \tag{4.30c}$$

It is a simple matter to establish from these definitions that
$$Q^{i+1} + Q^{i-1} = 0. \tag{4.30d}$$

Of greater relevance to the numerical solution is the fact that by use of (4.28) the value of Q^i in (4.30a) can be expressed, like $b^i_{\text{reg}}(0,\xi)$, entirely in terms of results from the sides $\mathscr{T}^{i\pm1}$ alone. There results
$$Q^i = -\bar{b}(\Delta\zeta^i) - \Delta b^i + \tfrac{1}{2}\{(\tilde{I}^{i+1}_+ - \tilde{I}^{i+1}_-) - (\tilde{I}^{i-1}_+ - \tilde{I}^{i-1}_-)\}. \tag{4.31}$$

Finally the Greens function solution on each side $\mathscr{T}^i$ is
$$\tilde{b}^i(\sigma,\xi) = Q^i G_0(\sigma,\xi) + \int_{-\infty}^{\infty} G_0(\sigma,\xi-\xi')\,\tilde{b}^i_{\text{reg}}(0,\xi')\,\mathrm{d}\xi'. \tag{4.32}$$

When $\sigma = 2$ it links again the start values $\tilde{b}^i(0,\xi)$ with the end values $\tilde{b}^i(2,\xi)$.

The essential idea behind the numerical solution is to specify an initial guess of $\tilde{b}^0(2,\xi)$ and $\tilde{b}^2(2,\xi)$. By (4.31), these values define $Q^1(=-Q^3$, see (4.30d)) and then with (4.29) they set up initial data on $\mathscr{T}^1$ and $\mathscr{T}^3$. The terminal values $\tilde{b}^1(2,\xi)$ and $\tilde{b}^3(2,\xi)$ then follow from (4.32). Again by (4.31), they define $Q^0(=-Q^2)$ and then with (4.29) they set up initial data on $\mathscr{T}^0$ and $\mathscr{T}^2$. The terminal values $\tilde{b}^0(2,\xi)$ and $\tilde{b}^2(2,\xi)$ then follow from (4.32). The numerical integrations are based on the values of $\tilde{b}^i_{\text{reg}}(0,\xi)$ being defined on points $\xi = j\,(\Delta\zeta_{\text{num}})$ ($j=$ integer). The end values $\tilde{b}^i(2,\xi)$ are evaluated at $\xi = j(\Delta\zeta_{\text{num}}) + \Delta\zeta^i$. Of course, for the numerical integrations the range of definition of $\tilde{b}^i_{\text{reg}}(0,\xi)$ is limited to $\xi^i_{-\infty} \leqslant \xi \leqslant \xi^i_{\infty}$ (see (4.15)) as are the integrals (cf. (3.42a) and (3.66a)). This means that our total range on each pair of sides $\mathscr{T}^{i+1}$ and $\mathscr{T}^{i-1}$ is $2[\zeta^c + (\zeta_\infty - \zeta_{-\infty})]$ (see (4.16)). In fact, we choose $\pm\zeta_{\pm\infty} = 16$. A Fortran NAG-library equation solver routine was used to find that initial set of $\tilde{b}^0(2, j(\Delta\xi_{\text{num}}) + \Delta\zeta^0)$ and $\tilde{b}^2(2, j(\Delta\zeta_{\text{num}}) + \Delta\zeta^2)$, which yielded the same set of values after processing by the operations described above. The results were used to set up the integrals $\tilde{I}^i$. For each value of i, $\tilde{I}^i$ defines by (4.28a) a value of A_0. Since all values so obtained should be the same, this provides a useful check of our numerical procedures.

Numerical solutions were obtained for flows with rational tangents (see (4.5)) and the results are illustrated in figures 9 and 10 for the cases listed in table 1. Those shown in figure 9 are for
$$\bar{\boldsymbol{g}}_{\text{H}} = (\Delta B)\,(-N, M), \quad \bar{\boldsymbol{B}}_{\text{H}} = (\Delta B)\,(M, N), \tag{4.33a, b}$$

TABLE 1. CHANNEL DATA USED FOR NUMERICAL INTEGRATIONS IN FIGURES 9–12

(Each of the data corresponds to the cases a, b, c and d shown on each set of figures. In the last row the values of above and below Δ_k and $\Delta\zeta_{\text{ch}}$ listed correspond to the short (k odd) and the long (k even) channels D_k respectively.)

(M,N)	$\Delta\zeta$	(η_x,η_y)	β	L	Λ	Δ_k	$\Delta\zeta_{\text{ed}}$	$\Delta\zeta_{\text{ch}}$	$\Delta\zeta_{\text{num}}$	$\pm\eta_{\pm\infty}$	ΔB
O-flows, L-odd											
$(0,1)$	24	$(0,24)$	7.64	1	1	1	5.01	5.01	0.5	16.0	1.0
$(1,2)$	24	$(24,48)$	17.08	3	1	1	5.01	8.68	1.0	16.0	1.0
$(1,6)$	13.26	$(13,80)$	25.68	7	1	1	5.01	13.26	1.105	16.0	1.0
E-flows, L-even											
						0.5		3.55			
$(1,1)$	24	$(24,24)$	10.80	2	0.75	1.5	5.01	6.14	0.75	16.0	1.0

PHILOSOPHICAL TRANSACTIONS OF THE ROYAL SOCIETY A MATHEMATICAL, PHYSICAL & ENGINEERING SCIENCES

which in the case of the magnetic problem corresponds to a mean magnetic field of magnitude

$$B_{\parallel} = (M^2 + N^2)^{\frac{1}{2}}(\Delta B) \tag{4.33c}$$

parallel to the mean motion. The asymptotic results of §5.2.2 below valid for large β (see (3.18)) expressed in terms of our boundary layer variables yield the channel and eddy solution

$$b = \begin{cases} \Delta_{k+1}\beta^{-1}B_{\parallel} & \text{on} \quad D_k, \qquad (4.34a) \\ 0 & \text{on} \quad \mathscr{D}^{\pm}_{m,n} \qquad (4.34b) \end{cases}$$

(see (5.21)) with

$$A_0 = \tfrac{1}{2}\Lambda\beta^{-1}B_{\parallel}\zeta^c \quad (\zeta^c = L(\Delta\zeta)) \tag{4.34c}$$

(see (5.22)), where, by (4.5a) and (4.33b),

$$\beta^{-1}B_{\parallel} = \pi(\boldsymbol{\eta}_{\mathrm{H}}\cdot\bar{\boldsymbol{B}}_{\mathrm{H}})/|\boldsymbol{\eta}_{\mathrm{H}}|^2 = \pi(\Delta B)/(\Delta\zeta), \tag{4.34d}$$

and the constants Δ_k and Λ are defined by (2.49) and (2.51) above. The values of the eddy constant A_0 given by (4.34c) are compared in table 2 with the computed values obtained from the numerical integrations of the boundary layer problem. They differ by about 10%. Similar differences occur with the channel values of b given by (4.34a) and the corresponding channel values for the full numerical integration illustrated in figure 9. The discrepancy occurs because of boundary layer corrections not included in (4.34). These are discussed in §6 below.

TABLE 2. PARALLEL FIELDS WITH CHANNEL DATA GIVEN IN TABLE 1, WHERE $\beta^{-1}B_{\parallel} = \pi(\Delta B)/(\Delta\zeta)$ (SEE (4.34d))

(The values of the two quantities proportional to Δ_{k+1} for L-even are partitioned as in table 1.)

$(\bar{B}_x, \bar{B}_y)$ (M, N)	$\Delta_{k+1}\beta^{-1}B_{\parallel}$	$\Delta_{k+1}\beta^{-1}B_{\parallel}(\Delta\zeta)$	$\frac{1}{2}\Lambda\beta^{-1}B_{\parallel}\zeta^c$	numerical A_0
L-odd				
(0, 1)	0.131	3.142	1.571	1.421
(1, 2)	0.131	3.142	4.713	4.422
(1, 6)	0.237	3.142	11.00	10.246
L-even				
(1, 1)	0.196 0.065	4.731 1.571	2.357	2.251

The results shown in figure 10 are for

$$\bar{\boldsymbol{g}}_{\mathrm{H}} = (\Delta B)(-M, -N), \quad \bar{\boldsymbol{B}}_{\mathrm{H}} = (\Delta B)(-N, M), \tag{4.35a, b}$$

which in the case of the magnetic problem corresponds to a mean magnetic field of magnitude

$$B_{\perp} = (M^2 + N^2)^{\frac{1}{2}}(\Delta B) \tag{4.35c}$$

perpendicular to the mean motion. The asymptotic results of §5.2.3 below for large β yield the channel and eddy solutions

$$b = \begin{cases} \left(\dfrac{2\bar{b}}{L\Delta_k}\right)\left(\dfrac{\zeta - \zeta_{k+\frac{1}{2}}}{\Delta\zeta}\right) & \text{on} \quad D_k, \qquad (4.36a) \\ \pm\bar{b} & \text{on} \quad \mathscr{D}^{\pm}_{m,n} \qquad (4.36b) \end{cases}$$

(see (5.32)), where $\zeta_{k+\frac{1}{2}}(=(k+\frac{1}{2})(\Delta\zeta)$, see (4.6)) defines the streamline in the middle of the channel D_k and, by (4.5a), (4.21) and (4.35b),

$$\bar{b} = -\tfrac{1}{8}\pi(M^2+N^2)(\Delta\zeta)(\Delta B). \tag{4.36c}$$

The numerical values of $-\bar{b}$ and the multiplicative factor $1/L\Delta_k$ in (4.36a) used to sketch the asymptotic solutions shown in figure 10 are listed in table 3. The numerical results show good agreement with the asymptotic formulas.

4.2.2. *The mean heat flux*

The determination of the mean heat flux $\bar{F}_{\mathrm{H}}$ from the formula (3.47) depends on the values of the functions $\mathscr{F}^i_{\mathrm{s}}$ defined by (3.45). In terms of our boundary layer coordinates the functions $\mathscr{F}^i_{\infty_{\mathrm{s}}}$ (see (3.42)), which define them, are

$$\mathscr{F}^i_{\infty_{\mathrm{s}}} = \hat{\mathscr{F}}^i_{\infty_{\mathrm{s}}} + \tilde{\mathscr{F}}^i_{\infty_{\mathrm{s}}}, \tag{4.37a}$$

where, ignoring the remainder term proportional to $\Delta A_{\pm\infty}$, which vanish as $\pm\zeta_{\pm\infty}\to\infty$,

$$\hat{\mathscr{F}}^i_{\infty_{\mathrm{s}}} = \frac{-1}{\pi}\int_0^{\pi}\left[\int_{\xi^i_{-\infty}}^{\xi^i_{\infty}} \xi\hat{b}^i\,\mathrm{d}\xi\right]\mathrm{d}s + \tfrac{1}{2}\bar{b}\{[\xi_{\infty}]^2+[\xi_{-\infty}]^2\}, \tag{4.37b}$$

$$\tilde{\mathscr{F}}^i_{\infty_{\mathrm{s}}} = \frac{-1}{\pi}\int_0^{\pi}\left[\int_{\xi^i_{-\infty}}^{\xi^i} \xi\tilde{b}^i\,\mathrm{d}\xi\right]\mathrm{d}s, \tag{4.37c}$$

(see (4.26a)). The integral of ξG_1 in (4.37b) (see (4.26b)) is evaluated using (4.24) and gives

$$\hat{\mathscr{F}}^i_{\infty_{\mathrm{s}}} = \frac{-\bar{b}}{\pi}\int_0^{\pi}[\tfrac{1}{2}\xi(G_2(\sigma,\xi)-|\xi|)-\sigma G_1(\sigma,\xi)]^{\xi^i_{\infty}}_{\xi^i_{-\infty}}\,\mathrm{d}s. \tag{4.38}$$

In view of the asymptotic results (4.25) only the term proportional to σ remains as $\pm\xi^i_{\pm\infty}\to\infty$. It yields the limit

$$\hat{\mathscr{F}}^i_{\mathrm{s}} = 2\bar{b} + \frac{2\bar{b}}{\pi}\int_0^{\pi}(\sigma-1)\,\mathrm{d}s = 2\bar{b}. \tag{4.39a}$$

Since $\sigma-1$ is antisymmetric about the midpoint $s=\frac{1}{2}\pi$ of each side $\mathscr{T}^i$. In the same limit, it is readily established from the heat conduction equation that

$$\int_{-\infty}^{\infty}\xi\tilde{b}^i\,\mathrm{d}\xi$$

is constant on each side $\mathscr{T}^i$ independent of σ. Hence (4.37c) yields the limit

$$\tilde{\mathscr{F}}^i_{\mathrm{s}} = -\int_{-\infty}^{\infty}\xi\tilde{b}^i\,\mathrm{d}\xi, \tag{4.39b}$$

which we find convenient to evaluate from the numerical results at the end $\sigma=2$ of each side $\mathscr{T}^i$. Substitution of (4.39) into (3.47) gives the formula

$$\pi R^{\frac{1}{2}}\bar{F}_x = \tfrac{1}{2}(\mathscr{F}^0_x-\mathscr{F}^2_x) - \tfrac{1}{2}\bar{b}\zeta^{\mathrm{c}}\eta_x - A_0\eta_y, \tag{4.40a}$$

$$\pi R^{\frac{1}{2}}\bar{F}_y = \tfrac{1}{2}(\mathscr{F}^1_y-\mathscr{F}^3_y) - \tfrac{1}{2}\bar{b}\zeta^{\mathrm{c}}\eta_y + A_0\eta_x, \tag{4.40b}$$

where

$$\mathscr{F}^i_{\mathrm{s}} = \hat{\mathscr{F}}^i_{\mathrm{s}} + \tilde{\mathscr{F}}^i_{\mathrm{s}}. \tag{4.40c}$$

PHILOSOPHICAL TRANSACTIONS OF THE ROYAL SOCIETY A MATHEMATICAL, PHYSICAL & ENGINEERING SCIENCES

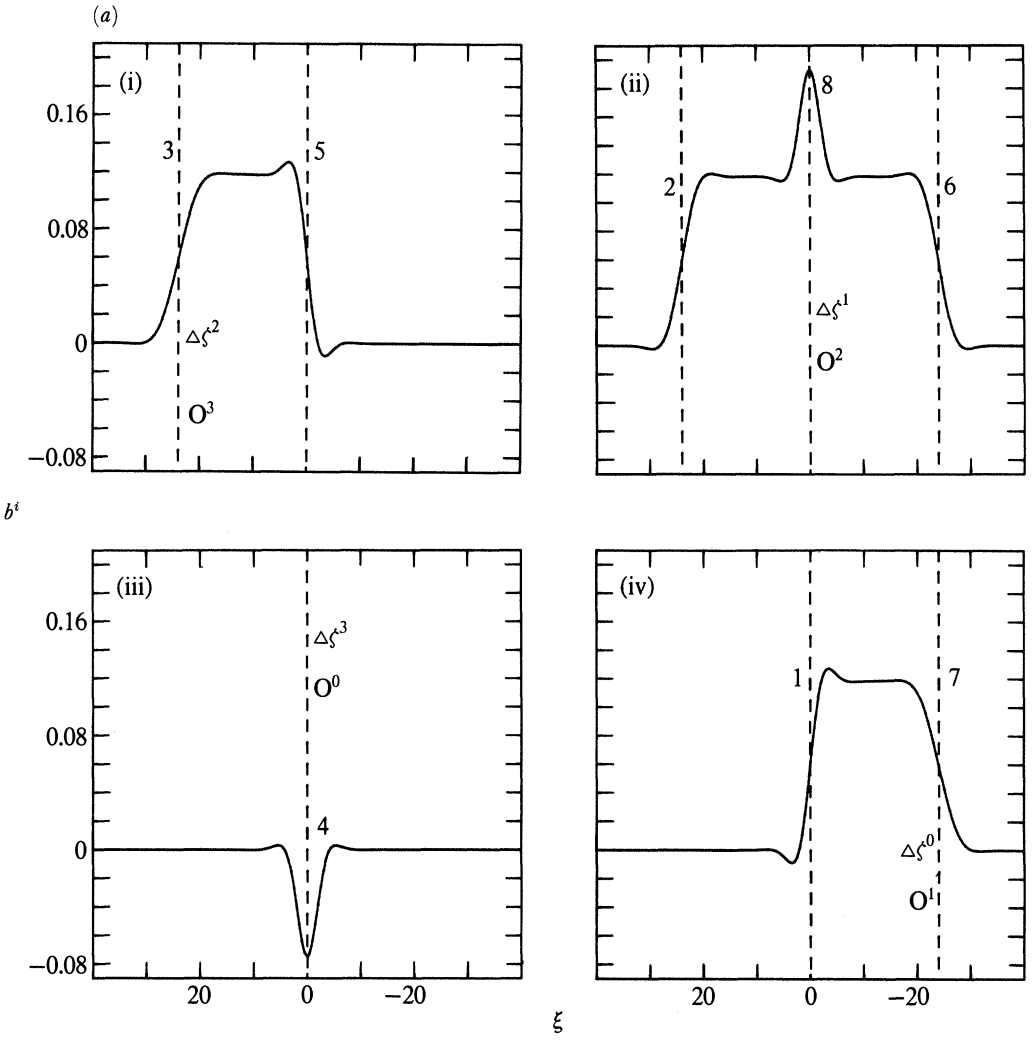

FIGURE 9. For description see page 693.

To determine the diffusion-matrix $\boldsymbol{D}$ defined by (3.6), it is sufficient to calculate $\bar{\boldsymbol{F}}_{\mathrm{H}}$ for the two cases of parallel and perpendicular mean magnetic fields (4.33) and (4.35) respectively. In general, this matrix has few simple properties. Nevertheless, in the case rapid mean flows $\bar{\boldsymbol{u}}_{\mathrm{H}} = \epsilon\hat{\boldsymbol{u}}_{\mathrm{H}}$ with rational tangents,

$$\beta \gg L^{\frac{1}{2}}(M^2+N^2)^{\frac{1}{2}} \tag{4.41}$$

(see (3.18)), the analysis of §5.2 below shows that the diffusion-matrix has the asymptotic form

$$\boldsymbol{D} = D_0\,\hat{\boldsymbol{u}}_{\mathrm{H}}\,\hat{\boldsymbol{u}}_{\mathrm{H}}, \tag{4.42a}$$

where, from (3.6) and (5.37),

$$\epsilon^{-3}R^{-1}D_0 = \pi^3/48\Lambda L(M^2+N^2)^{\frac{1}{2}}. \tag{4.42b}$$

Since Λ is of order unity (see (2.51)), the quantity $\epsilon^{-3}R^{-1}D_0$ tends to zero in the irrational limit and we are no longer necessarily left with the asymptotic form (4.42a). To test the asymptotic result (4.42) for rational tangents, we consider the case of perpendicular mean magnetic fields

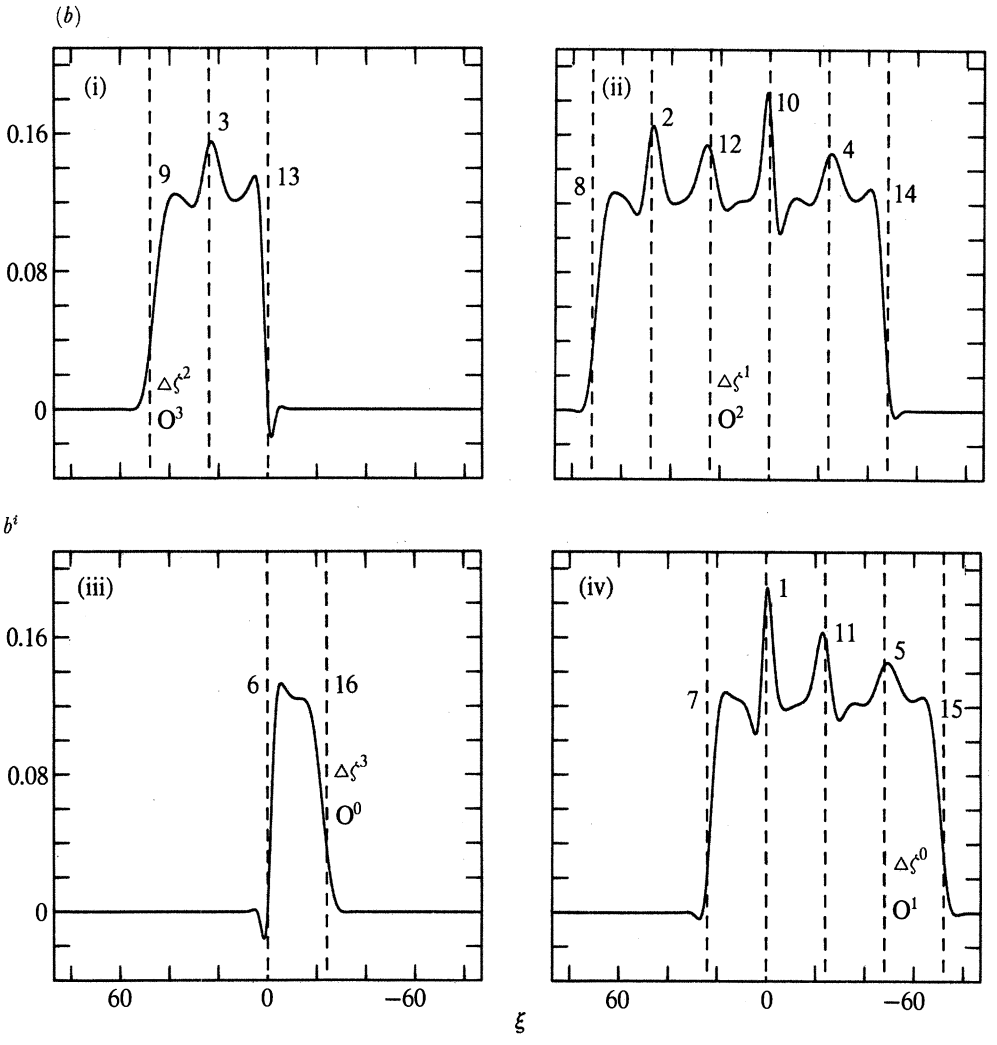

FIGURE 9. For description see page 693.

(4.35), for which the mean temperature gradient $\bar{\boldsymbol{g}}_{\mathrm{H}}$ is aligned with the mean motion, and use the results of the numerical integrations to evaluate

$$\tilde{D}^{\mathrm{num}} = -\beta^{-3}(R^{\frac{1}{3}}\bar{\boldsymbol{F}}_{\mathrm{H}}\cdot\bar{\boldsymbol{g}}_{\mathrm{H}}/|\bar{\boldsymbol{g}}_{\mathrm{H}}|^2) \quad (\bar{\boldsymbol{g}}_{\mathrm{H}} = |\bar{\boldsymbol{g}}_{\mathrm{H}}|\,\hat{\boldsymbol{u}}) \tag{4.43}$$

from (4.40). In the limit $\beta\to\infty$, the numerical results obtained from (4.43) should agree with the asymptotic result (4.42*b*).

Numerical results for $\tilde{D}^{\mathrm{num}}$ are presented in table 4 for low values of M and N in the two cases $|\boldsymbol{\eta}_{\mathrm{H}}|\,(=\pi\beta)$ equal to 30 and 60. They are used to give interpolated values at $\beta=\infty$ by use of the formula (6.10) below. These agree well with the asymptotic result (4.42*b*) when the sum $L\,(=M+N)$ is small. The poorer agreement achieved at larger values of L can be explained (see §6 below) by the stronger influence of the channel and eddy boundary layers. Finally the values of (4.43), for the complete range $0\leqslant M/N\leqslant 1$, are plotted on figure 13 below for the case $|\boldsymbol{\eta}_{\mathrm{H}}|=60$. The asymptotic values (4.42*b*) for the particular values of M/N listed in table 4 below are also indicated for comparison.

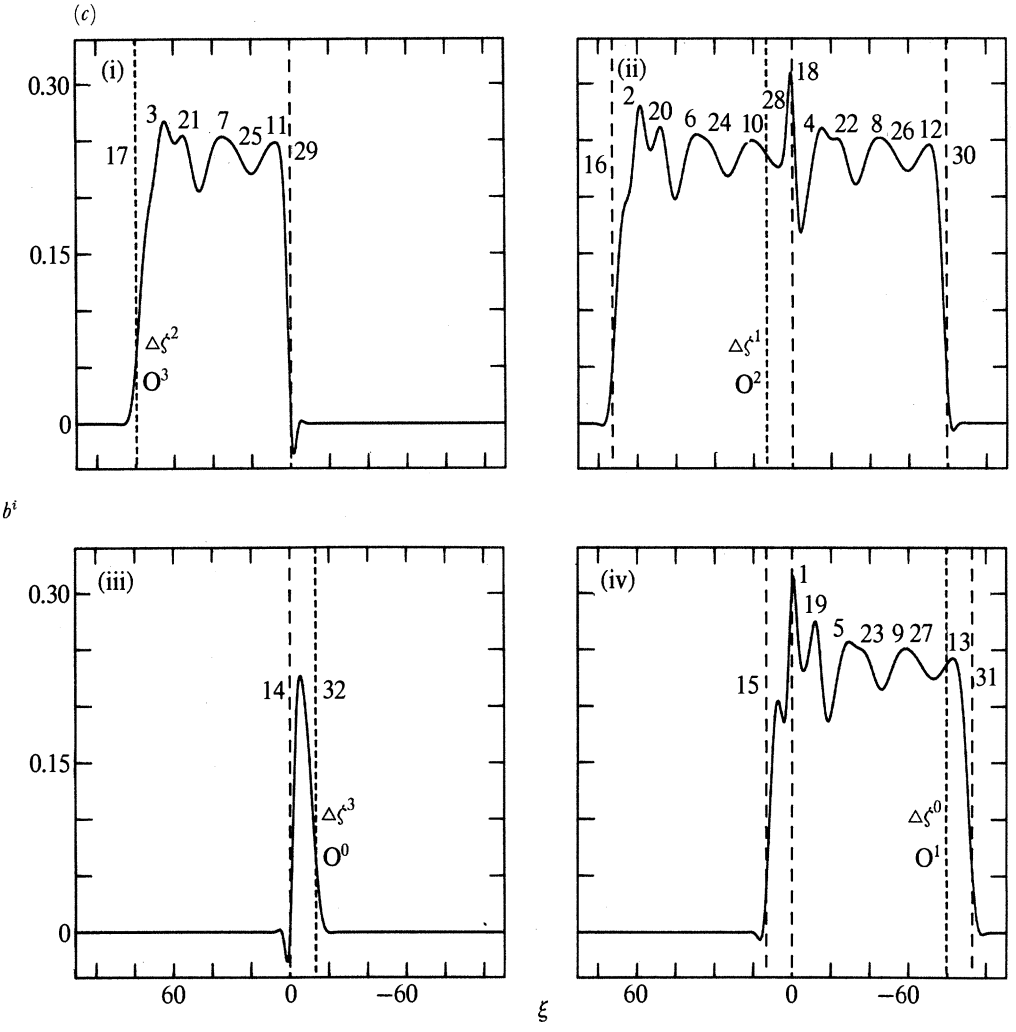

FIGURE 9. For description see opposite.

4.3. *The magnetic problem*

4.3.1. *The solution of the magnetic induction equation*

Our solution of the thermal problem solves part of the magnetic problem and, in particular, determines the horizontal magnetic field. It remains to solve the inhomogeneous heat conduction equation (3.12) for the vertical component of magnetic field, KB. In terms of our boundary layer coordinates its leading order approximation is

$$\partial B/\partial\sigma - \partial^2 B/\partial\zeta^2 = -\partial A/\partial\sigma + (\bar{\boldsymbol{u}}_{\mathrm{H}}\cdot\boldsymbol{\nabla}\zeta)\, b. \tag{4.44}$$

Just as (4.18) is the boundary layer extension of (3.20), so is (4.44) the boundary layer extension of (3.49a). Furthermore, like (3.49a), it can be recast in the form

$$\partial\mathscr{B}/\partial\sigma - \partial^2\mathscr{B}/\partial\zeta^2 = -\partial A/\partial\sigma\,, \tag{4.45a}$$

where

$$\mathscr{B}(\sigma,\zeta) = B + \bar{\zeta} b(\sigma,\zeta) \tag{4.45b}$$

(cf. (3.49b)).

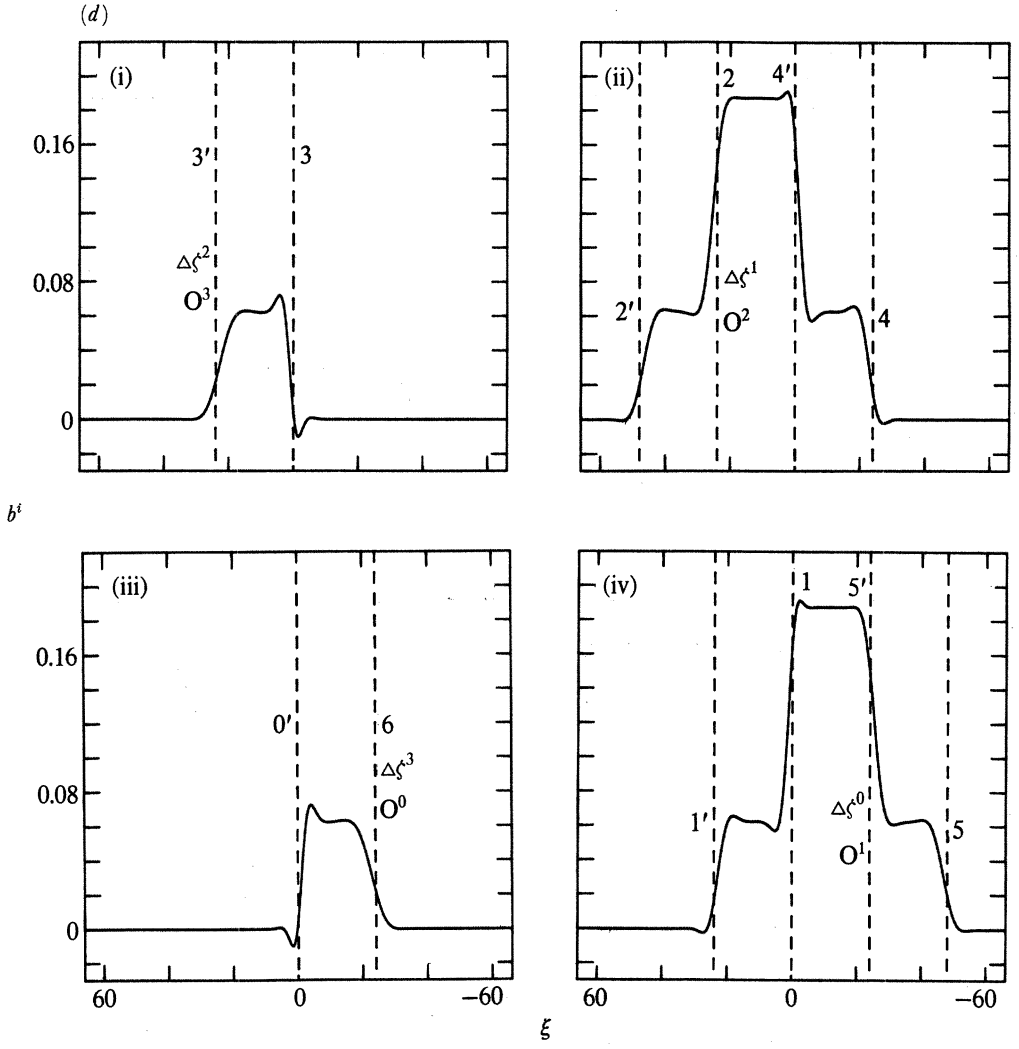

FIGURE 9. The functions b^i plotted solid against ξ at the end ($\sigma = 2$) of each side $\mathscr{T}^i$ of the primary square Π for parallel mean magnetic fields $\bar{\boldsymbol{B}}_{\mathrm{H}}$. The vertical broken lines identify the channel boundaries $C_k: \xi = \zeta_k - \zeta^i$. The origin $\xi = 0$ identifies the X-type stagnation point at the start of the side $\mathscr{T}^i$, while $\xi = \Delta\zeta^i$ identifies the X-type stagnation point O^{i+1} at the end of the side. The plots of b^i for the sides $\mathscr{T}^i$ at O^{+1i} are taken in cyclic order starting at the bottom right, with (iv) $i = 0$, (ii) $i = 1$, (i) $i = 2$, (iii) $i = 3$, just as for the flow (see figure 6). The location of the sequential points, identified in figures 3*a*, 4*a* and 5*a*, as mapped onto the primary square Π, are labelled. The following cases are illustrated. O-flows: (*a*) $\Delta\zeta = 24$, $(M, N) = (0, 1) = \bar{\boldsymbol{B}}_{\mathrm{H}}$; (*b*) $\Delta\zeta = 24$, $(M, N) = (1, 2) = \bar{\boldsymbol{B}}_{\mathrm{H}}$; (*c*) $\Delta\zeta = 13.25$, $(M, N) = (1, 6) = \bar{\boldsymbol{B}}_{\mathrm{H}}$. Only selected channel boundaries marked, namely the start and end X-type stagnation points and eddy boundaries. E-flows: (*d*) $\Delta\zeta = 24$, $(M, N) = (1, 1) = \bar{\boldsymbol{B}}_{\mathrm{H}}$.

TABLE 3. PERPENDICULAR FIELDS WITH CHANNEL DATA GIVEN IN TABLE 1, WHERE $\bar{b} = -\frac{1}{8}\pi(M^2 + N^2)\,(\Delta\zeta)\,(\Delta B)$ (SEE (4.36*c*))

(The value of the quantity proportional to Δ_{k+1} for L-even is partitioned as in table 1.)

(M, N)	$(\bar{B}_x, \bar{B}_y)$	$-\bar{b}$	$(L\Delta_k)^{-1}$	$-\bar{b}(\Delta\zeta)$	$\frac{1}{2}L$	$-\frac{1}{2}\bar{b}\zeta^e$
L-odd						
$(0, 1)$	$(-1, 0)$	9.426	1	226.2	$\frac{1}{2}$	113.1
$(1, 2)$	$(-2, 1)$	47.13	$\frac{1}{3}$	1131	$\frac{3}{2}$	1697
$(1, 6)$	$(-6, 1)$	192.7	$\frac{1}{7}$	2555	$\frac{7}{2}$	8943
L-even						
$(1, 1)$	$(-1, 1)$	18.85	$\frac{1}{3}$	452.4	1	452.4

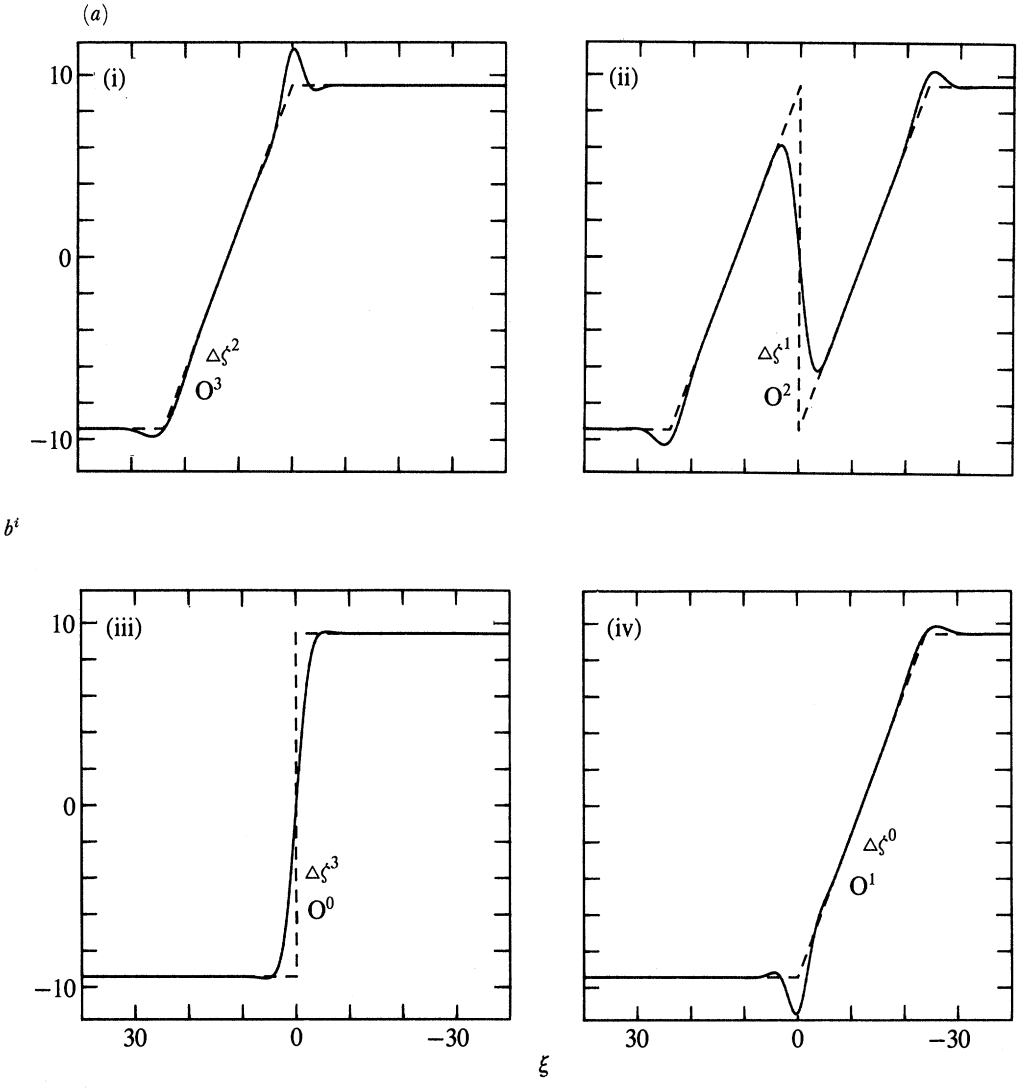

FIGURE 10. For description see page 697.

On each side $\mathscr{T}^i$ of the primary square Π, the stretched streamfunction $\bar{\zeta}(=\bar{\zeta}^i(\sigma))$ is a function of σ, which varies in value from

$$\bar{\zeta}^i(0) = \zeta^i \quad \text{to} \quad \bar{\zeta}^i(2) = \zeta^{i+1} \tag{4.46}$$

between the beginning and end of the side. Solutions are sought in the form

$$\mathscr{B} = \mathscr{B}^i(\sigma, \xi) = (\zeta^i + \tfrac{1}{2}\xi)\, b^i(\sigma, \xi) + C^i(\sigma, \xi). \tag{4.47a}$$

The first term, $(\zeta^i + \frac{1}{2}\xi)\, b^i$, is a particular integral of (4.45a) and so C^i is a solution of the homogeneous heat conduction equation

$$\partial C^i/\partial\sigma = \partial^2 C^i/\partial\xi^2. \tag{4.47b}$$

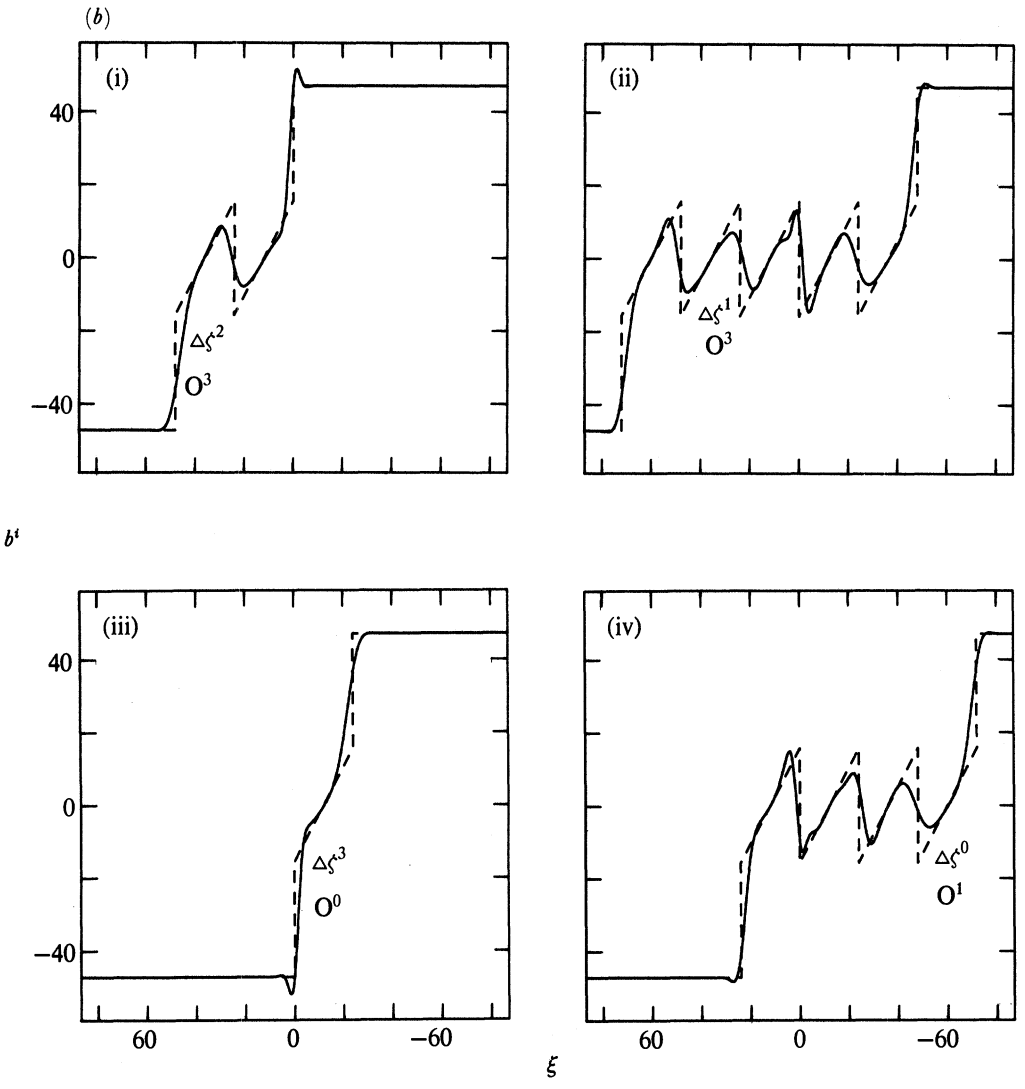

FIGURE 10. For description see page 697.

According to (4.47*a*), (4.45*b*) and (4.46) the beginning and end values of $B\,(=B^i(\sigma,\xi))$ are

$$B^i(0,\xi) = \tfrac{1}{2}\xi b^i(0,\xi) + C^i(0,\xi), \tag{4.48a}$$

$$B^i(2,\xi) = (\tfrac{1}{2}\xi - \Delta\zeta^i)\, b^i(2,\xi) + C^i(2,\xi) \tag{4.48b}$$

(see (4.10*b*)). The start value (4.48*a*), as in paper 1, provides the motivation for the representation (4.47*a*). For whereas both B and A can suffer discontinuities across $\xi = 0$ at $\sigma = 0$, the δ-function contribution to B from b^i at $\sigma = 0$ is unacceptable and is eliminated by the coefficient ξ of $b^i(0,\xi)$ in (4.48*a*). As a result the solution C^i of (4.47*b*), like B^i, has no δ-function source at $\sigma = 0$.

On each side $\mathscr{T}^i$, the result (3.56) with (4.13*f*) shows that $\mathscr{B}^i$ approaches $\frac{1}{2}\zeta^\beta \bar{b} + B_0$ as $\xi \uparrow \infty$ on the primary $\mathscr{D}^+_{0,0}$-eddy. On the neighbouring $\mathscr{D}^-_{m,n}$-eddies, $\mathscr{B}^i$ approaches

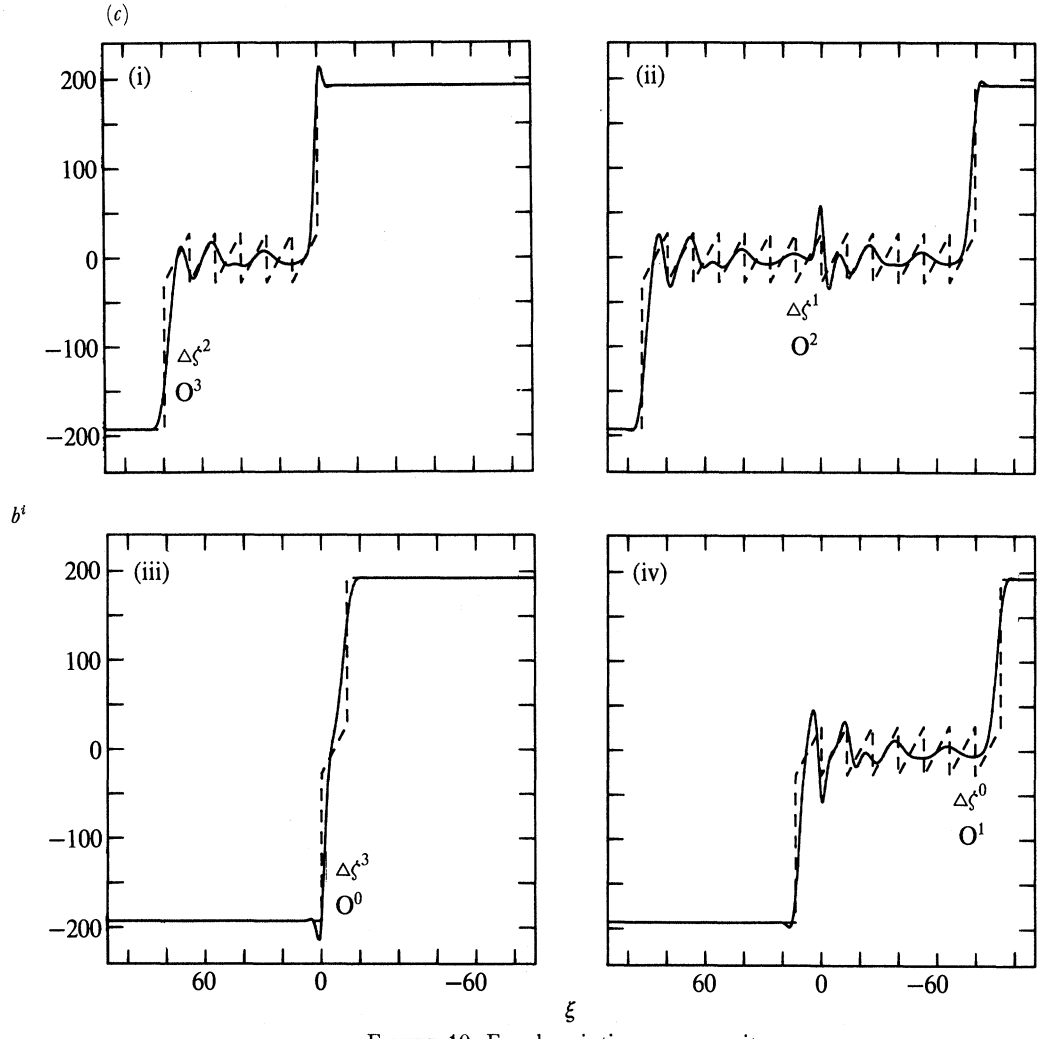

FIGURE 10. For description see opposite.

TABLE 4. CHANNEL DATA AND THE VALUES OF $\epsilon^{-3}R^{-1}D_0$

(The $\Delta\zeta_{ch}$ values for L-even are partitioned as in table 1.)

		$\lvert\eta_H\rvert = 30$		$\lvert\eta_H\rvert = 60$		$\lvert\eta_H\rvert \to \infty$	asymptotic value
(M, N)	$\Delta\zeta_{ch}$	$\Delta\zeta$	$\tilde{D}^{num}$	$\Delta\zeta$	$\tilde{D}^{num}$	$\tilde{D}_0^0$	$\epsilon^{-3}R^{-1}D_0$
L-odd							
(0, 1)	5.0	30.0	0.728	60.0	0.685	0.642	0.646
(1, 2)	8.7	13.4	0.254	26.8	0.170	0.086	0.096
(2, 3)	11.2	8.3	0.248	16.6	0.134	0.020	0.036
(1, 4)	11.2	7.3	0.253	14.6	0.130	0.006	0.031
(3, 4)	13.3	6.0	0.246	12.0	0.129	0.013	0.018
(2, 5)	13.3	5.6	0.259	11.1	0.129	−0.001	0.017
(1, 6)	13.3	4.9	0.269	9.9	0.126	−0.016	0.015
L-even							
(1, 1)	3.5 6.1	21.2	0.509	42.4	0.404	0.299	0.305
(1, 3)	6.1 7.9	9.5	0.281	19.0	0.162	0.043	0.054
(1, 5)	7.9 9.4	5.9	0.265	11.8	0.137	0.008	0.022

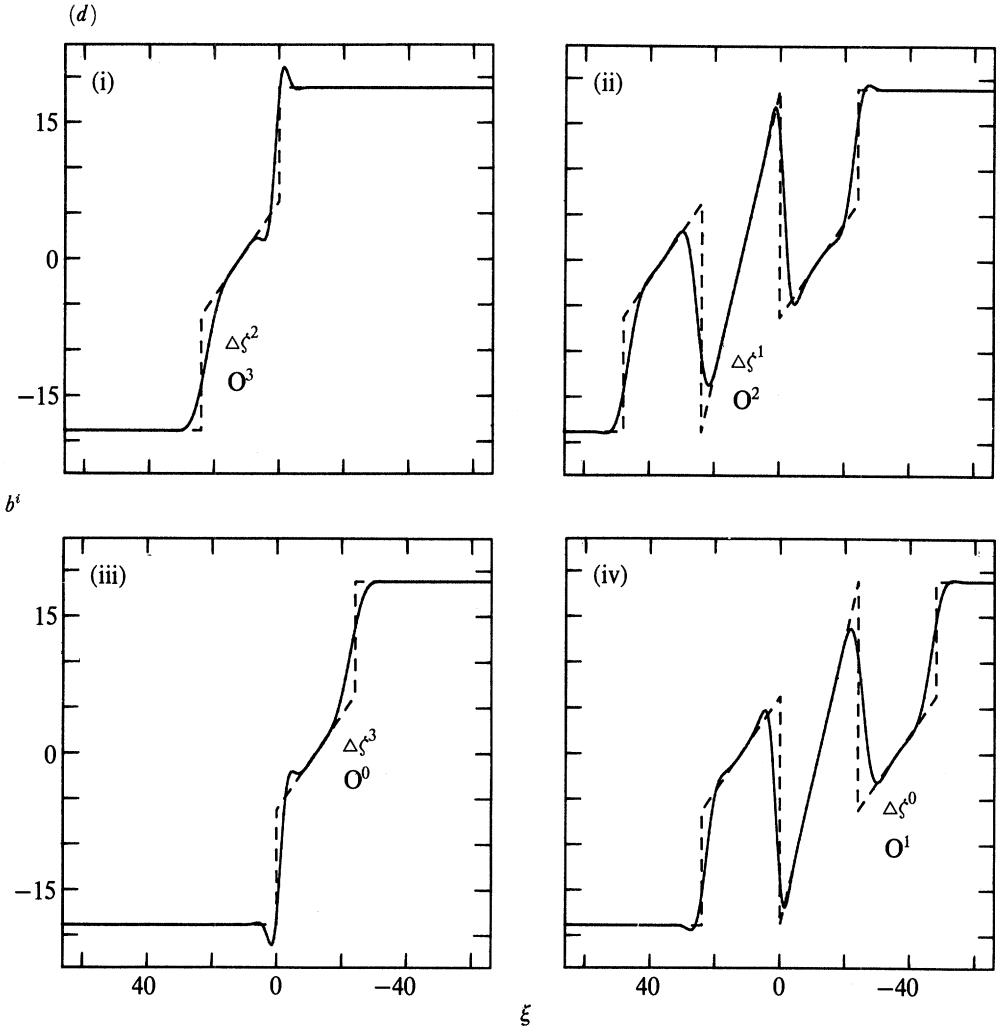

FIGURE 10. The function b^i plotted solid against ξ at the end ($\sigma = 2$) of each side $\mathscr{T}^i$ of the primary square Π for perpendicular mean magnetic fields $\bar{\boldsymbol{B}}_{\mathrm{H}}$. Taken in cyclic order starting at the bottom right they are (iv) $i = 0$, (ii) $i = 1$, (i) $i = 2$, (iii) $i = 3$. The broken lines are given by the asymptotic results (4.36). Other details are similar to figure 9 and the following cases are illustrated. O-flows: (*a*) $\Delta\zeta = 24$, $(M, N) = (0, 1)$, $\bar{\boldsymbol{B}}_{\mathrm{H}} = (-1, 0)$; (*b*) $\Delta\zeta = 24$, $(M, N) = (1, 2)$, $\bar{\boldsymbol{B}}_{\mathrm{H}} = (-2, 1)$; (*c*) $\Delta\zeta = 13.25$, $(M, N) = (1, 6)$, $\bar{\boldsymbol{B}}_{\mathrm{H}} = (-6, 1)$. E-flows: $\Delta\zeta = 24$, $(M, N) = (1, 1)$, $\bar{\boldsymbol{B}}_{\mathrm{H}} = (-1, 1)$.

$-\bar{\zeta}_{m+\frac{1}{2}, n+\frac{1}{2}}\bar{b} - B_0$ as $\xi \downarrow -\infty$. From (4.4) and (4.12) it is readily established that, on the side $\mathscr{T}^i$, this limit becomes $-(\frac{1}{2}\zeta^\beta - \Delta\zeta^{i+1})\bar{b} - B_0$. Further use of (4.13*d*) and (4.10*b*) shows that the boundary conditions on $\mathscr{B}^i$ take the form

$$\mathscr{B}^i \to \pm[\zeta^i + \tfrac{1}{2}(\Delta\zeta^i - \Delta\zeta^{i\mp1})]\,\bar{b} \pm B_0 \quad \text{as} \quad \pm\xi \uparrow \infty, \tag{4.49a}$$

where the upper and lower signs correspond to $\xi \uparrow \infty$ and $\xi \downarrow -\infty$ respectively. Consequently we thus have from (4.47*a*) that the asymptotic behaviour of C^i is

$$C^i \to \pm\tfrac{1}{2}[-\xi + \Delta\zeta^i - \Delta\zeta^{i\mp1}]\,\bar{b} \pm B_0 \quad \text{as} \quad \pm\xi \uparrow \infty. \tag{4.49b}$$

At the end of each side, B is carried to the start of another unaltered by diffusion. So, just as for A and b in §4.2.1, the initial value of B at the start of the side $\mathscr{T}^i$ is related to end values by

$$B^i(0, \zeta) = B^{i\mp1}(2, \xi + \Delta\zeta^{i\mp1}) \quad (\pm\xi > 0), \tag{4.50a}$$

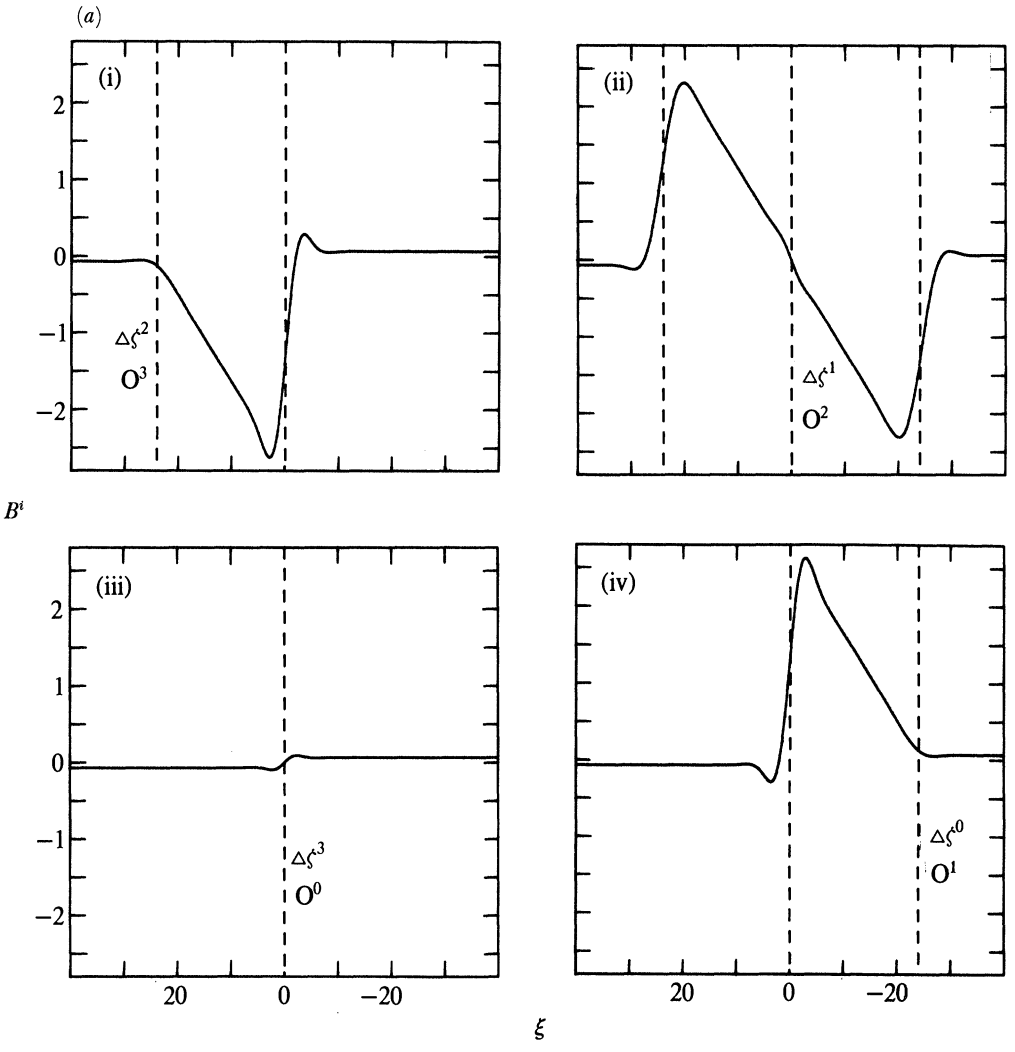

FIGURE 11. For description see page 701.

where the upper and lower signs correspond $\xi > 0$ and $\xi < 0$ respectively. Use of (4.48) shows that the corresponding result for C is

$$C^i(0,\xi) = C^{i\mp1}(2,\xi+\Delta\zeta^{i\mp1}) - \tfrac{1}{2}(\Delta\zeta^{i\mp1})\, b^{i\mp1}(2,\xi+\Delta\zeta^{i\mp1}) \quad (\pm\xi > 0). \tag{4.50b}$$

We express the solution of the heat conduction equation (4.47b) in the form

$$C^i(\sigma,\xi) = \hat{C}^i(\sigma,\xi) + \tilde{C}^i(\sigma,\xi), \tag{4.51a}$$

where

$$\hat{C}^i(\sigma,\xi) = -\tfrac{1}{2}\bar{b}G_2 + [\tfrac{1}{2}\bar{b}(\Delta\zeta^i) + B_0]\, G_1 + \tfrac{1}{2}\bar{b}(\Delta\zeta^{i+1}) \tag{4.51b}$$

is constructed from the elementary solutions (4.24) so that the boundary condition (4.49b) is satisfied. By this device the remaining part $\tilde{C}^i$ satisfies the heat conduction equation (4.47b) with the boundary condition

$$\tilde{C}^i(\sigma,\xi) \to 0 \quad \text{as} \quad \pm\xi \uparrow \infty. \tag{4.52}$$

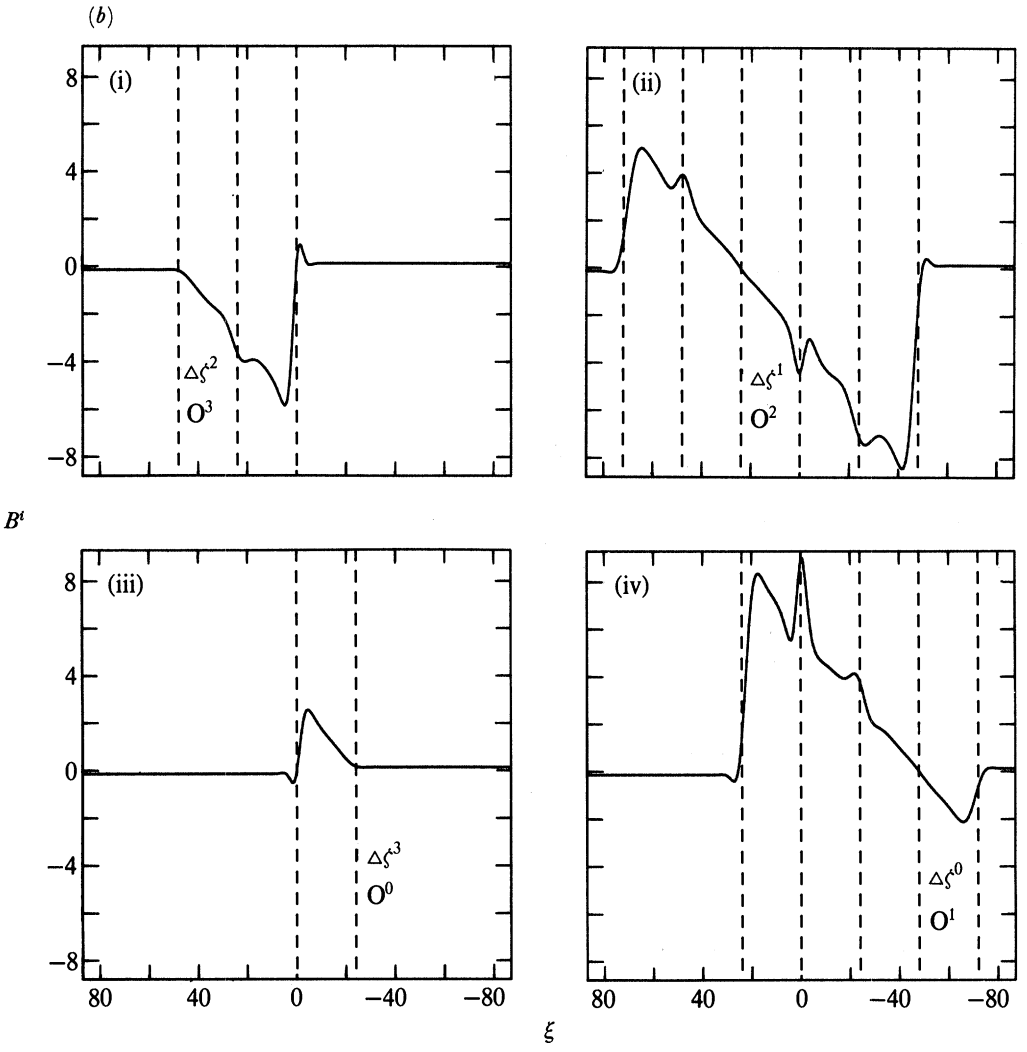

FIGURE 11. For description see page 701.

The initial condition on $\tilde{C}^i$ at the beginning of each side $\mathscr{T}^i$ follows from (4.50b) and (4.51). With the help of (4.24), (4.26) it reduces to

$$\tilde{C}^i(0,\xi) = \tilde{C}^{i\mp1}(2,\xi+\Delta\zeta^{i\mp1}) - \tfrac{1}{2}(\Delta\zeta^{i\mp1})\,\tilde{b}^{i\mp1}(2,\xi+\Delta\zeta^{i\mp1}) - \tfrac{1}{2}\bar{b}G_2^{\pm}(\xi+\Delta\zeta^{i\mp1}) + B_0\,G_1^{\pm}(\xi+\Delta\zeta^{i\mp1}) \quad (\pm\xi>0), \tag{4.53a}$$

where

$$G_2^{\pm}(\xi) = G_2(2,\xi)\mp\xi \tag{4.53b}$$

and $G_1^{\pm}(\xi)$ is defined by (4.29c) above. Finally the Greens function solution on each side $\mathscr{T}^i$ is

$$\tilde{C}^i(\sigma,\xi) = \int_{-\infty}^{\infty} G_0(\sigma,\xi-\xi')\,\tilde{C}^i(0,\xi')\,\mathrm{d}\xi'. \tag{4.54}$$

When $\sigma = 2$ it links the start value $\tilde{C}^i(0,\xi)$ to the end value $\tilde{C}^i(2,\xi)$.

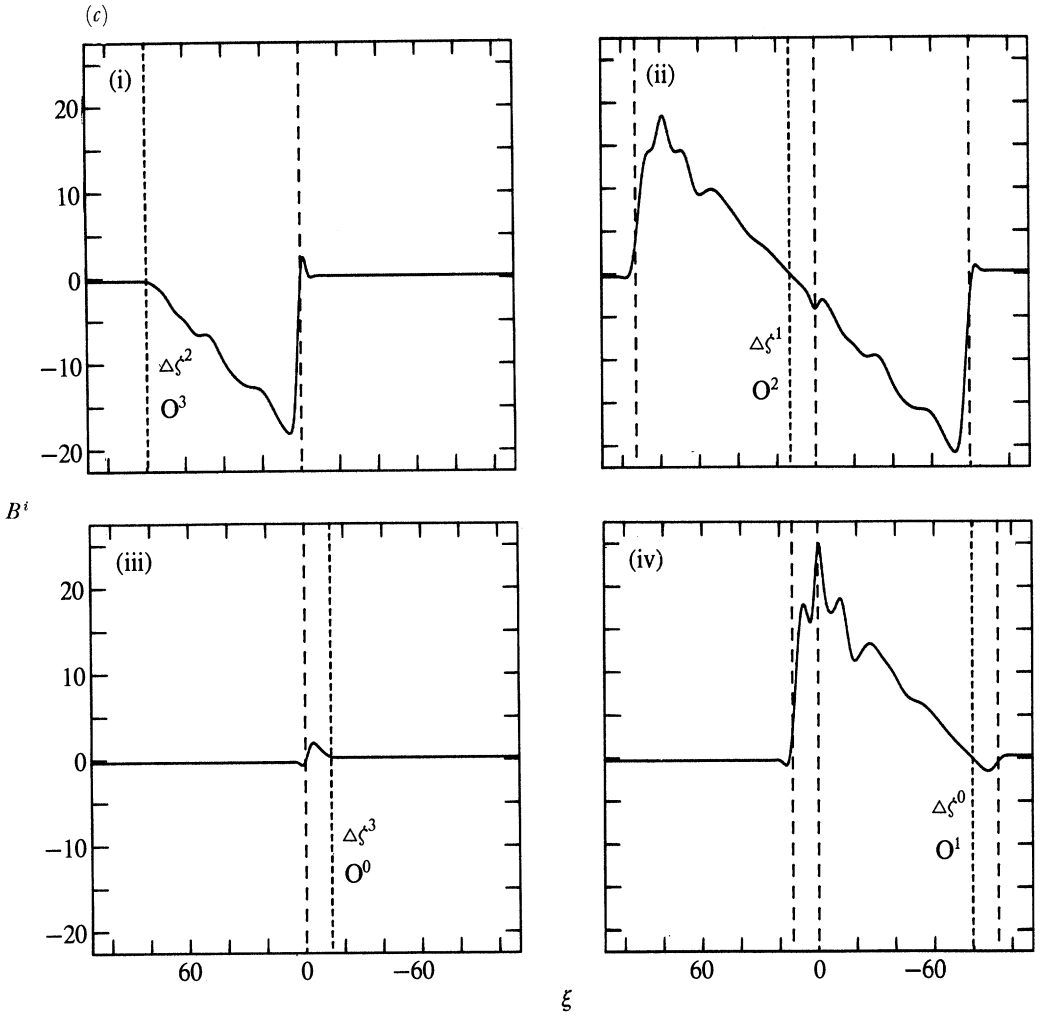

FIGURE 11. For description see opposite.

The mathematical problem posed by (4.53) and (4.54) for $\tilde{C}^i$ is similar to that for $\tilde{A}^i$ formulated in §4.2.1. In the numerical procedures, however, there is one difference. Whereas the iteration for $\tilde{b}^i(2,\xi)$ could proceed on the basis of an initial guess of $\tilde{b}^0(2,\xi)$ and $\tilde{b}^2(2,\xi)$ alone, here the iteration for $\tilde{C}^i(2,\xi)$ requires an initial guess of B_0 in addition to $\tilde{C}^0(2,\xi)$ and $\tilde{C}^2(2,\xi)$. Otherwise the procedures are the same.

Numerical results are illustrated in figures 11 and 12 for the cases listed in table 1. In the case of parallel mean magnetic fields (see (4.33)), the asymptotic results of §5.3.2 below for large β yields the channel and eddy solutions

$$B = \begin{cases} \Delta_{k+1}\beta^{-1}B_{\parallel}(\zeta-\bar{\zeta}) & \text{on} \quad D_k, \qquad (4.55a) \\ 0 & \text{on} \quad \mathscr{D}^{\pm}_{m,n} \qquad (4.55b) \end{cases}$$

(see (5.53)) for the vertical magnetic field, KB, where $\beta^{-1}B_{\parallel}$ is defined by (4.34d) above. The data used to produce the asymptotic solutions illustrated in figure 11 is listed in table 2. Note that, in each figure, B on the side $\mathscr{T}^i$ is plotted at the end $O^{i+1}(\sigma = 2)$ at which $\zeta-\bar{\zeta} = \xi-\Delta\zeta^i$. Consequently the asymptotic value of B defined by (4.55a) vanishes at $\xi = \Delta\zeta^i$. Just as in figure 9 before, the slope of the numerical solutions differ from those defined by (4.55a) by about

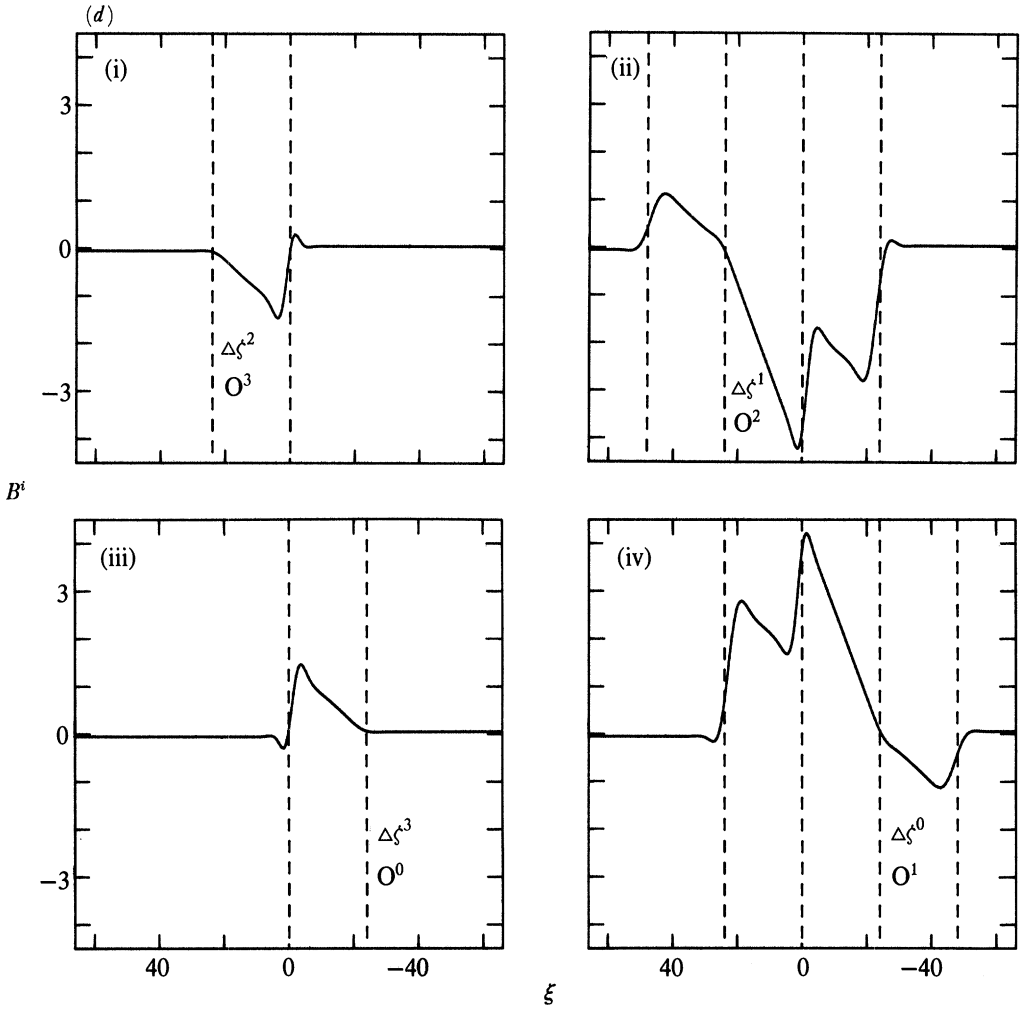

FIGURE 11. As in figure 9 except that B^i is plotted against ξ.

10 %. Note also that for O-flows Δ_k is unity and (4.55*a*) defines a straight line. For E-flows Δ_k alternates in value between one channel and the next. The resulting change in slope of B is illustrated well by figure 11*d*, just as the change in magnitude of b is clearly shown in figure 9*d*.

In the case of perpendicular mean magnetic fields (see (4.35)) the asymptotic results of §5.3.3 below for large β yield the channel and eddy solutions

$$B-B^s=\begin{cases}\left(\dfrac{\bar{b}}{L\Delta_k}\right)\left\{\dfrac{(\zeta-\bar{\zeta})^2-(\zeta_{k+1}-\bar{\zeta})\,(\zeta_k-\bar{\zeta})}{\Delta\zeta}\right\} & \text{on} \quad D_k, \qquad (4.56a)\\ \pm\bar{b}(\zeta^{\pm}_{m,n}-\bar{\zeta}) & \text{on} \quad \mathscr{D}^{\pm}_{m,n} \qquad (4.56b)\end{cases}$$

(see (5.63)) with $$B^s=-\tfrac{1}{2}\bar{b}\zeta^c \quad (\zeta^c=L(\Delta\zeta)) \qquad (4.57a)$$

(see (5.64)) and $$\zeta^{\pm}_{m,n}\equiv R_a^{\frac{1}{4}}\psi^{\pm}_{m,n}. \qquad (4.57b)$$

The expression (4.56*b*) gives the values achieved on the boundaries $\mathscr{C}^+_{m,n}=C_{k+1}$ and $\mathscr{C}^-_{m,n}=C_k$ as they are approached from the eddy interiors. The data used to produce the results

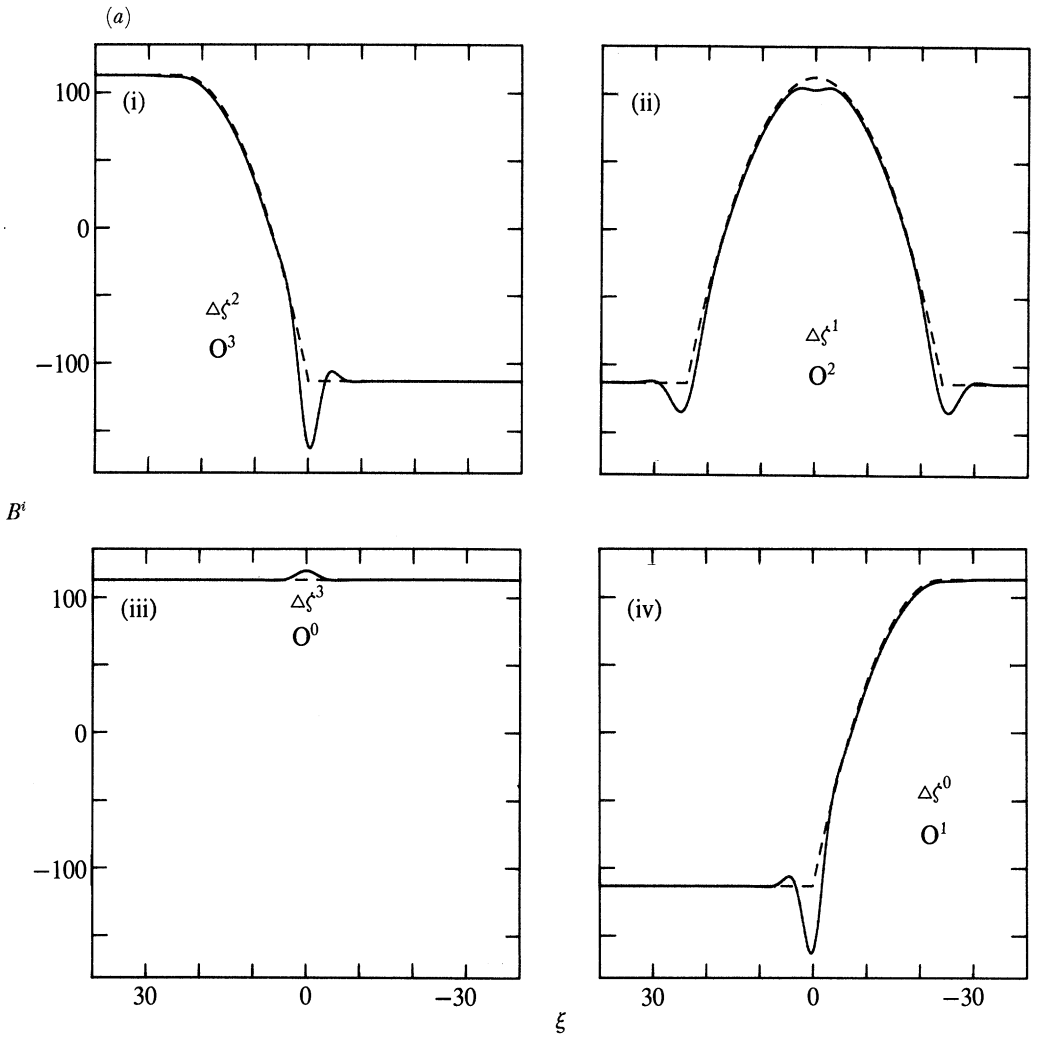

FIGURE 12. For description see page 705.

illustrated in figure 12 are listed in table 3. Note that the stagnation point at $O^{i+1}(\sigma = 2)$ on the side $\mathscr{T}^i$ is located at $\xi = \Delta\zeta^i$, on the streamline C_k (say). There $\zeta - \bar{\zeta}$ vanishes, as do $\zeta_k - \bar{\zeta}$ and $\zeta_{k+1} - \bar{\zeta}$ in the channels D_k and D_{k-1} respectively above and below the dividing streamline C_k. Consequently B is continuous across the dividing streamline C_k at the stagnation point, where it takes the value B^s. Finally we note that the agreement between the numerical and asymptotic results displayed in figure 12 is good despite complexity of the channel structure. The smoothing effect of diffusivity accounts for the disparity in the more complex cases.

4.3.2. *The mean electromotive force*

The determination of the mean electromotive force $K\bar{\boldsymbol{E}}_{\mathrm{H}}$ from the formula (3.65) depends on the values of the functions $\mathscr{E}^i_{\mathrm{s}}$ defined by (3.67). On each side $\mathscr{T}^i$ the integrand in (3.66a) is given by

$$\mathscr{E} \equiv R^{\frac{1}{2}}\psi b - \mathscr{B} = \tfrac{1}{2}\xi b^i(\sigma, \xi) - C^i(\sigma, \xi), \tag{4.58}$$

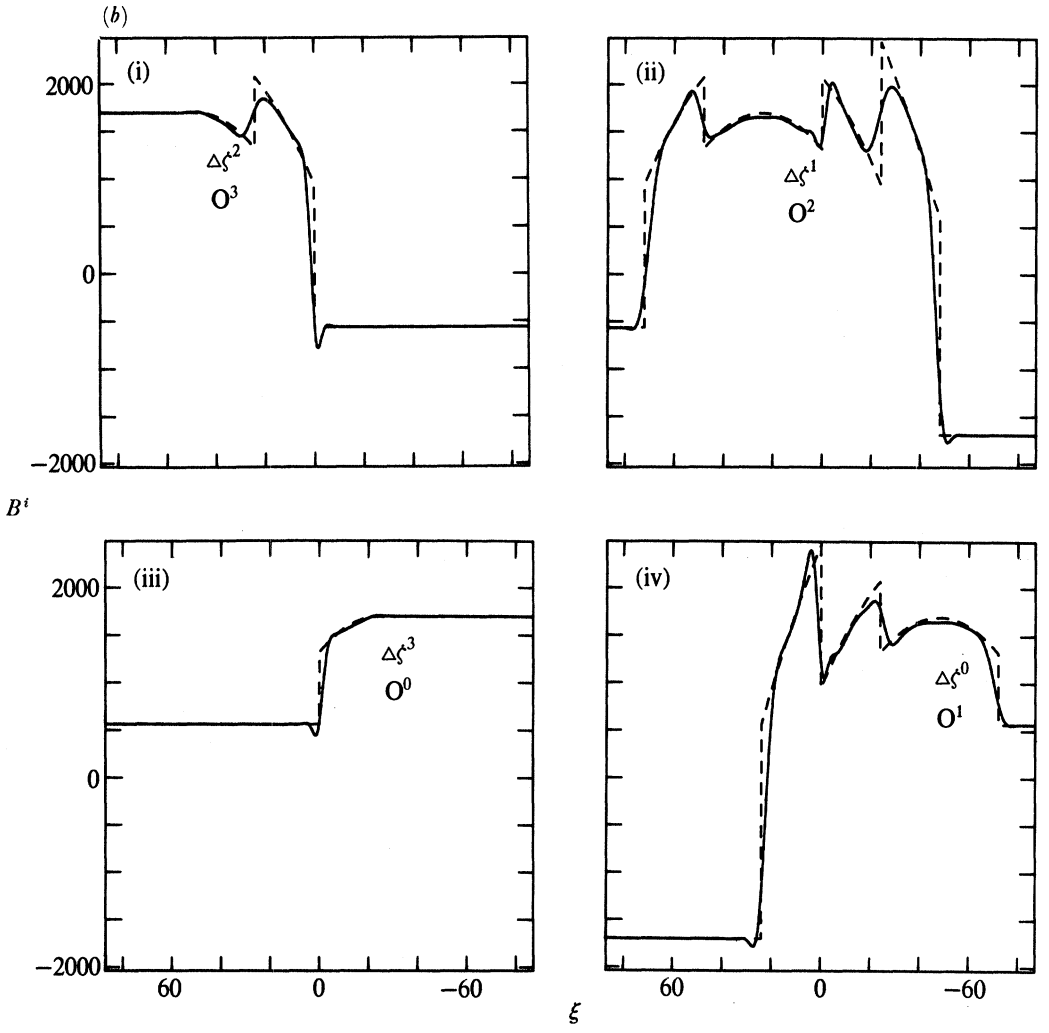

FIGURE 12. For description see page 705.

where use has been made of (4.3), (4.8) and (4.47*a*). With b^i and C^i expressed in the forms (4.26) and (4.51) the functions $\mathscr{E}^i_{\infty_s}$ (see (3.66*a*)), from which $\mathscr{E}^i_s$ are derived, are given by

$$\mathscr{E}^i_{\infty_s} = \hat{\mathscr{E}}^i_{\infty_s} + \tilde{\mathscr{E}}^i_{\infty_s}, \tag{4.59a}$$

where

$$\hat{\mathscr{E}}^i_{\infty_s} = \frac{1}{\pi}\int_0^\pi \left[\int_{\xi^i_{-\infty}}^{\xi^i_{\infty}} (\tfrac{1}{2}\xi\hat{b}^i - \hat{C}^i)\,\mathrm{d}\xi\right]\mathrm{d}s - (\mathscr{E}^i_\infty - \mathscr{E}^i_{-\infty}), \tag{4.59b}$$

$$\tilde{\mathscr{E}}^i_{\infty_s} = \frac{1}{\pi}\int_0^\pi \left[\int_{\xi^i_{-\infty}}^{\xi^i_{\infty}} (\tfrac{1}{2}\xi\tilde{b}^i - \tilde{C}^i)\,\mathrm{d}\xi\right]\mathrm{d}s, \tag{4.59c}$$

and, by use of (4.13*c*),

$$\mathscr{E}^i_{\pm\infty} = \pm\left[\tfrac{1}{2}\bar{b}(\xi^i_{\pm\infty} - \Delta\zeta^i - \Delta\zeta^{i\pm1}) - B_0\right]\xi^i_{\pm\infty}. \tag{4.59d}$$

PHILOSOPHICAL TRANSACTIONS OF THE ROYAL SOCIETY A MATHEMATICAL, PHYSICAL & ENGINEERING SCIENCES

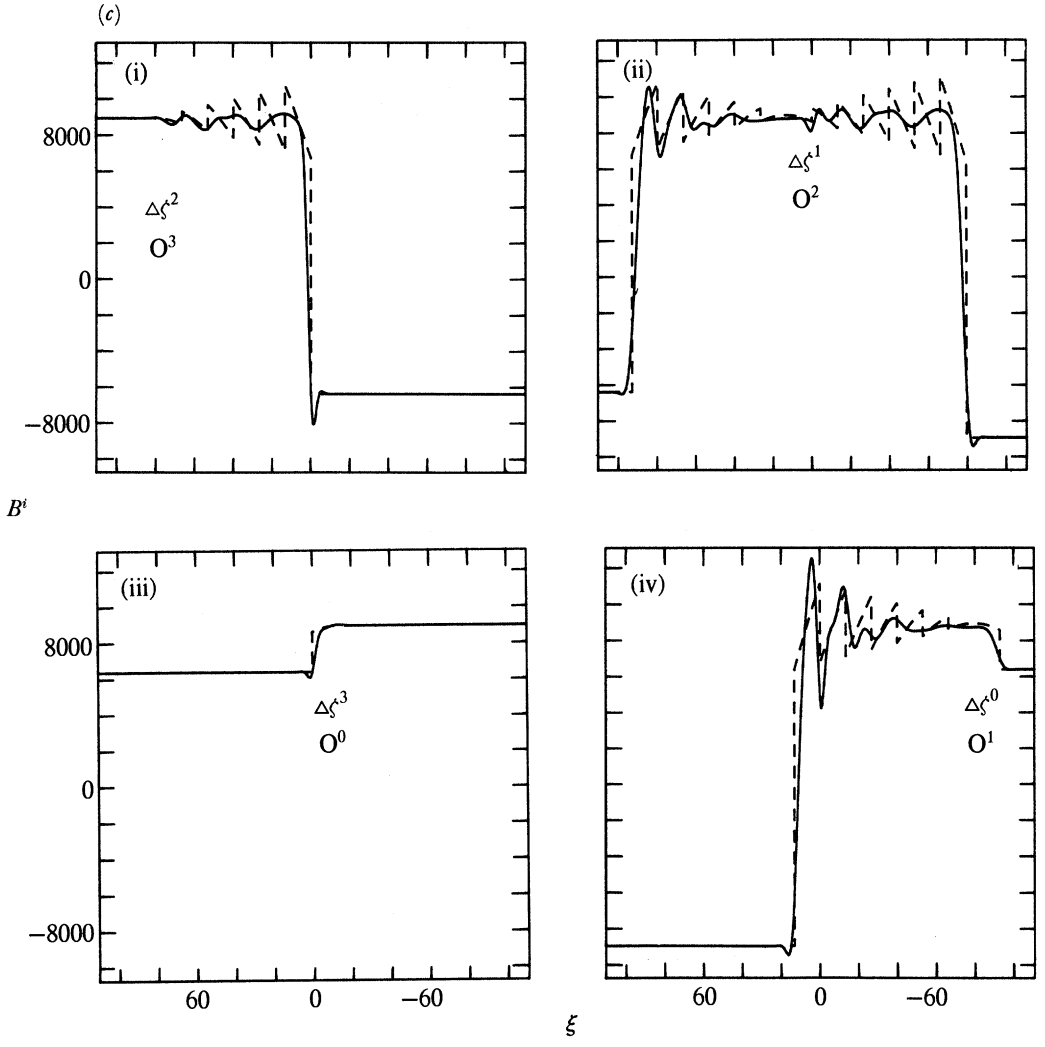

FIGURE 12. For description see opposite.

Substitution of (4.26*b*), (4.51*b*) into (4.59*b*) and use of (4.24) yields

$$\hat{\mathscr{E}}^i{}_{\infty_s} = \frac{1}{\pi}\int_0^\pi [\{\tfrac{1}{2}(\xi-\Delta\zeta^i)\,\bar{b}-B_0\}\{G_2(\sigma,\xi)-|\xi|\}]_{\xi^i_{-\infty}}^{\xi^i_\infty}\,\mathrm{d}s. \tag{4.60a}$$

In view of the asymptotic behaviour of G_2 defined by (4.25), this expression vanishes in the limit $\pm\xi^i_{\pm\infty}\to\infty$ giving

$$\hat{\mathscr{E}}^i_s = 0. \tag{4.60b}$$

It follows at once that

$$\mathscr{E}^i_s = \tilde{\mathscr{E}}^i_s = \int_{-\infty}^{\infty}(\tfrac{1}{2}\xi\tilde{b}^i-\tilde{C}^i)\,\mathrm{d}\xi \tag{4.61}$$

which, as for $\tilde{\mathscr{F}}^i_s$ defined by (4.39*b*) above, we find convenient to evaluate from our numerical results at $\sigma = 2$. To complete the evaluation of the mean electromotive force $K\bar{\boldsymbol{E}}_H$ defined by (3.69) we require

$$\mathscr{E}^i_\pm = \pm[\tfrac{1}{2}\bar{b}(-\xi^i_\pm\pm\zeta^c)-B_0]\,\xi^i_\pm \tag{4.62}$$

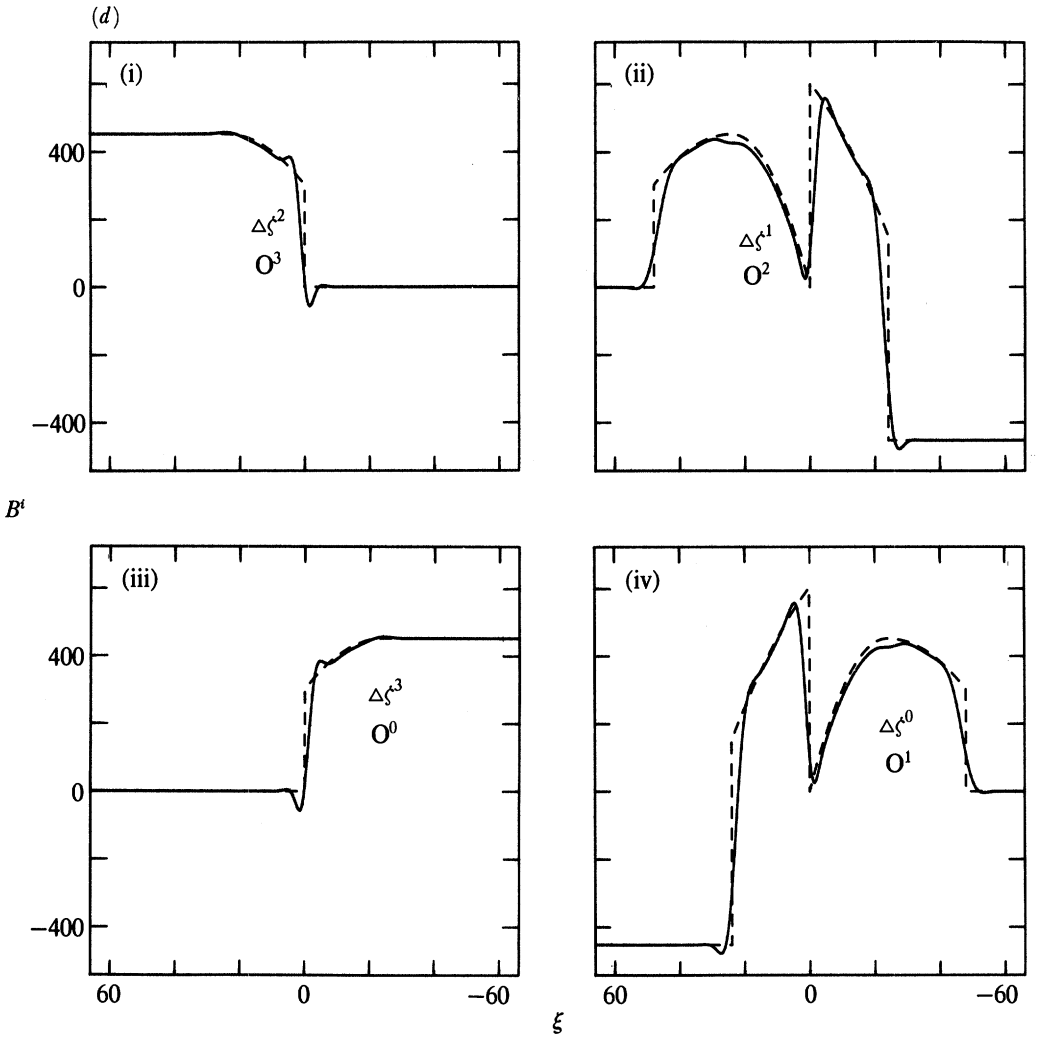

FIGURE 12. As in figure 10 except that B^i is plotted against ξ.

(see (3.66*b*)). Hence substitution of (4.62) into (3.65), (3.67), (3.68) and use of (4.12), (4.13*a*, *e*) recovers the result (3.69), namely

$$\pi R^{\frac{1}{2}}\bar{E}_x = -\tfrac{1}{2}(\mathscr{E}^1_x - \mathscr{E}^3_x) + B_0\,\eta_x, \tag{4.63a}$$

$$\pi R^{\frac{1}{2}}\bar{E}_y = \tfrac{1}{2}(\mathscr{E}^0_y - \mathscr{E}^2_y) + B_0\,\eta_y, \tag{4.63b}$$

where $\mathscr{E}^i_s$ are now determined from (4.61).

As in the case of the diffusion-matrix considered in §4.2.2, we determine the α-matrix $\boldsymbol{\alpha}$ in (3.14) by considering the value of $\bar{\boldsymbol{E}}_H$ defined by (4.63) for the two cases of parallel and perpendicular mean magnetic fields in the limit (4.41) of large β. The analysis of §5.3 below shows that the α-matrix has the asymptotic form

$$-\boldsymbol{\alpha} = \alpha_0(\boldsymbol{I} - \hat{\boldsymbol{u}}_H\,\hat{\boldsymbol{u}}_H), \tag{4.64a}$$

where from (5.68)

$$K^{-1}\epsilon^{-3}R^{-1}\alpha_0 = \frac{\pi^3 L}{16(M^2+N^2)^{\frac{1}{2}}}\left(1 - \frac{1}{3\Lambda L^2}\right). \tag{4.64b}$$

For mean flows with irrational tangents, (4.64*b*) yields

$$K^{-1}\epsilon^{-3}R^{-1}\alpha_0^{\mathrm{irr}} = \tfrac{1}{16}\pi^3(|\hat{u}_x| + |\hat{u}_y|) = \tfrac{1}{8\sqrt{2}}\pi^3 \sin(\theta_0 + \tfrac{1}{4}\pi) \tag{4.64c}$$

in the limit $L \to \infty$. Consequently we see that for mean flows with rational tangents D_0 (see (4.42*b*)) and α_0 are related by

$$K^{-1}\alpha_0 + D_0 = K^{-1}\alpha_0^{\mathrm{irr}}. \tag{4.65}$$

To test the asymptotic results (4.64*b*) for rational tangents, we again consider the case of perpendicular mean magnetic fields (4.35), and use the results of the numerical integrations to evaluate

$$K^{-1}\tilde{\alpha}^{\mathrm{num}} = -\beta^{-3}(R^{\frac{1}{2}}\bar{\boldsymbol{E}}_{\mathrm{H}} \cdot \bar{\boldsymbol{B}}_{\mathrm{H}}/|\bar{\boldsymbol{B}}_{\mathrm{H}}|^2) \quad (\hat{\boldsymbol{u}}_{\mathrm{H}} \cdot \bar{\boldsymbol{B}}_{\mathrm{H}} = 0) \tag{4.66}$$

from (3.69). In the limit $\beta \to \infty$, the numerical values for $\tilde{\alpha}^{\mathrm{num}}$ should agree with the asymptotic result (4.64*b*). Numerical results corresponding to those obtained for the heat flux calculations of §4.2 are presented in tabular form in table 5 below and graphically in figure 14 below.

TABLE 5. THE VALUES OF $K^{-1}\epsilon^{-3}R^{-1}\alpha_0$

(M, N)	$\lvert\boldsymbol{\eta}_{\mathrm{H}}\rvert = 30$ $K^{-1}\tilde{\alpha}^{\mathrm{num}}$	$\lvert\boldsymbol{\eta}_{\mathrm{H}}\rvert = 60$ $K^{-1}\tilde{\alpha}^{\mathrm{num}}$	$\lvert\boldsymbol{\eta}_{\mathrm{H}}\rvert \to \infty$ $K^{-1}\tilde{\alpha}_0^0$	asymptotic value $K^{-1}\epsilon^{-3}R\alpha_0$	irrational asymptotic value $K^{-1}\epsilon^{-3}R\alpha_0^{\mathrm{irr}}$
L-odd					
(0, 1)	1.255	1.273	1.291	1.292	1.938
(1, 2)	2.436	2.469	2.502	2.503	2.600
(2, 3)	2.549	2.608	2.667	2.652	2.687
(1, 4)	2.243	2.272	2.302	2.319	2.350
(3, 4)	2.593	2.640	2.687	2.694	2.712
(2, 5)	2.387	2.455	2.522	2.502	2.520
(1, 6)	2.102	2.168	2.234	2.215	2.230
L-even					
(1, 1)	2.339	2.387	2.435	2.436	2.740
(1, 3)	2.300	2.346	2.391	2.397	2.452
(1, 5)	2.150	2.202	2.254	2.259	2.281

5. THE CHANNEL SOLUTIONS

5.1. *Scope and objectives*

In this section we only consider mean flows with rational tangents for which

$$(\epsilon R^{\frac{1}{2}} \equiv)\ \beta \gg L^{\frac{1}{2}}(M^2 + N^2)^{\frac{1}{2}}, \quad R \gg 1 \gg \epsilon. \tag{5.1}$$

Diffusive effects are confined to eddy and channel boundary layers so that mainstream solutions exist inside the channels D_k as well as in the interior of the eddies $\mathscr{D}^{\pm}_{m,n}$. Here we construct these solutions and use them to determine the dominant contributions (4.42) and (4.64) to the diffusion and α-matrices as advocated in §3.3 above.

The method that we use is explained in paper 2, §3.1. Essentially we obtain consistency conditions as in §§3.4.1 and 3.5.1 above. However, whereas for the eddy solutions we considered closed domains $\mathscr{D}(\psi)$ bounded by closed streamlines $\mathscr{C}(\psi)$, we now consider the closed domain $\delta D(\psi)$ bounded by two neighbouring streamlines $C(\psi)$ and $C(\psi + \delta\psi)$ taken

over a periodicity section, P_0P_Δ (see (2.31a) and (2.16)). Both $C(\psi)$ and $C(\psi+\delta\psi)$ lie in the interior of the same channel D_k and the boundary of $\delta D(\psi)$ s completed by arcs, C^{P_0}, C^{P_Δ}, connecting $C(\psi)$ to $C(\psi+\delta\psi)$ at each end of the periodicity section. Just as we did for the eddy solutions, we assume that A and B are given by (3.21) and (3.49b), (3.50), where to leading order A and $\mathscr{B}$ are functions of ψ alone. To determine those functions we integrate the heat conduction equations (3.2b) and (3.12a) over the domain $\delta D(\psi)$. The differential equations (5.3) and (5.38) below governing A and $\mathscr{B}$ respectively are the consistency conditions obtained in the limit $\delta\psi\to 0$.

Some boundary conditions at the channel edges can be derived in a similar way. We consider the closed domain δD_k bounded on either side by the streamlines $C(\psi)$ and $C(\psi+\delta\psi)$ in the two distinct channels D_{k-1} and D_k on either side of the dividing streamline C_k. Taken over a periodicity section the domain contains, in addition to the streamline C_k, either a single $\mathscr{D}^{\pm}_{m,n}$-eddy for E-flows or both a $\mathscr{D}^{+}_{m,n}$ and a $\mathscr{D}^{-}_{m,n}$-eddy for O-flows (see §2.3). The particular case $C(\psi)\subset D_{-1}(\psi<0)$ and $C(\psi+\delta\psi)\subset D_0(\psi>0)$ is illustrated in figure 2. Again the heat conduction equations (3.2b) and (3.12a) are integrated over δD_k and two boundary conditions, one (5.11) for A and the other (5.43) for $\mathscr{B}$, are obtained in the limit $\delta\psi\to 0$. Unlike $\delta D(\psi)$, which has zero area in this limit, the region δD_k continues to include the eddy interiors of finite area (see (5.10) below). Not all boundary conditions can be obtained in this way. The complete solution to the mainstream problem requires matching the eddy and channel boundary layers. As mentioned in §3.4.1, such matching was achieved to all orders of inverse powers of R in paper 2 by constructing the boundary layer solutions using the Weiner–Hopf method. This powerful method is not available to us here and so we do not attempt to solve the boundary-layer problem in detail. When we consider the two particular cases of parallel and perpendicular fields (see (4.33) and (4.35) above), we make use of the limited information available to construct the lowest order mainstream solutions compatible with boundary layers. Using the language of the magnetic problem, it is the latter case of perpendicular field ρ, which is the more interesting. Just as for the cat's-eye problem of paper 2, and as explained in §1 above, the magnetic field is stretched out and intensified by an order of magnitude in the channels. This gives the dominant contributions (4.42) and (4.64) to the diffusion and α-matrices. In the former case of parallel fields, magnetic flux is simply expelled from the closed eddies and aligns itself with the channel flow giving negligible contributions to the mean heat flux (3.6) and mean electromotive force (3.14).

The approach presented in this section is based upon the detailed channel geometry of §2 and is thus in the spirit of the boundary-layer analysis of §4. However, for the specific purpose of obtaining the dominant mainstream channel solution, other approaches of a more algebraic nature are possible. For example, the increments or shifts $\Delta\psi^i$ in ψ given by (2.43) and utilized in (4.11)–(4.13) can be represented by a shift map mod ψ^c on the real line. The properties of this map can be used to deduce the values of the circulation integrals (2.48) needed in the asymptotic evaluation of transport. Since such alternative approaches might be useful for other examples with mean flow, we outline this approach to the computation of the mainstream contributions to $\boldsymbol{D}$ in Appendix A.

PHILOSOPHICAL TRANSACTIONS OF THE ROYAL SOCIETY A MATHEMATICAL, PHYSICAL & ENGINEERING SCIENCES

5.2. *The thermal problem*

5.2.1. *The mainstream solution*

At leading order we assume that both A and $R^{\frac{1}{2}}b\,(=\partial A/\partial\psi)$ are functions of ψ alone as in (3.21) and (3.23b) above. Integration of the heat conduction equation (3.2) over our channel periodicity domain $\delta D(\psi)$ yields, upon application of the divergence theorem,

$$[A]_{P_0}^{P_\Delta}\delta\psi-\bar{E}\delta\Sigma=R^{-\frac{1}{2}}\delta(\gamma b), \tag{5.2a}$$

where $\delta\Sigma$ is the area of $\delta D(\psi)$, γ is the circulation integral (2.31a) (cf. (3.24b)), $[A]_{P_0}^{P_\Delta}$ denotes the jump in value of A between the terminal arcs C^{P_0} and C^{P_Δ}, and

$$\delta(\gamma b)=\gamma(\psi+\delta\psi)\,b(\psi+\delta\psi)-\gamma(\psi)\,b(\psi). \tag{5.2b}$$

In the limit $\delta\psi\to 0$, the consistency condition (5.2a) becomes

$$[A]_{P_0}^{P_\Delta}=\bar{E}\frac{\mathrm{d}\Sigma}{\mathrm{d}\psi}+R^{-\frac{1}{2}}\frac{\mathrm{d}}{\mathrm{d}\psi}(\gamma b), \tag{5.3a}$$

in which

$$\frac{\mathrm{d}\Sigma}{\mathrm{d}\psi}=\int_{P_0}^{P_\Delta}\frac{1}{q}\,\mathrm{d}s,\quad \frac{\mathrm{d}\gamma}{\mathrm{d}\psi}=\int_{P_0}^{P_\Delta}\frac{1}{q}\nabla^2\psi\,\mathrm{d}s \tag{5.3b}$$

(cf. (3.25b), but note that $\mathrm{d}\Sigma$ is of opposite sign). Now within the framework of our small-ϵ approximation the derivative of γ is negligible in comparison with that of b. We therefore assume it to be a constant, which according to (2.48) is given by

$$[\sigma]_{P_0}^{P_\Delta}=\gamma=\Gamma_k=(8/\tau)\,\Delta_k L, \tag{5.4}$$

where σ is the streamline coordinate (3.39). We then define the mean σ-derivative of A on the channel D_k by

$$\left(\overline{\frac{\partial A}{\partial\sigma}}\right)_k=\frac{1}{\Gamma_k}[A]_{P_0}^{P_\Delta}, \tag{5.5a}$$

where, by (2.16) and (3.4),

$$[A]_{P_0}^{P_\Delta}=(2/\tau)\,\bar{A}_{M,N}. \tag{5.5b}$$

The value of $\bar{E}$, on the other hand, is determined by (2.10), (3.1) and (3.2c) and is given by

$$\bar{E}=\pi^{-2}(\Delta\psi)\,\bar{A}_{M,N}=O(\epsilon). \tag{5.6}$$

Since $\mathrm{d}\Sigma/\mathrm{d}\psi$ is of order unity, it follows from (5.5b) and (5.6) that $\bar{E}(\mathrm{d}\Sigma/\mathrm{d}\psi)$ is smaller than $[A]_{P_0}^{P_\Delta}$ by a factor of order ϵ and so can be neglected. Within the framework of our approximations, (5.3a) now reduces to

$$\mathrm{d}b/\mathrm{d}\psi=R^{\frac{1}{2}}(\overline{\partial A/\partial\sigma})_k\quad\text{on}\quad D_k, \tag{5.7a}$$

where, by (5.4)–(5.6),

$$\left(\overline{\frac{\partial A}{\partial\sigma}}\right)_k=\tfrac{1}{4}\pi^2\frac{\bar{E}}{\Delta_k\psi^{\mathrm{c}}}\quad(\psi^{\mathrm{c}}=L(\Delta\psi)). \tag{5.7b}$$

Integration of (5.7*a*) yields

$$b = R^{\frac{1}{2}}(\overline{\partial A/\partial\sigma})_k\,(\psi-\psi_{k+\frac{1}{2}}) + R^{-\frac{1}{2}}\bar{b}_k \quad \text{on} \quad D_k, \tag{5.8a}$$

where

$$\psi_{k+\frac{1}{2}} = (k+\tfrac{1}{2})\,(\Delta\psi) = \tfrac{1}{2}(\psi_k+\psi_{k+1}), \tag{5.8b}$$

and the constant $R^{-\frac{1}{2}}\bar{b}_k$ are the mean values of ψ and b respectively across the channel. Further integration of (5.8*a*) yields

$$A = (\overline{\partial A/\partial\sigma})_k\,[\tfrac{1}{2}R(\psi-\psi_k)\,(\psi-\psi_{k+1})+\sigma] + \bar{b}_k(\psi-\psi_{k+\frac{1}{2}}) + \text{const.} \tag{5.9}$$

Here we have included the secular term proportional to σ, which is formally small compared with the term $R(\psi-\psi_k)\,(\psi-\psi_{k+1})$ in our large β limit (5.1). The corresponding eddy solutions are given by (3.27*b*).

Now we integrate the heat conduction equation (3.2) over the boundary periodicity domain δD_k to obtain (5.2*a*) as before. Now, however, we have

$$\delta\Sigma \to (2/\tau)\,\pi^2 \quad \text{as} \quad \delta\psi \to 0, \tag{5.10}$$

which is the area of one ($\tau = 2$, E-flows) or two ($\tau = 1$, O-flows) $\mathscr{D}^{\pm}_{m,n}$-eddies inside δD_k. Consequently, in this limit, the consistency condition (5.2*a*) yields the jump condition

$$[\gamma b]^+_- \equiv \lim_{\psi\downarrow\psi_k}(\gamma b) - \lim_{\psi\uparrow\psi_k}(\gamma b) = -(2/\tau)\,R^{\frac{1}{2}}\bar{E} \quad \text{across} \quad C_k. \tag{5.11}$$

Substitution of (5.8*a*) into (5.11) and use of (5.5*a*) yields

$$\Gamma_k\,\bar{b}_k = \Gamma_{k-1}\,\bar{b}_{k-1}. \tag{5.12a}$$

According to (5.4) and (2.48), this relation is satisfied when

$$\bar{b}_k = \Delta_{k+1}\,\bar{b}^M, \tag{5.12b}$$

where $\bar{b}^M$ is as yet an unknown constant that defines the mean value of $\bar{b}_k$ on two adjacent channels;

$$\bar{b}^M = \tfrac{1}{2}(\bar{b}_k+\bar{b}_{k+1}). \tag{5.12c}$$

The determination of $\bar{b}^M$ and the remaining constant in (5.9) requires more detailed information about the channel boundary layers. Some simple properties are noted in our consideration of the two particular cases of parallel and perpendicular fields in the following two sections.

5.2.2. *Parallel fields*

When the mean field $\bar{\boldsymbol{B}}_{\mathrm{H}}$ is aligned to the mean flow $\bar{\boldsymbol{u}}_{\mathrm{H}}$ (see (4.33)), it follows from (3.4) that

$$\bar{A}_{m,n} = \epsilon^{-1}B_{\parallel}(-mN+nM)\,(\Delta\psi) \tag{5.13}$$

and, in particular, that $\bar{A}_{M,N}$ vanishes. In addition (5.6) and (5.7) show that

$$\bar{E} = 0, \quad (\overline{\partial A/\partial\sigma})_k = 0. \tag{5.14a, b}$$

Since there is no secular increase of A down the channel, the term proportional to $(\overline{\partial A/\partial\sigma})_k$ in (5.9) is lost. As a result it is possible to demand that A be continuous across all channel and

eddy boundaries, thus fixing the unknown constant in (5.9). Continuity across channel boundaries is met when

$$A = \Delta_{k+1}\,\bar{b}^M(\psi-\psi_{k+\frac{1}{2}}) + (k+\tfrac{1}{2})\,\bar{b}^M(\Delta\psi) + \bar{A}^M \quad \text{on} \quad D_k, \tag{5.15}$$

where $\bar{A}^M$ is a constant independent of k. The result (5.15) is established by noting that, when applied to two neighbouring channels D_k and D_{k-1}, it yields the same result

$$A = [k-\tfrac{1}{2}(1-\Delta_k)]\,\bar{b}^M(\Delta\psi) + \bar{A}^M \quad \text{on} \quad C_k, \tag{5.16}$$

in both the limits $\psi \downarrow \psi_k$ and $\psi \uparrow \psi_k$. In the case of O-flows, for which Δ_k is unity, this result is obvious. On the other hand, in the case of E-flows we make use of the property (2.50) of Δ_k. It implies that

$$-\tfrac{1}{2}(1-\Delta_k) = \pm\tfrac{1}{2}(1-\Delta_0) \quad \text{on} \quad \mathscr{C}^{\pm}_{m,n}, \tag{5.17a}$$

since, by (2.30a), k is odd and even on $\mathscr{C}^{+}_{m,n}$ and $\mathscr{C}^{-}_{m,n}$-eddy boundaries respectively and, by (2.11), (2.27), takes the values

$$k = (n+\tfrac{1}{2})\,M - (m+\tfrac{1}{2})\,N \pm \tfrac{1}{2}L \quad \text{on} \quad \mathscr{C}^{\pm}_{m,n}. \tag{5.17b}$$

Since $\bar{E}$ vanishes, so does $\bar{b}$ defined by (3.26b). More specifically it implies by (3.24a) that b vanishes in the interior of the closed eddies. There $\bar{A}$ is constant and takes the value

$$A = \bar{A}_{m+\frac{1}{2},\,n+\frac{1}{2}} \pm A_0 \quad \text{on} \quad \mathscr{D}^{\pm}_{m,n}. \tag{5.18}$$

From (5.13) and (5.16)–(5.18), continuity of A across eddy boundaries yields

$$\begin{aligned}\{[(n+\tfrac{1}{2})\,M-(m+\tfrac{1}{2})\,N] \pm \tfrac{1}{2}[L+1-\Delta_0]\}\,\bar{b}^M(\Delta\psi) + \bar{A}^M \\ = [(n+\tfrac{1}{2})\,M-(m+\tfrac{1}{2})\,N]\,\epsilon^{-1}B_{\parallel}(\Delta\psi) \pm A_0 \quad \text{on} \quad \mathscr{C}^{\pm}_{m,n}.\end{aligned} \tag{5.19}$$

This result holds on all $\mathscr{D}^{\pm}_{m,n}$-eddies when

$$\bar{b}^M = \epsilon^{-1}B_{\parallel}, \quad \bar{A}^M = 0, \tag{5.20a, b}$$

$$A_0 = \tfrac{1}{2}A\epsilon^{-1}B_{\parallel}\,\psi^{\mathrm{c}} \quad (\psi^{\mathrm{c}} = L(\Delta\psi)) \tag{5.20c}$$

(see (2.49) and (2.51)).

As the channel and eddy solutions (5.15) and (5.18) are continuous across all boundaries when the constants $\bar{b}^M$, $\bar{A}^M$ and A_0 are given by (5.20), we are not obliged to consider the δ-function sources of b triggered at the X-type stagnation points. These sources were incorporated in the general boundary layer formulation of §4 above. Nevertheless to the lowest order of approximation attempted here, we see that they are negligible for the special case of parallel fields discussed in this section.

The picture which emerges is as follows. From the thermal point of view the closed eddies are isothermal with temperature given by (5.18). On the other hand, from the magnetic point of view, flux is expelled from the eddies and concentrated in the channel regions. Specifically the ψ-derivatives of (5.15) and (5.18) yield using more primitive variables,

$$\frac{\boldsymbol{u}_{\mathrm{H}}\cdot\boldsymbol{B}_{\mathrm{H}}}{|\boldsymbol{u}_{\mathrm{H}}|^2} = \frac{\partial A}{\partial\psi} = \begin{cases}\Delta_{k+1}(\bar{\boldsymbol{u}}_{\mathrm{H}}\cdot\bar{\boldsymbol{B}}_{\mathrm{H}}/|\bar{\boldsymbol{u}}_{\mathrm{H}}|^2) & \text{on} \quad D_k, \qquad (5.21a)\\ 0 & \text{on} \quad \mathscr{D}^{\pm}_{m,n}, \qquad (5.21b)\end{cases}$$

where

$$\bar{\boldsymbol{B}}_{\mathrm{H}} = \bar{b}^{M}\bar{\boldsymbol{u}}_{\mathrm{H}}. \tag{5.21c}$$

The remaining constant A_0 in (5.20c) is given by

$$A_0 = \tfrac{1}{2}A\psi^{c}(\bar{\boldsymbol{u}}_{\mathrm{H}}\cdot\bar{\boldsymbol{B}}_{\mathrm{H}}/|\bar{\boldsymbol{u}}_{\mathrm{H}}|^2). \tag{5.22}$$

Finally we note that by (3.11) the thermal and magnetic problems are related by

$$(\bar{\boldsymbol{u}}_{\mathrm{H}}\times\bar{\boldsymbol{g}}_{\mathrm{H}})_z = \bar{\boldsymbol{u}}_{\mathrm{H}}\cdot\bar{\boldsymbol{B}}_{\mathrm{H}}. \tag{5.23}$$

We finish the section by using our results to calculate the fluxes $\bar{F}_{\mathrm{s}}^{i}$ defined by (3.36), which determine the mean heat flux $\bar{\boldsymbol{F}}_{\mathrm{H}}$ defined by (3.46). Since A is constant in the interior of the eddies and, furthermore, because we are ignoring the boundary layer contributions, it is not necessary to take the formal limit $\pm R^{\frac{1}{2}}\psi_{\pm\infty}\to\infty$ in (3.46). Instead we taken our integrations in (3.36) only up to the eddy boundaries and set $\psi_{\pm\infty}=0$. With (3.37) and (3.38) this yields

$$\pi\bar{F}_{\mathrm{s}}^{i} = \int_{\psi_-^i}^{\psi_+^i} A\,\mathrm{d}\psi - \tfrac{1}{2}(\bar{A}_+^i+\bar{A}_-^i)\,(\psi^{c}+\Delta\psi^{i+1}). \tag{5.24}$$

With A given by (5.15) and (5.20) the contribution to the integral for each channel section D_k is

$$\int_{\psi_k}^{\psi_{k+1}} A\,\mathrm{d}\psi = (k+\tfrac{1}{2})\,\bar{b}^{M}(\Delta\psi)^2 \tag{5.25}$$

and so the complete integral is

$$\int_{\psi_-^i}^{\psi_+^i} A\,\mathrm{d}\psi = \sum_{k=k_-^i}^{k_+^i-1}(k+\tfrac{1}{2})\,\bar{b}^{M}(\Delta\psi)^2 = \tfrac{1}{2}\{[k_+^i]^2-[k_-^i]^2\}\,\bar{b}^{M}(\Delta\psi)^2. \tag{5.26}$$

Since equations (2.37)–(2.41) imply that

$$(k_+^i-k_-^i)\,(\Delta\psi) = \psi_+^i-\psi_-^i = \psi^{c}+\Delta\psi^{i+1} \tag{5.27a}$$

and since (3.38), (5.13) and (5.20a) yield

$$(k_+^i+k_-^i)\,\bar{b}^{M}(\Delta\psi) = \bar{A}_+^i+\bar{A}_-^i, \tag{5.27b}$$

it follows that each of the fluxes (5.24) vanish;

$$\bar{F}_{\mathrm{s}}^{i} = 0. \tag{5.28a}$$

So to the order of accuracy attempted here there is no mean heat flux,

$$\bar{\boldsymbol{F}}_{\mathrm{H}} = 0. \tag{5.28b}$$

Smaller non-zero contributions to $\bar{\boldsymbol{F}}_{\mathrm{H}}$ are only encountered when the boundary-layer effects are included. Since the isotherms (or magnetic field lines) are almost aligned with the flow, the result is not particularly surprising and is in accord with the earlier results of paper 2 for the cat's-eye flow.

PHILOSOPHICAL TRANSACTIONS OF THE ROYAL SOCIETY A MATHEMATICAL, PHYSICAL & ENGINEERING SCIENCES

5.2.3. *Perpendicular fields*

When the mean field $\bar{\boldsymbol{B}}_{\mathrm{H}}$ is directed normal to the mean flow $\bar{\boldsymbol{u}}_{\mathrm{H}}$ (see (4.35)), it follows from (3.4) that

$$\bar{A}_{m,n} = -\epsilon^{-1} B_{\perp}(mM+nN)\,(\Delta\psi). \tag{5.29}$$

Substitution into (5.6) and (5.7*b*) yields

$$\bar{E} = -\epsilon B_{\perp}, \quad \left(\overline{\frac{\partial A}{\partial \sigma}}\right)_k = -\tfrac{1}{4}\pi \frac{(M^2+N^2)^{\frac{1}{2}}}{L\Delta_k} B_{\perp}. \tag{5.30\,a, b}$$

Since $(\overline{\partial A/\partial\sigma})_k$ is of order unity, the leading order R term of (5.9) dominates the channel solution. We ignore the higher-order terms, which depend on boundary-layer corrections, and so obtain the channel solutions,

$$A = (\overline{\partial A/\partial\sigma})_k\,[\tfrac{1}{2}R(\psi-\psi_k)\,(\psi-\psi_{k+1})+(\sigma-\sigma_k)] \quad \text{on} \quad D_k, \tag{5.31\,a}$$

where σ_k is a constant. To the same order of accuracy the eddy solutions (3.27*b*) close to the boundary are

$$A = \pm R^{\frac{1}{2}}\bar{b}(\psi-\psi^{\pm}_{m,n}) + \bar{A}_{m+\frac{1}{2},n+\frac{1}{2}} \quad \text{on} \quad \mathscr{C}^{\pm}_{m,n}, \tag{5.31\,b}$$

where, from (3.26*b*) and (5.30*a*),

$$\bar{b} = -\tfrac{1}{8}\pi^2\beta B_{\perp}, \tag{5.31\,c}$$

in which $\beta\,(=\epsilon R^{\frac{1}{2}})$ is large (see (5.1)). In both (5.31*a*) and (5.31*b*), we have retained the formally small secular contributions. When they are neglected we see that the dominant order β^2 terms vanish at (and therefore continuous across) all channel and eddy boundaries. When, on the other hand, the secular terms in (5.31*a*) are included, it is clear that continuity of A must be abandoned and δ-function sources of b are triggered at the X-type stagnation points.

As in the previous section we recast the results (5.31*a*, *b*) in terms of primitive variables. They become

$$\frac{\boldsymbol{u}_{\mathrm{H}}\cdot\boldsymbol{B}_{\mathrm{H}}}{|\boldsymbol{u}_{\mathrm{H}}|^2} = \frac{\partial A}{\partial\psi} = \begin{cases} -\tfrac{1}{4}R\pi^2(\bar{\boldsymbol{u}}_{\mathrm{H}}\times\bar{\boldsymbol{B}}_{\mathrm{H}})_z\,(\psi-\psi_{k+\frac{1}{2}})/\Delta_k\,\psi^{\mathrm{c}} & \text{on} \quad D_k, \qquad (5.32\,a) \\ \mp\tfrac{1}{8}R\pi^2(\bar{\boldsymbol{u}}_{\mathrm{H}}\times\bar{\boldsymbol{B}}_{\mathrm{H}})_z & \text{on} \quad \mathscr{D}^{\pm}_{m,n}, \qquad (5.32\,b) \end{cases}$$

where for the thermal problem

$$\bar{E} = \bar{\boldsymbol{u}}_{\mathrm{H}}\cdot\bar{\boldsymbol{g}}_{\mathrm{H}} = -(\bar{\boldsymbol{u}}_{\mathrm{H}}\times\bar{\boldsymbol{B}}_{\mathrm{H}})_z. \tag{5.33}$$

Finally we compute the heat fluxes from (3.36), which at lowest order reduce to

$$\pi\bar{F}^i_{\mathrm{s}} = \int_{\psi^i_-}^{\psi^i_+} A\,\mathrm{d}\psi. \tag{5.34\,a}$$

Each channel contribution to the integral obtained from (5.31*a*), with the term proportional to $(\sigma-\sigma_k)$ ignored, is

$$\int_{\psi_k}^{\psi_{k+1}} A\,\mathrm{d}\psi = -\tfrac{1}{12}R(\overline{\partial A/\partial\sigma})_k\,(\Delta\psi)^3. \tag{5.34\,b}$$

Since $(\overline{\partial A/\partial\sigma})_k$ alternates in value from one channel to the next, it is simplest to evaluate the two components of (3.46) directly. They are given by

$$\tfrac{1}{2}\pi(\bar{F}_{\rm s}^{i-1}-\bar{F}_{\rm s}^{i+1}) = \frac{1}{2}\int_{\psi_-^{i-1}}^{\psi_-^{i+1}} A\,\mathrm{d}\psi, \tag{5.35a}$$

because the upper limits $\psi_+^{i\pm1}$ of the two separate integrals $\bar{F}_{\rm s}^{i\pm1}$ are identical. Furthermore since the ψ-range of integration in (5.35a) is $2(\Delta\psi^i)$ (see (2.45c)) it includes an even number of channels. Consequently with (5.34b), equation (5.35a) reduces to

$$\tfrac{1}{2}\pi(\bar{F}_{\rm s}^{i-1}-\bar{F}_{\rm s}^{i+1}) = -\tfrac{1}{12}\mathrm{R}\left(\overline{\frac{\partial A}{\partial\sigma}}\right)^M(\Delta\psi)^2(\Delta\psi^i), \tag{5.35b}$$

where

$$\left(\overline{\frac{\partial A}{\partial\sigma}}\right)^M = \frac{1}{2}\left[\left(\overline{\frac{\partial A}{\partial\sigma}}\right)_k+\left(\overline{\frac{\partial A}{\partial\sigma}}\right)_{k+1}\right] = -\tfrac{1}{4}\pi\frac{(M^2+N^2)^{\frac{1}{2}}}{AL}B_\perp \tag{5.35c}$$

is the mean value of $(\overline{\partial A/\partial\sigma})_k$ over two neighbouring channels (see also Appendix A, particularly (A 1)). Finally with $i=1$ and 2, (5.35) gives

$$\bar{\boldsymbol{F}}_{\rm H} = -\tfrac{1}{12}R\left(\overline{\frac{\partial A}{\partial\sigma}}\right)^M(\Delta\psi)^2\bar{\boldsymbol{u}}_{\rm H} = R\epsilon^3\left(\frac{\pi^3}{48}\right)\frac{1}{AL(M^2+N^2)}B_\perp(M,N). \tag{5.36}$$

The result (5.36) always yields the dominant contribution to $\bar{\boldsymbol{F}}_{\rm H}$, whatever the orientation of $\bar{\boldsymbol{B}}_{\rm H}$, except for the special case in which it is aligned to $\bar{\boldsymbol{u}}_{\rm H}$. In that case, as we have shown in the previous section, $\bar{\boldsymbol{F}}_{\rm H}$ reduces to boundary-layer contributions. So, for the general case, (5.36) yields the result

$$\bar{\boldsymbol{F}}_{\rm H} = -R\left(\frac{\pi^2}{48}\right)\left(\frac{\psi^{\rm c}}{AL^2}\right)\bar{\boldsymbol{u}}_{\rm H}(\bar{\boldsymbol{u}}_{\rm H}\cdot\bar{\boldsymbol{g}}_{\rm H}) \tag{5.37}$$

for the heat flux which, in turn, gives the asymptotic result (4.42) above for the diffusion-matrix, $\boldsymbol{D}$.

5.3. *The magnetic problem*

5.3.1. *The mainstream solution*

At leading order the mainstream problem for the vertical magnetic field, KB, is (3.49), as formulated for the eddy solution. Thus B is given by (3.49b) in which $\mathscr{B}$ continues to be a function of ψ alone. We now follow the development of the thermal problem in §5.2.1. We, therefore, begin by integrating the inhomogeneous heat conduction equation (3.12) over our channel periodicity domain $\delta D(\psi)$ and proceed to the limit $\delta\psi\to0$. The result is

$$[A]_{P_0}^{P_{\rm A}} = \frac{\mathrm{d}}{\mathrm{d}\psi}\left[\int_{C(\psi)}\frac{1}{q}\{\bar{\psi}\bar{E}+R^{-\frac{1}{2}}(\bar{\psi}\nabla^2\psi-\nabla\bar{\psi}\cdot\nabla\psi)\,b\}\,\mathrm{d}s\right]+R^{-1}\frac{\mathrm{d}}{\mathrm{d}\psi}\left(\gamma\frac{\mathrm{d}\mathscr{B}}{\mathrm{d}\psi}\right). \tag{5.38}$$

Its derivation is similar to the eddy argument which proceeds via equations (3.52), (3.53) to the result (3.54). The conspicuously new terms are $[A]_{P_0}^{P_{\rm A}}$ on the left and the term involving $\nabla\bar{\psi}$ on the right. The former emerges from the term, $-\boldsymbol{u}_{\rm H}\cdot\nabla A$, in (3.12$b$), while the latter arises from the final integral in (3.53). In the eddy case neither gives a contribution. Since the jump

$[A]_{P_0}^{P_A}$ over a periodicity interval is constant independent of ψ, differentiation of (5.3a) yields the result

$$0 = \frac{\mathrm{d}}{\mathrm{d}\psi}\left[\int_{C(\psi)} \frac{1}{q}\{\bar{E} + R^{-\frac{1}{2}}(\nabla^2\psi)\, b\}\,\mathrm{d}s\right] + R^{-\frac{1}{2}}\frac{\mathrm{d}}{\mathrm{d}\psi}\left(\gamma\frac{\mathrm{d}b}{\mathrm{d}\psi}\right). \tag{5.39}$$

If we now restrict attention to a channel D_k, it is convenient to multiply (5.39) by $\psi_{k+\frac{1}{2}}$ and subtract the result from (5.38). This yields

$$[A]_{P_0}^{P_A} = \frac{\mathrm{d}}{\mathrm{d}\psi}\left[\int_{C(\psi)} \frac{1}{q}\{(\bar{\psi} - \psi_{k+\frac{1}{2}})\,\bar{E} + R^{-\frac{1}{2}}[(\bar{\psi} - \psi_{k+\frac{1}{2}})\,(\nabla^2\psi) - \nabla\bar{\psi}\cdot\nabla\psi]\, b\}\,\mathrm{d}s\right] + R^{-1}\frac{\mathrm{d}}{\mathrm{d}\psi}\left(\gamma\frac{\mathrm{d}\mathscr{B}_k}{\mathrm{d}\psi}\right), \tag{5.40a}$$

where

$$\mathscr{B}_k(\psi) = \mathscr{B} - R^{\frac{1}{2}}\psi_{k+\frac{1}{2}}\, b. \tag{5.40b}$$

By this device the multiplicative factors $\bar{\psi} - \psi_{k+\frac{1}{2}}$ and $\nabla\bar{\psi}$, both of order ϵ, ensure that the derivative of the $C(\psi)$-integral on the right of (5.40a) is of order ϵ in comparison with $[A]_{P_0}^{P_A}$ on the left, the latter turn being of order unity. (See, for example, the solutions for perpendicular fields in §5.2.3, which render the $C(\psi)$-integral of order ϵ^2. Differentiation with respect to ψ only increases its magnitude by a factor of order ϵ^{-1}.) With this term dropped (5.40a) is readily integrated twice giving

$$\mathscr{B}_k = \tfrac{1}{2}R(\overline{\partial A/\partial\sigma})_k\,(\psi - \psi_{k+\frac{1}{2}})^2 + \bar{f}_k(\psi - \psi_{k+\frac{1}{2}}) + \bar{h}_k \quad \text{on} \quad D_k, \tag{5.41}$$

where $\bar{f}_k$ and $\bar{h}_k$ are as yet unknown constants. To determine the mean electromotive force it is necessary to evaluate $\mathscr{E}$ defined by (3.58b). Use of (5.40b) yields the alternative formula

$$\mathscr{E} = R^{\frac{1}{2}}(\psi - \psi_{k+\frac{1}{2}})\, b - \mathscr{B}_k \quad \text{on} \quad D_k, \tag{5.42a}$$

which with (5.8a) and (5.41) gives

$$\mathscr{E} = \tfrac{1}{2}R(\overline{\partial A/\partial\sigma})_k\,(\psi - \psi_{k+\frac{1}{2}})^2 + (\bar{b}_k - \bar{f}_k)\,(\psi - \psi_{k+\frac{1}{2}}) - \bar{h}_k \quad \text{on} \quad D_k. \tag{5.42b}$$

We now integrate (3.12) over the boundary periodicity domain δD_k and proceed to the limit $\delta\psi \to 0$. It leads to the differential form of (5.38), for which the left hand side is $[A]_{P_0}^{P_A}\mathrm{d}\psi$ and where the differentials denote jumps in values. With the jump in the $C(\psi)$-integral neglected, as above, we obtain the result,

$$[\gamma\,\mathrm{d}\mathscr{B}/\mathrm{d}\psi]_-^+ = 0 \quad \text{across} \quad C_k, \tag{5.43}$$

which corresponds to our earlier thermal result (5.11). From (5.8) and (5.41) is readily shown that

$$\mathrm{d}\mathscr{B}/\mathrm{d}\psi = R(\overline{\partial A/\partial\sigma})_k\,\psi + \bar{f}_k \quad \text{on} \quad D_k. \tag{5.44}$$

Since (5.5a) says that $\Gamma_k(\overline{\partial A/\partial\sigma})_k$ is the same for all channels and since ψ is continuous across C_k, the jump condition (5.43) is satisfied when

$$\Gamma_k\bar{f}_k = \Gamma_{k-1}\bar{f}_{k-1}. \tag{5.45a}$$

Like (5.12a) before it is met by

$$\bar{f}_k = \Delta_{k+1}\bar{f}^M, \tag{5.45b}$$

where $\bar{f}^M$ is some constant taking the same value on all channels.

The jump in the value of A across a channel boundary C_k includes a δ-function source of b

at the X-type stagnation points. No such source is present in B and this is guaranteed only when $\mathscr{B}-R^{\frac{1}{2}}\psi_k b$ has no δ-function source. This observation was the basis of the representation (4.47a) of the boundary layer solutions on the sides $\mathscr{T}^i$ of the primary square. The representation (4.47a) can also be used as the starting point of an investigation of channel boundary layers. Hence the heat conduction equation (4.47b) must be solved subject to the matching condition as $R^{\frac{1}{2}}(\psi-\psi_k)\to\pm\infty$, that $\mathscr{B}-R^{\frac{1}{2}}\psi_k b$ is proportional to $R^{\frac{1}{2}}(\psi-\psi_k)$ plus a constant, whose value in the two neighbouring channels D_{k-1} and D_k differs by at most an order one amount. Since this difference is an order $R^{-\frac{1}{2}}$ smaller than the dominant part which increases linearly with $R^{\frac{1}{2}}(\psi-\psi_k)$, it may be ignored at lowest order and yields the jump condition, which is most conveniently expressed in terms of $\mathscr{E}$ defined by (4.58), namely

$$[\mathscr{E}]^+_- = -[\mathscr{B}-R^{\frac{1}{2}}\psi_k b]^+_- = 0 \quad \text{across} \quad \begin{cases} C_k, & (5.46a) \\ C^{\pm}_{m,n}. & (5.46b) \end{cases}$$

Here we have noted that, unlike the other jump conditions (5.11) and (5.43) which only hold across channel boundaries, this new result is also applicable to eddy boundaries.

In the following two sections we use (5.46) to find the lowest order solutions for the cases of parallel and perpendicular fields separately.

5.3.2. *Parallel fields*

When the magnetic field $\bar{\boldsymbol{B}}_{\mathrm{H}}$ is parallel to $\bar{\boldsymbol{u}}_{\mathrm{H}}$, the horizontal part of the magnetic field is given by the solution to the thermal problem presented in §5.2.2. In particular there is no horizontal magnetic field in the eddies ($\bar{b}=0$) and there is no secular increase of A down the channels. The jump condition (5.46a) implies that $\mathscr{E}$ defined by (5.42b) takes the same value on the channel boundary C_k when evaluated on D_k and D_{k-1}. With (5.12b) and (5.45b) it yields

$$\mathscr{E} = \begin{cases} -\frac{1}{2}\mathcal{A}_{k+1}(\bar{b}^M-\bar{f}^M)\,(\Delta\psi)-\bar{h}_k & \text{as} \quad \psi\downarrow\psi_k \\ \frac{1}{2}\mathcal{A}_k(\bar{b}^M-\bar{f}^M)\,(\Delta\psi)-\bar{h}_{k-1} & \text{as} \quad \psi\uparrow\psi_k \end{cases} \quad \text{on} \quad C_k, \tag{5.47a}$$

and so, by (2.50),

$$(\bar{f}^M-\bar{b}^M)\,(\Delta\psi) = \bar{h}_k-\bar{h}_{k-1}. \tag{5.47b}$$

For O-flows all channels are the same. Hence $\bar{h}_k$ is independent of k with the consequence that $\bar{f}^M=\bar{b}^M$. For E-flows, $\bar{h}_k$ alternates its value from one channel to the next so that the difference $\bar{h}_k-\bar{h}_{k-1}$ is proportional to $(-1)^k$. This only compatible with (5.47b) for all channels when

$$\bar{f}^M=\bar{b}^M, \quad \bar{h}_k=\bar{h}^M \quad \text{(say)}. \tag{5.48}$$

Together, (5.47) and (5.48) show that $\mathscr{E}$ takes the same constant value

$$\mathscr{E} = -\bar{h}^M \quad \text{on} \quad C_k, \tag{5.49a}$$

i.e. on all channel boundaries. When in addition we apply (5.46b) to eddy boundaries, the results (3.56) show that

$$\mathscr{E} = -\bar{h}^M = \mp B_0 \quad \text{on} \quad \mathscr{C}^{\pm}_{m,n}. \tag{5.49b}$$

Clearly this can only hold for both $\mathscr{C}^+_{m,n}$ and $\mathscr{C}^-_{m,n}$-boundaries when

$$B_0=0, \quad \bar{h}^M=0. \tag{5.50}$$

PHILOSOPHICAL TRANSACTIONS OF THE ROYAL SOCIETY A MATHEMATICAL, PHYSICAL & ENGINEERING SCIENCES

The results (5.48) and (5.50) then show that $\mathscr{B}_k$, given by (5.41), is

$$\mathscr{B}_k = \Delta_{k+1}\bar{b}^M(\psi-\psi_{k+\frac{1}{2}}) = R^{\frac{1}{2}}(\psi-\psi_{k+\frac{1}{2}})\,b, \tag{5.51}$$

by (5.15). It follows from (5.40*b*) and (3.49*b*) that

$$\mathscr{B} = R^{\frac{1}{2}}\psi b, \quad B = R^{\frac{1}{2}}(\psi-\bar{\psi})\,b \tag{5.52a, b}$$

everywhere inside the channel regions. In terms of primitive variables, our results are

$$B = \begin{cases} \Delta_{k+1}(\bar{\boldsymbol{u}}_{\mathrm{H}}\cdot\bar{\boldsymbol{B}}_{\mathrm{H}}/|\bar{\boldsymbol{u}}_{\mathrm{H}}|^2)\,(\psi-\bar{\psi}) & \text{on} \quad D_k, \qquad (5.53a) \\ 0 & \text{on} \quad \mathscr{D}^{\pm}_{m,n}. \qquad (5.53b) \end{cases}$$

Furthermore the channel value of $\mathscr{E}$ defined by (5.42*b*) vanishes as does the eddy value by (3.56*b*). Since $\mathscr{E}$ vanishes everywhere so does the horizontal electric field $\boldsymbol{E}_{\mathrm{H}}$ defined by (3.58*a*). An obvious consequence is that there is no mean horizontal electromotive force,

$$K\bar{\boldsymbol{E}}_{\mathrm{H}} = 0, \tag{5.54}$$

a result which is completely analogous to the thermal result (5.28*b*). Again, as in that problem, the small non-zero contributions to $\bar{\boldsymbol{E}}_{\mathrm{H}}$ only emerge at higher order, when the boundary layers corrections are incorporated.

5.3.3. *Perpendicular fields*

When the mean magnetic field $\bar{\boldsymbol{B}}_{\mathrm{H}}$ is perpendicular to $\bar{\boldsymbol{u}}_{\mathrm{H}}$, the horizontal part of the magnetic field is given by the solution to the thermal problem presented in §5.2.3. The lowest-order approximation to be determined from (5.31*a*) is

$$b = R^{\frac{1}{2}}(\overline{\partial A/\partial\sigma})_k\,(\psi-\psi_{k+\frac{1}{2}}) \quad \text{on} \quad D_k, \tag{5.55}$$

while to the same order of accuracy $\mathscr{E}$ is given by (5.42*b*) with $\bar{b}_k = 0$. Consequently continuity of $\mathscr{E}$ across the channel boundary C_k yields with (5.45*b*) the result

$$\mathscr{E} = \begin{cases} \frac{1}{8}R(\overline{\partial A/\partial\sigma})_k\,(\Delta\psi)^2+\frac{1}{2}\Delta_{k+1}\bar{f}^M(\Delta\psi)-\bar{h}_k & \text{as} \quad \psi\downarrow\psi_k \\ \frac{1}{8}R(\overline{\partial A/\partial\sigma})_{k-1}\,(\Delta\psi)^2-\frac{1}{2}\Delta_k\bar{f}^M(\Delta\psi)-\bar{h}_{k-1} & \text{as} \quad \psi\uparrow\psi_k \end{cases} \quad \text{on} \quad C_k \tag{5.56a}$$

and so, by (2.50),

$$\bar{f}^M(\Delta\psi) = [\bar{h}_k-\tfrac{1}{8}(\overline{\partial A/\partial\sigma})_k\,(\Delta\psi)^2]-[\bar{h}_{k-1}-\tfrac{1}{8}R(\overline{\partial A/\partial\sigma})_{k-1}\,(\Delta\psi)^2]. \tag{5.56b}$$

Using the argument following (5.47*b*) we obtain

$$\bar{f}^M = 0, \quad \bar{h}_k = \tfrac{1}{8}R(\overline{\partial A/\partial\sigma})_k\,(\Delta\psi)^2+B^{\mathrm{s}}, \tag{5.57}$$

where B^{s} is a constant independent of k. Together (5.56*a*) and (5.57) show that $\mathscr{E}$ takes the same constant value

$$\mathscr{E} = -B^{\mathrm{s}} \quad \text{on} \quad C_k, \tag{5.58}$$

that is, on all channel boundaries. The corresponding value of $\mathscr{E}$ on the eddy boundaries, given by (3.62) with $\psi = \psi^{\pm}_{m,n}$, is

$$\mathscr{E} = \tfrac{1}{2}R^{\frac{1}{2}}\bar{b}\psi^{\mathrm{c}}\mp B_0 \quad \text{on} \quad \mathscr{C}^{\pm}_{m,n}. \tag{5.59}$$

Since $\mathscr{E}$ takes the same value, $-B^{\mathrm{s}}$, on both $\mathscr{C}^{+}_{m,n}$ and $\mathscr{C}^{-}_{m,n}$-boundaries, it follows immediately that

$$B_0 = 0, \quad B^{\mathrm{s}} = -\tfrac{1}{2}R^{\frac{1}{3}}\bar{b}\psi^{\mathrm{c}}. \tag{5.60}$$

We now substitute the results (5.57), (5.60) into (5.41) and use (5.40b) and (5.55) to obtain

$$\mathscr{B} = \tfrac{1}{2}R(\overline{\partial A/\partial\sigma})_k\{(\psi-\psi_{k+\frac{1}{2}})(\psi+\psi_{k+\frac{1}{2}})+\tfrac{1}{4}(\Delta\psi)^2\}+B^{\mathrm{s}} \quad \text{on} \quad D_k. \tag{5.61}$$

It follows from (3.49b), after making use of (5.55) again, that

$$B = \tfrac{1}{2}R(\overline{\partial A/\partial\sigma})_k\{(\psi-\bar{\psi})^2-(\psi_{k+1}-\bar{\psi})(\psi_k-\bar{\psi})\}+B^{\mathrm{s}} \quad \text{on} \quad D_k. \tag{5.62a}$$

In the closed eddies, on the other hand, near the the boundaries $\mathscr{C}^{\pm}_{m,n}$, we have from (2.9d), (3.26a), (3.56b) and (5.60) that

$$B = \pm R^{\frac{1}{3}}\bar{b}(\psi^{\pm}_{m,n}-\bar{\psi})+B^{\mathrm{s}} \quad \text{on} \quad \mathscr{D}^{\pm}_{m,n}. \tag{5.62b}$$

In terms of primitive variables the results (5.62a, b) are

$$B-B^{\mathrm{s}} = \begin{cases} -\tfrac{1}{8}R\pi^2(\bar{\boldsymbol{u}}_{\mathrm{H}}\times\bar{\boldsymbol{B}}_{\mathrm{H}})_z\{((\psi-\bar{\psi})^2-(\psi_{k+1}-\bar{\psi})(\psi_k-\bar{\psi}))/\Delta_k\psi^{\mathrm{c}}\} & \text{on} \quad D_k, \quad (5.63a) \\ \mp\tfrac{1}{8}R\pi^2(\bar{\boldsymbol{u}}_{\mathrm{H}}\times\bar{\boldsymbol{B}}_{\mathrm{H}})_z(\psi^{\pm}_{m,n}-\bar{\psi}) & \text{on} \quad \mathscr{D}^{\pm}_{m,n} \end{cases} \tag{5.63b}$$

(cf. the thermal problem results (5.32)), where, by (5.60),

$$B^{\mathrm{s}} = \tfrac{1}{16}R\pi^2(\bar{\boldsymbol{u}}_{\mathrm{H}}\times\bar{\boldsymbol{B}}_{\mathrm{H}})_z\psi^{\mathrm{c}}. \tag{5.64}$$

To calculate the mean electromotive force we first require the channel value of $\mathscr{E}$. Substitution of (5.55), (5.61) into (3.58b) yields

$$\mathscr{E} = \tfrac{1}{2}R(\overline{\partial A/\partial\sigma})_k(\psi-\psi_k)(\psi-\psi_{k+1})-B^{\mathrm{s}}. \tag{5.65}$$

To calculate $\mathscr{E}^i_{\mathrm{s}}$ defined by (3.67) we may proceed as in the case of the thermal problem in §5.2 and set $\psi_{\pm\infty} = 0$. By this device $\bar{E}^i_{\mathrm{s}}$ defined by (3.65) reduces to

$$\pi\bar{E}^i_{\mathrm{s}} = \int_{\psi^i_-}^{\psi^i_+}\mathscr{E}\,\mathrm{d}\psi, \tag{5.66a}$$

where each channel contribution determined from (5.65) is

$$\int_{\psi_k}^{\psi_{k+1}}\mathscr{E}\,\mathrm{d}\psi = -\tfrac{1}{12}R(\overline{\partial A/\partial\sigma})_k(\Delta\psi)^3-B^{\mathrm{s}}(\Delta\psi). \tag{5.66b}$$

Except for the additional term, $-B^{\mathrm{s}}(\Delta\psi)$, this is the same as the result (5.34b). Following the arguments which lead to (5.35) we obtain from (5.66) the result

$$\tfrac{1}{2}\pi(\bar{E}^{i-1}_{\mathrm{s}}-\bar{E}^{i+1}_{\mathrm{s}}) = -\{\tfrac{1}{12}R(\overline{\partial A/\partial\sigma})^M(\Delta\psi)^2+B^{\mathrm{s}}\}(\Delta\psi^i), \tag{5.67a}$$

in which it is readily shown from the definitions that

$$B^{\mathrm{s}} = -\tfrac{1}{4}R\Lambda(\overline{\partial A/\partial\sigma})^M[\psi^{\mathrm{c}}]^2. \tag{5.67b}$$

Hence it follows from (3.68) with $i = 1$ and 2 in (5.67a) that

$$\bar{\boldsymbol{E}}_{\mathrm{H}} = -\left(1-\frac{1}{3\Lambda L^2}\right)B^{\mathrm{s}}(-\bar{u}_y, \bar{u}_x), \tag{5.68a}$$

$$= -R\epsilon^3\left(\frac{\pi^3}{16}\right)\frac{L}{(M^2+N^2)}\left(1-\frac{1}{3\Lambda L^2}\right)B_{\perp}(-N, M). \tag{5.68b}$$

As in the thermal problem, the result (5.68) gives the dominant contribution to $\bar{\boldsymbol{E}}_{\mathrm{H}}$, whatever the orientation of $\bar{\boldsymbol{B}}_{\mathrm{H}}$ except for the special case in which it is aligned to $\bar{\boldsymbol{u}}_{\mathrm{H}}$, when it is small anyway. So, for the general case, (5.68) yields the result

$$K\bar{\boldsymbol{E}}_{\mathrm{H}} = \tfrac{1}{16}KR\pi^2\left(1-\frac{1}{3\Lambda L^2}\right)\psi^{\mathrm{c}}\bar{\boldsymbol{u}}_{\mathrm{H}}\times(\bar{\boldsymbol{u}}_{\mathrm{H}}\times\bar{\boldsymbol{B}}_{\mathrm{H}}) \tag{5.69}$$

for the mean electromotive force which, in turn, gives us the asymptotic result (4.64) above for the α-matrix, $\boldsymbol{\alpha}$.

Finally we remark briefly about the large L limit. In that case $\Delta\psi$ tends to zero and so ψ_{k+1} and ψ_k tend to the value ψ on D_k. This means that B defined by (5.62a) is given asymptotically by

$$B = B^{\mathrm{s}} \quad \text{on} \quad D_k \quad \text{as} \quad L\to\infty, \tag{5.70}$$

while the mean electromotive force (5.68a) becomes

$$K\bar{\boldsymbol{E}}_{\mathrm{H}} = \bar{\boldsymbol{u}}_{\mathrm{H}}\times(0, 0, KB^{\mathrm{s}}) \quad \text{as} \quad L\to\infty. \tag{5.71}$$

The latter result is not that surprising as the mean flow linked with $\bar{\boldsymbol{u}}_{\mathrm{H}}$ is constrained to follow the channel regions, where the vertical field, KB, is uniform.

6. Boundary layers and error estimates

6.1. *Boundary-layer widths*

The estimates of mainstream channel solutions, upon which the results of §5 depend requires the ratio of the channel boundary layer width, $R^{-\frac{1}{2}}(\Delta\zeta)_{\mathrm{ch}}$, to the channel width, $R^{-\frac{1}{2}}(\Delta\zeta)$, to be small;

$$\mu \equiv (\Delta\zeta_{\mathrm{ch}})/(\Delta\zeta) \ll 1, \tag{6.1}$$

where $\Delta\zeta$ is defined by (4.5b). On the basis of this inequality an order of magnitude estimate was obtained in §3.3, which led to the inequality (5.1). In this section we make quantitive estimates of $\Delta\zeta_{\mathrm{ch}}$ (see (6.3) below) to determine the conditions under which our asymptotic results should reasonably approximate the numerical results of §4.

Consider, for example, the streamline C_0 over the periodicity interval OO_Δ illustrated in figure 2. The boundary layer solution on one side of it, either in the channel D_0 above or in the channel D_{-1} below, can be constructed of modes with σ-periodicity, $2\pi/\Gamma_k$, where k is either 0 or -1 respectively. The corresponding solutions of the heat conduction equation

$$\partial\theta/\partial\sigma = \partial^2\theta/\partial\zeta^2 \tag{6.2a}$$

governing a scalar θ, which underlies our boundary layer problems, are composed of modes proportional to

$$\theta_n = \exp\left[2in\pi\sigma/\Gamma_k - (1-i)\,(n\pi/\Gamma_k)^{\frac{1}{2}}|\zeta|\right] \quad (n = 1, 2, \ldots). \tag{6.2b}$$

The lowest mode $n = 1$ is the least damped in the ζ-direction and provides the dominant contribution to the solution at large $|\zeta|$. We quantify its width by the ζ-distance

$$\Delta\zeta_{\mathrm{ch}} = (\Gamma_k \pi)^{\frac{1}{2}} \tag{6.3}$$

between two successive zeros of the real or imaginary part of θ_1 at fixed σ. The boundary layer width, $(\Delta\zeta)_{\mathrm{ed}}$, on the interior of the closed eddies may be defined in a similar way. There the circulation integral Γ is ± 8 (see (2.33)) and so the formula (6.3) yields

$$\Delta\zeta_{\mathrm{ed}} = (8\pi)^{\frac{1}{2}}. \tag{6.4}$$

With the result (2.48) and (6.3) it gives

$$\Delta\zeta_{\mathrm{ch}} = (L\Delta_k/\tau)^{\frac{1}{2}}(\Delta\zeta_{\mathrm{ed}}). \tag{6.5}$$

It follows from (4.5b) that the ratio μ in (6.1) is

$$\mu_k = (8\Delta_k/\pi)^{\frac{1}{2}} L^{\frac{1}{2}}(M^2 + N^2)^{\frac{1}{2}}\beta^{-1}. \tag{6.6}$$

The two interior boundary layers of a channel D_k adjacent to its bounding streamlines C_k and C_{k+1} decay exponentially and will not interact when well separated. In practice this condition is met when $\mu_k + \mu_{k+1}$ is less than about unity. At fixed ϵ, this condition is always met by flows with rational tangents for sufficiently large R. We will call such solutions resonances. At fixed β, on the other hand, the condition is only met by resonances with sufficiently small values of M and N. That subset of resonant solutions will be referred to as strong resonances.

The values of $\Delta\zeta$, $\Delta\zeta_{\mathrm{ch}}$ and $\Delta\zeta_{\mathrm{ed}}$ for the results illustrated in figures 9–12 are listed in table 1. Strong resonances occur for the O-flows $(M, N) = (0, 1), (1, 2)$ and the E-flow $(M, N) = (1, 1)$ shown in a, b and d of the above figures, all of which have $\Delta\zeta = 24$. Agreement of the analytic with the numerical results is reasonably good for the case of perpendicular mean fields shown in figures 10 and 12, but the discrepancies are larger for the case of parallel mean fields shown in figures 9 and 11. Consider, for example, the case $(M, N) = (0, 1)$. The channel value of about 0.12 shown in figure 9a is approximately 10% smaller than the asymptotic value 0.13 listed in table 2. Here a comparison with the corresponding analytic result (4.30) of paper 2 for cat's-eye flows, which includes the boundary layer corrections is interesting. That result shows that, in the notation of paper 2, the boundary layer correction is $4\Gamma\beta^{-1}$, where the channel width is 2β, the channel boundary layer width is approximately 3.5 (paper 2, equation (4.51b)) and Γ is approximately 0.25 (paper 2, equation (A 7a)). Hence for the paper 2 cat's-eye problem, we have

$$\mu_{\mathrm{CS}} = (\Delta\zeta_{\mathrm{ch}})/(\Delta\zeta) \doteqdot (7/4)\,\beta^{-1}, \tag{6.7}$$

(cf. (6.6) above). It follows that the discrepancy in b for those results is approximately $(4\Gamma\beta^{-1} =)\,\frac{4}{7}\mu_{\mathrm{CS}}$. For our problem, namely $(M, N) = (0, 1)$, $\Delta\zeta = 24$, $\Delta\zeta_{\mathrm{ch}} \doteqdot 5$ (see table 1), we have μ approximately equal to 0.2, for which the paper 2 result $\frac{4}{7}\mu$ also gives a discrepancy of about 10%. This is a very reassuring check of the validity of our results. Further direct comparisons of the numerical and analytic results are provided by the numerical and

asymptotic value of A_0 listed in table 2. For the case $(M, N) = (0, 1)$ the discrepancy between the two values is again about 10%, as it is for the other O-flows $(M, N) = (1, 2)$ and $(1, 6)$; even though the latter case is not a strong resonance. In the E-flow case $(M, N) = (1, 1)$, the discrepancy is less, about 5%.

For our three strong resonant cases $(M, N) = (0, 1)$, $(1, 2)$ and $(1, 1)$ of non-interacting boundary layers, the distances $\Delta\zeta_{\mathrm{ch}}$ and $\Delta\zeta_{\mathrm{ed}}$ measure the distances between the successive zeros of the boundary layer corrections. They are not always clearly identifiable on figures 9–12 but, when they are, they evidently agree.

So far we have stressed channel and eddy periodicity in order to understand the characteristics of our boundary layer solutions. The other fundamental point of view, which we introduced in §3.3, is that boundary layers are triggered at the X-type stagnation points and evolve downstream either on the eddy or channel boundary (see figure 7). In order to interpret this downstream evolution from figures 9–12 it is necessary to appreciate the nature of the division of boundary layer solutions portrayed in the figures upon arrival at the end of the side $\mathscr{T}^i$. Data is divided at the stagnation point O^{i+1} with coordinate $\xi = \Delta\zeta^i$. The subsequent mapping of data for positive (negative) $\xi - \Delta\zeta^i$ to the start of the next (previous) side $\mathscr{T}^{i+1}(\mathscr{T}^{i-1})$ is accomplished by (A 3) and illustrated symbolically in figure 8. Since ξ increases to the left on figures 9–12, the pictured terminal data to the left (right) of $\xi = \Delta\zeta^i$ provides the initial data to the left (right) of $\xi = 0$ for the results shown in the next (previous) picture, taken in cyclic (anticyclic) order. By this device it is a simple matter to follow in sequence the development along any streamline. For the O-flows $(M, N) = (0, 1)$ and $(1, 2)$ single streamline sequences 1–8 and 1–16 are indicated in figures 3 and 4 respectively, while for the E-flow $(M, N) = (1, 1)$ a pair of streamline sequences 1–6 and 0′–5′ are indicated in figure 5. The location of these points for the solutions at the end of the sides $\mathscr{T}^i$ is indicated on figures 9*a*, *b* and *d*. A single streamline sequence 1–32 is also indicated for the O-flow $(M, N) = (1, 6)$ on figure 9*c*. Note, in particular, that the interior $\mathscr{C}^+_{0,0}$-boundary layer is easily identified by the left hand vertical broken lines in figures 9 and 11. The interior of the $\mathscr{D}^+_{0,0}$-eddy lies to the left of these lines. The downstream development follows the structure at the stagnation point $\mathrm{O}^0, \mathrm{O}^1, \mathrm{O}^2, \mathrm{O}^3$ taken in cyclic order (see (A 4*a*)). The exterior $\mathscr{C}^-_{m,n}$-boundary layers are identified by the right hand broken lines with the corresponding $\mathscr{D}^-_{m,n}$-eddy interiors on their right. Now the downstream development follows the stagnation points $\mathrm{O}^3, \mathrm{O}^2, \mathrm{O}^1, \mathrm{O}^0$ taken in anticyclic order (see (A 4*b*) and also figure 6). In case of the channels, identified by the regions between pairs of vertical broken lines in figures 9 and 11*a*, *b* and *d*, a sequence generally consists both of cyclic and anticyclic movements (see (A 5)) and as a result a channel visits the same stagnation point on a number of separate occasions.

The resonant O-flow $(M, N) = (1, 6)$ solution on figures 9–12*c* was chosen with $(\Delta\zeta)$ and $(\Delta\zeta)_{\mathrm{ch}}$ equal. If we look, for example, at the parallel field case, which illustrates *b* in figure 9*c*, we see how the boundary layer triggered at the X-type stagnation point O^0 evolves through the sequence 1–13 (the X-type stagnation point O^1). Through diffusion it thickens and smears out to leave oscillations whose period is two channel widths, compatible with our periodicity arguments. Of course, boundary-layer thickening is also apparent in the strong resonant cases as a streamline boundary sequence is followed.

PHILOSOPHICAL TRANSACTIONS OF THE ROYAL SOCIETY A MATHEMATICAL, PHYSICAL & ENGINEERING SCIENCES

6.2. *The eddy-diffusivity and α-effect*

The results of paper 2 lead us to believe that all mainstream solutions have power series expansions in inverse powers of β, when the boundary layers on either side of channels are non interacting. So in particular, for strong resonances, we postulate that the computed quantities $\tilde{D}^{\rm num}$ and $\tilde{\alpha}^{\rm num}$ defined by (4.43) and (4.66) have the expansions

$$\tilde{D}^{\rm num} = \tilde{D}^0_0 + (\Delta\zeta)^{-1}\tilde{D}^1_0 + \ldots, \tag{6.8a}$$

$$\tilde{\alpha}^{\rm num} = \tilde{\alpha}^0_0 + (\Delta\zeta)^{-1}\tilde{\alpha}^1_0 + \ldots, \tag{6.8b}$$

in which the leading coefficients

$$\tilde{D}^0_0 = \epsilon^{-3}R^{-1}D_0, \quad \tilde{\alpha}^0_0 = \epsilon^{-3}R^{-1}\alpha_0 \tag{6.9a, b}$$

take the values (4.42b), (4.64b) respectively. Of course, in the limit $\Delta\zeta \to \infty$, the diffusion and α-matrices take on the limiting forms (4.42a) and (4.64a) respectively. On the basis of this hypothesis, we interpolate the numerically computed values of $\tilde{D}^{\rm num}$ and $\tilde{\alpha}^{\rm num}$ listed in tables 4 and 5 to obtain better numerical estimates of $\tilde{D}^0_0$ and $\tilde{\alpha}^0_0$. The value of $\tilde{D}^0_0$ is given by the formula,

$$\tilde{D}^0_0 = 2[\tilde{D}^{\rm num}]_{|\boldsymbol{\eta}_{\rm H}|=60} - [\tilde{D}^{\rm num}]_{|\boldsymbol{\eta}_{\rm H}|=30} + O[(\Delta\zeta)^{-2}], \tag{6.10}$$

while a similar expression gives the value of $\tilde{\alpha}^0_0$.

Of course, the order $(\Delta\zeta)^{-2}$ error in (6.10) is for fixed M and N. The separation of the channel boundary layers depends on the ratio $(\mu = (\Delta\zeta_{\rm ch})/(\Delta\zeta))$. So for our solutions obtained at the two values of $|\boldsymbol{\eta}_{\rm H}|$, namely 30 and 60, the channel width $\Delta\zeta$ decreases with M and N. Consequently the condition, μ small, is only met by small values of M and N. In the case of the diffusion coefficient $\tilde{D}^0$, its irrational tangent limit is zero (see (4.42b)). It is clear from table 4 that there is good agreement with the numerical value of $\tilde{D}^0_0$ obtained from (6.10) with the asymptotic value for the strong resonances $(M, N) = (0, 1)$ and $(1, 1)$, and reasonable agreement for the resonances $(M, N) = (1, 2)$ and $(1, 3)$ for which μ is close to unity for the case $|\boldsymbol{\eta}_{\rm H}| = 30$. The larger values of M, N listed do not meet the non-interacting boundary-layer condition and we do not expect the asymptotic theory, upon which (6.10) depends, to apply. Nevertheless there is a clear tendency for the remaining values of $\tilde{D}^0_0$ to approach the irrational tangent limit zero. A more comprehensive coverage of the values of $[\tilde{D}^{\rm num}]_{|\boldsymbol{\eta}_{\rm H}|=60}$ is illustrated in figure 13 over the range $0 \leqslant M/N \leqslant 1$. The strong resonances $M/N = 0, 1$ at either end of the range are clearly visible, as are the resonances $M/N = \frac{1}{3}, \frac{1}{2}$. The asymptotic values of $\tilde{D}^0_0$ listed in table 4 are indicated by the stars. The corresponding results for $[\tilde{\alpha}^{\rm num}]_{|\boldsymbol{\eta}_{\rm H}|=60}$ are illustrated in figure 14, with the irrational limit (4.64c) given by the upper smooth curve.

The general trend, highlighted by the numerical results illustrated in figures 13 and 14, is for the computed values of $\tilde{D}^{\rm num}$ and $\tilde{\alpha}^{\rm num}$ to approach their corresponding irrational tangent limits. As this happens the resonances (or rational tangents), on becoming strong, poke through, adding a spike to the curve. The corresponding half-width $\Delta_{\rm sp}$ is determined by that misalignment of the streamlines which lie within the channel boundary layer width. Specifically suppose we consider a strong resonance $(\Delta\zeta)\,(M, N)$ and consider neighbouring mean flows $\boldsymbol{\eta}_{\rm H}$ of the same magnitude, then the mismatch of the streamlines of $\boldsymbol{\eta}_{\rm H}$ with the resonant case is of order

$$|(\eta_x/\eta_y) - (M/N)||\boldsymbol{\eta}_{\rm H}| \tag{6.11}$$

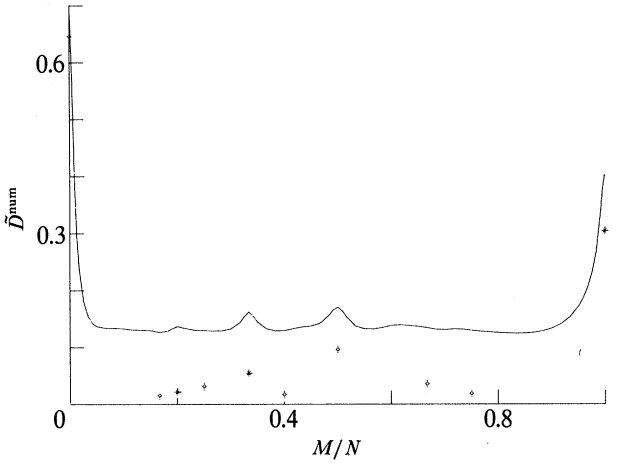

FIGURE 13. The numerical values of $\tilde{D}^{\mathrm{num}}$ for the case $|\boldsymbol{\eta}_{\mathrm{H}}| = 60$ plotted against the tangent M/N over the range $0 \leqslant M/N \leqslant 1$. The asymptotic values given in table 4 are marked individually. Those for E-flows are identified by ✷ and those for O-flows are identified by ✧ . The irrational tangent limit is the axis $\epsilon^{-3}R^{-1}D_0 = 0$.

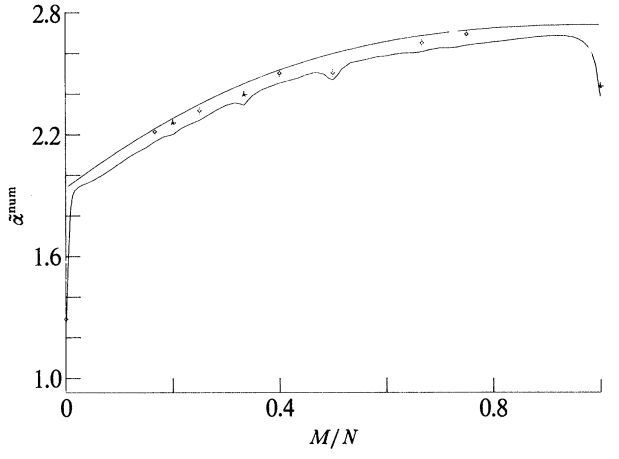

FIGURE 14. The numerical values of $\tilde{\alpha}^{\mathrm{num}}$ for the case $|\boldsymbol{\eta}_{\mathrm{H}}| = 60$ plotted against the tangent M/N, as in figure 13. The irrational tangent limit is the smooth upper curve.

at the end of one side $\mathscr{T}^i$ of the primary square Π. Along the length of that side the circulation integral is 2 and so the relevant channel boundary layer width is obtained by setting $\Gamma_k = 2$ in (6.3). It gives the rough estimate

$$\Delta_{\mathrm{sp}} = |(\eta_x/\eta_y) - (M/N)| = (2\pi)^{\frac{1}{2}}/|\boldsymbol{\eta}_{\mathrm{H}}| = (2/\pi)^{\frac{1}{2}}\beta^{-1}. \tag{6.12}$$

For $|\boldsymbol{\eta}_{\mathrm{H}}| = 60$, used in figures 13 and 14, this gives

$$\Delta_{\mathrm{sp}} \approx 0.025, \tag{6.13}$$

which appears to be roughly in agreement with the widths of the spikes shown.

Even for the relatively moderate value of $|\boldsymbol{\eta}_{\mathrm{H}}|$ used in figures 13 and 14 much fine structure has emerged, which we have not completely resolved. It should be noted, however, that because of the finite magnetic diffusivity the curves are smooth. The apparent roughness stems from the fact that we have joined the computed points by straight line segments. As $|\boldsymbol{\eta}_{\mathrm{H}}|$ increases more and more spikes poke through and existing spikes sharpen according to the

criterion (6.12). In the limit $|\eta_H| \to \infty$, the spikes are dense on the line $0 \leqslant M/N \leqslant 1$ and the resulting curve is nowhere differentiable.

It is perhaps worth commenting on the asymptotic behaviour, at large β, for which strong resonances occur when

$$L = O(\beta^{\frac{2}{3}}) \quad (\beta \gg 1), \tag{6.14}$$

(see (5.1)). Since the corresponding number of strong resonances is of order $L^2 (= \beta^{\frac{4}{3}})$ and the spike widths is of order β^{-1}, (see (6.12)) the spikes more than fill the unit interval $0 \leqslant M/N \leqslant 1$. This means that the curves portrayed in figures 13 and 14 become everywhere spiky for large β with only the strongest resonances being distinguishable.

7. Concluding remarks

In this paper we have presented a comprehensive investigation of the nature of scalar diffusion and magnetic induction in a particular spatially periodic steady flow with mean motion. The main objective of the work has been to describe a class of steady flows with complicated streamline topology, which lie between simpler examples such as the cat's-eye flow of paper 2, and the three-dimensional ABC-flows mentioned in the introduction. Although our analysis has not produced explicit fast dynamos within this family of motions, the methods may be useful in tackling the more complicated but also more promising question of fast dynamo action in steady flows with chaotic streamlines.

There are some features of chaotic streamline geometry which are mirrored in our almost-periodic geometry here appropriate to the irrational limit. In both cases steady flow patterns generally have boundary-layer structure which is dense in some finite region. While there is undoubtedly a different topology (for example, that of a Cantor set) that arises in chaotic flows, the basic response of the magnetic field at large R is similar in the two problems. As the discussion of §6 explains, magnetic field structure on finer and finer length scales emerges in the limit $R \to \infty$ in the irrational case. This structure tends to produce fluctuations in the α-effect as a function of R, which tend to decrease in amplitude for large R. In this way the occurrence of fast dynamo action is characterized by a well-defined limit as $R \to \infty$, although numerically large values of R may be needed. Indeed Soward (1989) showed that in the two-dimensional Roberts case discussed by Galloway & Frisch (1986), the asymptotic behaviour is not reached until values of R of order 10^4. If this estimate applies to the three-dimensional ABC flows, an asymptotic régime, where fast dynamo action can be assessed, may require R to be 10 or 100 times larger than the maximum value in Galloway & Frisch (1986).

The above remarks relate to the magnitude of the α-matrix when the vertical z-dependence of the mean magnetic field proportional to e^{iqz} is included. To estimate the range of validity of the present theory and the magnitude of modifications which ensue at finite q, we must investigate the role of vertical advection. In paper 2 we noted that for the cat's-eye problem the asymptotic validity with increasing q is first broken by the vertical advection of magnetic field in the channels. For our mean flow problem the effect of vertical advection is more potent in the eddies themselves, where it gives rise to a new term of order $K\psi' \partial A/\partial z$ on the right of (3.25a). This yields the estimate

$$\frac{\mathrm{d}}{\mathrm{d}\psi}\left(\gamma \frac{\mathrm{d}\bar{A}}{\mathrm{d}\psi}\right) - R\bar{E}\frac{\mathrm{d}\Sigma}{\mathrm{d}\psi} \sim \mathrm{i}KR(\psi - \bar{\psi})\, q\bar{A}. \tag{7.1}$$

Our earlier result (3.24) thus continues to hold when KRq is small. When KRq is large, on the other hand, a boundary layer is formed and the mainstream solution of (7.1), which ignores the first term on the left, gives $\bar{A}$ of order $\bar{E}/Kq(\psi-\bar{\psi})$ in the eddy interior. This means that the size of $\bar{b}$ on the eddy boundaries is of order $R^{-\frac{1}{2}}\bar{E}/Kq\epsilon^2$, smaller by a factor $(KqR\epsilon^2)^{-1}$ than that given by (3.26b). This in turn reduces the vertical B-field in the eddy by an order of magnitude. Thus the vertical channel field, which is controlled by the boundary value (3.57), is likewise reduced causing a corresponding reduction of the α-effect.

We must distinguish carefully between the cases of rational and irrational tangents. In the irrational limit the horizontal field b in the channel tends to zero. A similar expulsion of vertical field occurs, leaving the uniform component B^s (cf. (5.64)). This is fixed by the matching across the eddy boundary. So, when KRq is large and the eddy B-field is small, the electromotive force is reduced in concert. It is difficult to estimate the exact size of the α-effect in this limit but we may reasonably suppose that it is smaller than (4.64c) by the vertical eddy B-field reduction factor of order $(KqR\epsilon^2)^{-1}$:

$$\alpha_0^{\mathrm{irr}} = O(\epsilon/q) \quad (q \gg (KR)^{-1}). \tag{7.2}$$

For rationals, on the other hand, the expulsion of flux from the eddies does not effect the order of magnitude of the channel fields and the estimate $\alpha_0 = O(K\epsilon^3 R)$ given by (4.64b) remains valid. The limitations on the validity of this estimate now emerges from the channel solutions. So, in place of (7.1), we consider the corresponding modification of the channel equation (5.7a), namely

$$\mathrm{d}^2\bar{A}/\mathrm{d}\psi^2 - R(\overline{\partial A/\partial\sigma})_k \sim \mathrm{i}K\epsilon RqA. \tag{7.3}$$

This forces $\bar{A}$ to decay on the boundary layer width $(K\epsilon Rq)^{-\frac{1}{2}}$. It is comparable to the channel width when

$$q = O(K\epsilon^3 R)^{-1}. \tag{7.4}$$

Consequently, our order $K\epsilon^3 R$ estimate for α_0 remains valid for $q \ll (K\epsilon^3 R)^{-1}$. For shorter vertical length scales q^{-1} the magnitude of α_0 is reduced by an order of magnitude.

We comment now on the interesting question of fast dynamo action. The α-matrices, which we have calculated for large R (cf. (4.64)), are singular and do not by themselves lead to a dynamo at all. To test whether dynamo action is possible it is necessary to calculate the induced mean electromotive force when the mean magnetic field is parallel to the mean flow as in paper 2. Instead, we explore the possibility of a dynamo when the mean flow (1.2c) varies its orientation slowly with z. In other words, we consider the case

$$0 < l \ll 1 \tag{7.5}$$

instead of the limit $l \to 0$, which leads to (1.9). To estimate the growth rate of magnetic field we may assume that the α-effect is constant independent of the orientation of the mean flow. The problem then coincides with a model considered by Soward & Childress (1986). Their results showed that the fastest growing mode had a wavenumber (q in (1.3a)) equal to l in the vertical z-direction and that the growth rate p is

$$p \sim \alpha_0 l. \tag{7.6}$$

It is likely that this is maximized with increasing l when KRl is of order unity, i.e. precisely at the point where our estimate $\alpha_0 \sim K\epsilon^3 R$ is no longer strictly valid. If we nevertheless suppose that it is, we obtain the fast dynamo estimate $p \sim \alpha_0 l \sim \epsilon^3$. Alternatively we might increase l yet further and adopt (7.2) valid for $l \gg (KR)^{-1}$, appropriate because during the rotation of the mean velocity vector $\bar{\boldsymbol{u}}_{\mathrm{H}}$ with z it is largely the irrational tangents that are sampled. In that region of parameter space we obtain $p \sim \epsilon$. The discrepancy between the order ϵ and ϵ^3 estimates for p reflects our use of asymptotic formulas outside their formal range of validity, and we emphasize only the disappearance of R in both cases.

Moreover, fast dynamo action is achieved here by adjusting the vertical length scale, l^{-1}, of the mean motion so that it increases linearly with R. The long vertical wavelength is needed for technical reasons, to allow our theory to be applied locally in z. If the wavelength does not grow in this way as R increases, vertical structure, which produces chaotic webs and disrupts the asymptotic channel structure, will influence the magnetic field generation. If we anticipate that the chaos will not inhibit, and indeed will more likely enhance, dynamo activity, then the limit of large R at fixed ϵ, l should exhibit fast dynamo action, although the present theory can not be applied to prove this.

The corresponding issue for scalar diffusion is the existence of a 'turbulent' effective diffusivity which is positive and independent of R as $R \to \infty$. The present result (4.42b) is interesting because of its behaviour in the irrational limit. The divergence of

$$\boldsymbol{D} \sim \frac{(\pi\epsilon)^3 R}{48\Lambda L(M^2+N^2)^{\frac{1}{2}}} \hat{\boldsymbol{u}}_{\mathrm{H}} \hat{\boldsymbol{u}}_{\mathrm{H}} + o(R) \tag{7.7}$$

with increasing R is typical of steady flows with channel structure in a preferred direction. However, the coefficient in (7.7) vanishes in the irrational limit. This behaviour thus allows a finite effective diffusivity in the irrational case, although without further analysis we cannot assume that the next term in the expansion (7.7) is order unity and non trivial. A general abstract discussion of the effective diffusivity generated by a large class of steady periodic flows without mean motion has been given by Avellaneda & Majda (1989). Closely related is the work on diffusion in porus media by Koch *et al.* (1989). Our irrational limit would indeed correspond to a finite effective diffusivity according to the analysis of the latter paper, since there the streamlines are dense mod $2\pi^3$. In that case boundary layers should not contribute intermediate terms of order $R^{\frac{1}{2}}$, and therefore it may be feasible to calculate the leading term of the expansion in $\boldsymbol{D}$ in the irrational case using asymptotic channel theory. In any event analysis of the present example in the more abstract setting of Avellaneda & Majda (1989) may prove very fruitful.

The limitations of the present theory are highlighted by the above remarks. Nevertheless the flows we have studied do confirm, in so far as diffusion and α-effect are concerned, their anticipated status as providing a bridge between simple periodic and chaotic three-dimensional flows. The irrational limit suggests but does not establish fast dynamo action for flows of fixed structure in the irrational case, and it would be interesting to confirm this and relate growth rate to the structure of the flow, e.g. the rates of stretching of line elements, for the irrational limit.

For the analysis of steady motion at least, the next step in this line of investigation is to introduce small regions of lagrangian chaos, for example in the chaotic webs of the flow (1.2) with $\delta \sim \epsilon \ll 1$. Unfortunately, both three-dimensionality and full chaotic behaviour are then

introduced simultaneously, this being a consequence of treating chaos only in the context of steady flow. Whether or not the present asymptotic methods will then prove useful remains to be seen. One hopeful point is that there is clearly an analogous boundary layer structure when $\delta \sim \epsilon \ll 1$; and also there remains the simplification to long vertical length scale, $l \ll 1$ in (1.2c). Our results suggest that such calculations would lead to explicit examples of fast dynamo action and order one 'turbulent diffusion' in steady flows, in the limit of infinite R.

This research was begun under SERC grant number GR/D/87121 during June and July 1986. The work was continued at New York University under Grants NSF-DMS-831 2229 and NASD-NAGW-781. Part of the study was carried out at the 1987 Woods Hole Summer Study Program in Geophysical Fluid Dynamics. We thank the Director of the 1987 Program, W. V. R. Malkus for his encouragement and support. In Autumn 1989, S. Childress was supported at Cambridge University by a Royal Society Guest Research Fellowship, and by a Visiting Fellow Commonorship at Trinity College. He thanks H. K. Moffatt for his hospitality and encouragement during this visit.

Appendix A. Mainstream solutions using shift maps

The basic formula (4.42) for the diffusion-matrix and (4.64) for the α-matrix depends on knowledge of the number of sides of each square $\Pi_{m,n}$, which are transversed by individual streamlines before they repeat themselves. This transit defines a shift $(\Delta x, \Delta y)$ in the xy plane and the streamline between two end points $P_0(x_0, y_0)$ and $P_\Delta(x_0+\Delta x, y_0+\Delta y)$ we called a periodicity section (see (2.14), (2.16), (2.31a)). So, for example, in calculating the A-field (5.31a) for perpendicular fields the coefficient $(\overline{\partial A/\partial\sigma})_k$ is determined by dividing the jump $[A]_{P_0}^{P_\Delta}$ over a peridicity section, which is the same for all streamlines, by the circulation integral Γ_k, which takes constant values $2S_k$ in each channel D_k (see (2.32)). The magnitude of the diffusion coefficient D_0 in (4.42a) is proportional to the mean value $(\overline{\partial A/\partial\sigma})^M$ of $(\overline{\partial A/\partial\sigma})_k$ (see (5.35c)). That in turn is proportional to the mean value of $1/S_k$, namely

$$\left(\frac{1}{S}\right)^M = \frac{1}{2}\left(\frac{1}{S_k}+\frac{1}{S_{k+1}}\right) = \frac{\tau L}{4[L^2-(\tau-1)]} \tag{A 1}$$

(see (2.48)–(2.51)).

In this Appendix, we provide an alternative derivation of the result (A 1) of §2, by use of shift maps. Whilst this approach is basically only a restatement of the results of §2 together with their application in §5, it perhaps suggests how the present analysis might be formalized for applications to yet more complicated topology.

We consider a scalar function f which satisfies the periodicity condition, $f(x+\pi, y\pm\pi) = f(x,y)$, and has the special property that is constant upon the streamlines of the flow, $f = f(\psi)$; for example, the mainstream solutions $b(\psi)$ and $\mathscr{B}(\psi)$ of §5. In the case of slow mean flows ($|\bar{\boldsymbol{u}}_H| \ll 1$, see §2.3), it is convenient to treat the flow near the corners O^i, at which $\psi = \psi^i$ (see (2.35), (2.36)), of the primary square Π by introducing the coordinate

$$\phi = \psi - \psi^i \equiv R^{-\frac{1}{2}}\xi \tag{A 2a}$$

as in (4.8) and writing

$$F_i(\phi) = f(\psi). \tag{A 2b}$$

The symmetries of the flow yield the connections defined by (4.15), which are

$$F_i(\phi) = \begin{cases} F_{i-1}(\phi + \Delta\psi^{i-1}), & \phi > 0, \\ F_{i+1}(\phi + \Delta\psi^{i+1}), & \phi < 0, \end{cases} \tag{A 3}$$

and were used extensively in §4. Here the end values at $\sigma = 2$ on sides $\mathscr{T}^{i\mp1}$ determine the start value at $\sigma = 0$ on the side $\mathscr{T}^i$.

The relations (A 3) provide transition sequences connecting F_0 to F_0. Two of them,

$$f(\psi) = F_0 \to \begin{cases} F_1 \to F_2 \to F_3 \to F_0, & \psi^0_+ < \psi, \quad (A\,4a) \\ F_3 \to F_2 \to F_1 \to F_0, & \psi < \psi^0_-, \quad (A\,4b) \end{cases}$$

distinguished by their initial ψ-range on $\mathscr{T}^0$, are associated with closed eddy streamlines. The former ($\psi^0_+ < \psi$) lie on $\mathscr{D}^+_{0,0}$, the latter ($\psi < \psi^0_-$) lie on $\mathscr{D}^-_{m,n}$ neighbouring the primary square Π. In the channel regions we may identify three sequences

$$f(\psi) = F_0 \to \begin{cases} F_1 \to F_2 \to F_1 \to F_0, & \psi^2 < \psi < \psi^0_+ \quad (\mathrm{I}), \quad (A\,5a) \\ F_1 \to F_0, & \psi^1 < \psi < \psi^2 \quad (\mathrm{II}), \quad (A\,5b) \\ F_3 \to F_0, & \psi^0_- < \psi < \psi^1 \quad (\mathrm{III}), \quad (A\,5c) \end{cases}$$

again distinguished by their initial ψ-range. As a result of map $F_i \to F_{i\pm1}$, the transitions (A 3) indicate that there is a ψ-shift $-\Delta\psi^i$. Thus (A 5) defines a mapping

$$\tilde{m}(\psi) = \psi + \begin{cases} -\psi^\beta - \psi^c, & (\mathrm{I}): \psi^0_+ - \psi^2 = \pi\bar{u}_y, \quad (A\,6a) \\ -\psi^\beta, & (\mathrm{II}): \psi^2 - \psi^1 = \pi\bar{u}_x, \quad (A\,6b) \\ +\psi^c, & (\mathrm{III}): \psi^1 - \psi^0_- = \pi\bar{u}_x \quad (A\,6c) \end{cases}$$

(see (2.38), (2.39), (2.42) and figures 6 and 8) of the initial ψ-range $\psi^0_- < \psi < \psi^0_+$ ($i = 0$ in (2.40)) onto itself, where $\psi^c = \pi(\bar{u}_x + \bar{u}_y)$, $\psi^\beta = \pi(\bar{u}_x - \bar{u}_y)$ as defined by (2.7 d). The mappings (A 6) from I, II and III involve 4, 2 and 2 transitions respectively (see (A 5)).

The map $\tilde{m}(\psi)$ is not, however, into or onto for each of the ranges I, II and III separately. Some transition sequences from II return to II after a shift $-\psi^\beta$. On the other hand, the transition sequence from III is always into I ∪ II. It is, therefore, convenient to contract the sequence of double maps I ∪ II → III → I ∪ II so forming a single mapping $m(\psi)$ of I ∪ II into and onto itself. In this way the transition sequence I → III → I also corresponds to a shift $-\psi^\beta$. Other possible transition sequences depend on the sign of ψ^β. When $\psi^\beta > 0$, they are II → III → I with shift $-\psi^\beta + \psi^c$ and I → III → II with shift $-\psi^\beta$. When $\psi^\beta < 0$, they are II → I with shift $-\psi^\beta$ and I → I ∪ II with shift $-\psi^\beta - \psi^c$. Since the ψ-range of I ∪ II is ψ^c, all possibilities are accounted for by the single statement

$$m(\psi) + \pi\bar{u}_y = (\psi + \pi\bar{u}_y - \psi^\beta) \,(\mathrm{mod}\, \psi^c), \quad -\pi\bar{u}_y \leqslant \psi < \pi\bar{u}_x \quad (\mathrm{I} \cup \mathrm{II}). \tag{A 7a}$$

In the special case $\psi^\beta = 0$, map (A 7a) reduces to the identity $m(\psi) = \psi$. Henceforth, we restrict attention to the case $\bar{u}_y \geqslant \bar{u}_x \geqslant 0$ (see (2.6)), for which $\psi^\beta \leqslant 0$.

Now each transition $F_i \to F_{i\pm1}$ corresponds to the passage of one side of the primary eddy. The aim is to determine, for each streamline in the neighbourhood of the origin, the number of transitions (or sides traversed) before the shifted value of ψ returns to its initial value. In order

to accomplish this calculation for $\psi^\beta \leqslant 0$, we need to count carefully the number of transitions involved in the mapping (A 7a). The transition sequences with upward shift $-\psi^\beta$ are of two types: type (A) with initial range $-\pi\bar{u}_y < \psi < \psi^\beta$, II$\rightarrow$I $\cup$ II with two transitions, and type (B) with initial range $\psi^\beta < \psi < \pi\bar{u}_x + \psi^\beta$, I$\rightarrow$III$\rightarrow$I with six transitions. The only transition with downward shift $-\psi^\beta - \psi^c$ is type (C) with initial range $\pi\bar{u}_x + \psi^\beta < \psi < \pi\bar{u}_x$, I$\rightarrow$I $\cup$ II with four transitions, occurring only when $\psi^\beta < 0$.

To form a link with the channel structure, we set $\pi(\bar{u}_x, \bar{u}_y) = (\Delta\psi)\,(M, N)$ as in (2.10) and write $\psi = x(\Delta\psi)$. Accordingly, the map (A 7a) becomes

$$m(x) + N = [x + N + (N - M)] \,(\mathrm{mod}\, L) \quad (-N \leqslant x \leqslant M), \tag{A 7b}$$

where $L\,(= M + N)$ is the sum of the relatively prime integers M and N. The unit interval $k < x < k+1$ corresponds to the channel D_k (see (2.30)). Since $m(x)$ constitutes a linear shift map on a one-dimensional torus (a circle), we may also regard it as a shift map $m(x) = x + (N - M)$ on the infinite line, where x in (A 7b) is now the equivalence class $\{x\}$ of all points $x + qL$ generated by all integers q. Consequently, when after p repetitions of the shift (A 7b) a particular point x returns to its start position

$$m^p(x) = x \quad (-N \leqslant x < M), \tag{A 8}$$

the linearity of m implies that all points on the interval $-N \leqslant x < M$ return simultaneously. An immediate objective is to determine the smallest number p for which (A 8) is satisfied together with the number of transitions $S(x)$ involved as a function of the start position x. It is not defined for integer values of x but elsewhere, we will show that

$$S(x) = S_k \quad (k < x < k+1) \tag{A 9a}$$

takes the constant values

$$S_k = (4/\tau)\, \Delta_k L \tag{A 9b}$$

on each of the channels D_k. This result (see (2.48)), which was determined by an alternative method in §2, gives the number of sides S involved in a channel periodicity section P_0 to P_Δ (see (2.31)).

Consider first the simpler case of O-flows, L odd, $\tau = 1$. We first note that $N - M$ and $M + N$ are relatively prime. Indeed if $M + N$ is odd and $N - M = ra$, $M + N = rb$ for relatively prime integers a, b and integer $r\,(> 1)$, then we have $2N = r(a + b)$ and $2M = r(b - a)$. Now r must be odd, in which case 2 is a factor of $a + b$ and $b - a$, so that M and N have a common factor $r\,(> 1)$, which is a contradiction. Accordingly, a point $x \in D_k$ only returns to its start position after $p = L\,(= M + N)$ applications of the map (A 7b): This is the smallest positive number for which $p(N - M) + q(M + N) = 0$. Since there are $L - 1$ non-repetitive maps, each of the L channels $D_k (-N \leqslant k \leqslant M - 1)$ is visited once and only once. The visits involve M upward shifts of type (A), M upward shifts of type (B) and $N - M$ downward shifts of type (C). This gives the total transition count

$$S_k = 2M + 6M + 4(N - M) = 4L. \tag{A 10}$$

Consider the case of E-flows, L even, $\tau = 2$. Now $N - M$ and $N + M$ are no longer relatively prime but have the common factor 2. This means that our argument that a point x eventually enters every channel D_k under repeated application of m no longer applies. Instead, $\frac{1}{2}(N - M)$

and $\frac{1}{2}(M+N)$ are relatively prime. As a result it is convenient to split the domain $\bigcup_{k=-N}^{M-1} D_k$ of our mapping (A 7*b*) into two distinct subdomains

$$D_+ = \bigcup_{k\,\text{even}} D_k, \quad D_- = \bigcup_{k\,\text{odd}} D_k \tag{A 11}$$

each of which are mapped into and onto themselves by m. Since both D_+ and D_- consist of $\frac{1}{2}(M+N)$ distinct intervals D_k, the arguments of the previous paragraph imply that each point x returns to its initial position after $p = \frac{1}{2}L$ applications of the map (A 7*b*) having entered every distinct unit interval D_k of one of the two subdomains once. To count the number of transitions we need the number of intervals D_k in each range I and II for the two subdomains D_+ and D_- separately. Use of the fact, that the location of the boundary $\psi\,(=\psi^2) = \psi^\beta$ between ranges I and II is characterized by $N-M = -\psi^\beta/(\Delta\psi)$ even, yields the number of intervals

$$\left.\begin{aligned} &\tfrac{1}{2}(N+1) \text{ in I}, \quad \tfrac{1}{2}(M-1) \text{ in II} \quad (k \text{ even}),\\ &\tfrac{1}{2}(N-1) \text{ in I}, \quad \tfrac{1}{2}(M+1) \text{ in II} \quad (k \text{ odd}). \end{aligned}\right\} \tag{A 12}$$

The number of transition sequences of type (A), (B) and (C) are easily determined by noting their initial ψ-ranges in conjunction with (A 12). The number of type (A) from II is $\frac{1}{2}(M\mp 1)$, of type (B) from I is $\frac{1}{2}(M\pm 1)$ and of type (C) from I is $\frac{1}{2}(N-M)$, where the upper and lower signs correspond to the subdomains D_+ and D_- respectively. These results give the total transition count

$$S_k = [M-(-1)^k]+3[M+(-1)^k]+2(N-M) = 2[L+(-1)^k]. \tag{A 13}$$

The results (A 10) and (A 13) agree with (2.48) and are used to derive the main result (A 1).

Appendix B. Glossary

We summarize the key notation either giving or referencing their definitions.

Dimensionless numbers

R = magnetic Reynolds number, $R \gg 1$;
$\beta = \epsilon R^{\frac{1}{2}}$, $\epsilon \ll 1$, (3.16);
M, N are relatively prime integers, $L = M+N$, (1.10*b*);
$\Delta\psi = R^{-\frac{1}{2}}(\Delta\zeta) = \pi\epsilon/(M^2+N^2)^{\frac{1}{2}}$, (2.10*b*), (4.5*b*).

Geometry

$\Pi^{\pm}_{m,n} = [m\pi, (m+1)\,\pi] \times [n\pi, (n+1)\,\pi]$, $\pm = (-1)^l$, $l = m+n$: (1.4), (2.4*b*);
$\left.\begin{aligned} &\mathscr{T}_x(m+\tfrac{1}{2}, n): m\pi < x < (m+1)\,\pi, y = n\pi,\\ &\mathscr{T}_y(m, n+\tfrac{1}{2}): x = m\pi, n\pi < y < (n+1)\,\pi, \end{aligned}\right\}$ (3.30);
$\Pi = \Pi^+_{0,0}$: primary square with edges $\mathscr{T}^i$ (4.9) connecting the corners O^i to O^{i+1}, (2.35), also (4.10*a*);
$(\Delta x, \Delta y) = (2\pi/\tau)\,(M, N)$: periodicity shift (2.16), $\tau = 2$ (L even), 1 (L odd), (2.14).

Flow

$$\left.\begin{aligned}
&\boldsymbol{u} = \begin{Bmatrix} \bar{\boldsymbol{u}}_{\mathrm{H}} + \boldsymbol{u}' \\ (\partial\psi/\partial y, -\partial\psi/\partial x, K\psi') \end{Bmatrix}\!: \quad \text{velocity,} \\
&\psi = \bar{\psi} + \psi' : \text{streamfunction,} \\
&\psi' = \sin x \sin y, \\
&\bar{\psi} = y\bar{u}_x - x\bar{u}_y = \pi^{-1}(\Delta\psi)\,(yM - xN) : (2.10c),
\end{aligned}\right\} \quad (2.1);$$

$\bar{\psi}_{m,n} = \bar{\psi}(m\pi, n\pi) = (\Delta\psi)\,(nM - mN)$: (2.3);
$\psi^{\mathrm{c}} = L(\Delta\psi), \psi^{\beta} = (M-N)\,(\Delta\psi)$: (2.7*d*), (2.27*b*);
$\bar{\boldsymbol{u}}_{\mathrm{H}} = \pi^{-1}(\Delta\psi)\,(M, N)$: mean velocity, (2.10);
$\boldsymbol{\eta}_{\mathrm{H}} = R^{\frac{1}{2}}\pi\bar{\boldsymbol{u}}_{\mathrm{H}}$: stretched boundary layer mean velocity, (4.2);

E-flows: L even,
O-flows: L odd,
$\Big\}$ $L = M + N$, below (2.16);

ζ-notation means $R^{\frac{1}{2}}$ times corresponding ψ variable.

Eddy structure

$\mathscr{C}(\psi)$: closed eddy streamline $\psi =$ constant, above (3.22);
$\mathscr{D}(\psi)$: region bounded by $\mathscr{C}(\psi)$, above (3.22);

$\gamma(\psi) = \oint_{\mathscr{C}} \boldsymbol{u}_{\mathrm{H}} \cdot \mathrm{d}\boldsymbol{x}$: circulation, (3.24*b*);

$\Sigma(\psi) = \oint_{\mathscr{D}} \mathrm{d}\Sigma$: area enclosed by $\mathscr{C}(\psi)$, (3.22) and below;

$\psi^{\pm}_{m,n}$: $\psi = \psi^{\pm}_{m,n}$ at X-type stagnation point on eddy boundary, (2.9);
$\mathscr{C}^{\pm}_{m,n} = \mathscr{C}(\psi^{\pm}_{m,n})$: eddy boundary, above (2.8);
$\mathscr{D}^{\pm}_{m,n} = \mathscr{D}(\psi^{\pm}_{m,n})$: eddy interior $\subset \Pi^{\pm}_{m,n}$, above (2.8);
$\mathscr{C}^{\pm\infty}_{m,n} = \mathscr{C}(\psi^{\pm}_{m,n} + \psi_{\pm\infty})$: particular eddy streamline where $\pm\psi_{\pm\infty}$ are positive constants, (2.24);
$\pm\Gamma = \gamma(\psi^{\pm}_{m,n}) \doteqdot \pm 8$, $\Sigma(\psi^{\pm}_{m,n}) \doteqdot \pi^2$, above (3.26);
$R^{-\frac{1}{2}}(\Delta\zeta_{\mathrm{ed}})$: eddy boundary layer width (6.4); μ_k: (6.6).

Primary eddy structure ($i = 0, 1, 2, 3$)

$\psi^i = k^i(\Delta\psi)$: $\psi \doteqdot \psi^i$ at X-type stagnation point near O^i (integer k^i), (2.36);
C^i: streamline through O^i, (4.7*b*);
$\Delta\psi^i = \psi^{i+1} - \psi^i$: (2.43);

$\psi^i_{\pm}$: $\begin{cases} \psi = \psi^i_+ \text{ on boundary } \mathscr{C}^+_{0,0} \text{ of primary eddy } \mathscr{D}^+_{0,0}, \text{ (2.38)}, \\ \psi = \psi^i_- \text{ on boundary } \mathscr{C}^-_{m,n} \text{ of eddies adjacent to } \mathscr{D}^+_{0,0}, \text{ (2.39)}, \\ \text{specifically on side } \mathscr{T}^i; \end{cases}$

$\psi^i_{\pm\infty} = \psi^i_{\pm} + \psi_{\pm\infty}$, (2.37*a*);

$\left.\begin{aligned} &\xi = R^{\frac{1}{2}}(\psi - \psi^i) \\ &\sigma = \int_{\mathrm{O}^i}^{P} \boldsymbol{u}_{\mathrm{H}} \cdot \mathrm{d}\boldsymbol{x} \end{aligned}\right\}$: boundary layer coordinates of point P on side $\mathscr{T}^i$, (4.8), (4.9);

ξ-notation means corresponding ζ variable less $\zeta^i\,(= R^{\frac{1}{2}}\psi^i)$.

Channel structure

$C(\psi)$: open channel streamline $\psi =$ constant, below (5.1);
$\psi_k = k(\Delta\psi)$: $\psi \doteqdot \psi_k$ at some X-type stagnation point where
$\psi_k^{\pm} \equiv \psi_k \doteqdot \psi^{\pm}_{m,n}, k = (n+\frac{1}{2})M-(m+\frac{1}{2})N+(-1)^{l}\frac{1}{2}L$, (2.27), (2.30);
$C_k = C(\psi_k)$: channel boundary, (2.30);
D_k: $\psi_k < \psi < \psi_{k+1}$: channel interior, (2.30);
P_0, P_Δ: end points of channel periodicity section defined by shift $(\Delta x, \Delta y)$, (2.31) and below;
S_k: number of sides in periodicity section, (2.32) and above;

$$\Gamma_k = \int_{P_0}^{P_\Delta} \boldsymbol{u}_{\mathrm{H}} \cdot \mathrm{d}\boldsymbol{x}\text{: circulation; } \sigma = \int \boldsymbol{u}_{\mathrm{H}} \cdot \mathrm{d}\boldsymbol{x};$$

Δ_k, Δ: parameters, (2.49), (2.51);
$R^{-\frac{1}{2}}(\Delta\zeta_{\mathrm{ch}})$: channel boundary layer width; μ: (6.1).

Thermal and magnetic variables and constants

$\boldsymbol{g}_{\mathrm{H}} = \boldsymbol{\nabla} A$: thermal gradient;
$\boldsymbol{B} = (\partial A/\partial y, -\partial A/\partial x, KB)$: magnetic field;
$\bar{A} = x\bar{g}_x + y\bar{g}_y = y\bar{B}_x - x\bar{B}_y$: (3.1), (3.9);
$\bar{A}_{m,n} = \bar{A}(m\pi, n\pi)$: (3.4$b$);
$B_{\parallel}, B_{\perp}, \Delta B$: parallel (4.33) and perpendicular (4.35) fields;
$\bar{E} = \bar{\boldsymbol{u}}_{\mathrm{H}} \cdot \bar{\boldsymbol{g}}_{\mathrm{H}} = -(\bar{\boldsymbol{u}}_{\mathrm{H}} \times \bar{\boldsymbol{B}}_{\mathrm{H}})_z$: (3.2$c$), (3.10);
$\bar{\boldsymbol{F}}_{\mathrm{H}} = \overline{\boldsymbol{u}_{\mathrm{H}} A} - \bar{\boldsymbol{u}}_{\mathrm{H}} \bar{A} = -\boldsymbol{D} \cdot \bar{\boldsymbol{g}}_{\mathrm{H}}$: mean heat flux, (3.5), (3.6);
$\boldsymbol{D}$: diffusion-matrix; D_0: (4.42); $\tilde{D}^{\mathrm{num}}$: (4.43);
$K\bar{\boldsymbol{E}}_{\mathrm{H}} = (\overline{\boldsymbol{u} \times \boldsymbol{B}})_{\mathrm{H}} = \boldsymbol{\alpha} \cdot \bar{\boldsymbol{B}}_{\mathrm{H}}$: mean electromotive force, (3.13), (3.14);
$\boldsymbol{\alpha}$: α-matrix; $\alpha_0, \alpha_0^{\mathrm{irr}}$: (4.64); $\tilde{\alpha}^{\mathrm{num}}$: (4.66);

$b = R^{-\frac{1}{2}}\partial A/\partial\psi$: (3.40)
$\mathscr{B} = B + R^{\frac{1}{2}}\bar{\psi} b$: (3.59)
$\mathscr{E} = R^{\frac{1}{2}}\psi b - \mathscr{B}$: (3.58)

} { Principal quantities of interest which are functions of the σ, ψ coordinates.

Eddy constants

$\bar{A}_{m+\frac{1}{2}, n+\frac{1}{2}}$: value of $\bar{A}$ at centre of square $\Pi^{\pm}_{m,n}$, (3.27a) and below;
A_0: $A \sim \bar{A}_{m+\frac{1}{2}, n+\frac{1}{2}} \pm A_0$, (3.27): mainstream eddy values on $\mathscr{C}^{\pm}_{m,n}$;
$\bar{b}$: $b \sim \pm\bar{b}$, (3.26);
B_0: $B^{\pm}_{m,n} = \pm B_0$: mean value of B on eddy $\mathscr{D}^{\pm}_{m,n}$, (3.56);
B^{s}: mainstream X-type stagnation point values of B, (4.57a), (5.64);
$\bar{\boldsymbol{F}}^{\mathrm{loc}}, F^{\pm\infty}_{m+\frac{1}{2}, n+\frac{1}{2}}$: (3.31), (3.34);
$\bar{\boldsymbol{E}}^{\mathrm{loc}}, E^{\pm\infty}$: (3.60), (3.63).

Primary eddy constants

i-superscripts refers to side $\mathscr{T}^i$.

$\bar{A}^i_{\pm}$: $\begin{cases} \bar{A}^i_+ = \bar{A}_{\frac{1}{2},\frac{1}{2}}, & \text{centre value on primary square } \Pi \equiv \Pi^+_{0,0}, \quad (3.37) \\ \bar{A}^i_- = \bar{A}_{m+\frac{1}{2},n+\frac{1}{2}}, & \text{centre value on squares } \Pi^-_{m,n} \text{ adjacent to } \Pi, \quad (3.38) \end{cases}$

$\Delta b^i = -(\bar{A}^i_+ - \bar{A}^i_-)$: (3.43);

$\bar{F}^i_s, F^i_{\pm\infty}$: $s = x, y$, (3.35), (3.37), (3.38);

$\bar{E}^i_s$: (3.64);

$\mathscr{F}^i_{\infty s}, \mathscr{F}^i_{\pm}, \mathscr{F}^i_{\pm\infty}, \mathscr{F}^i_s$: (3.42), (3.45);

$\mathscr{E}^i_{\infty s}, \mathscr{E}^i_{\pm}, \mathscr{E}^i_{\pm\infty}, \mathscr{E}^i_s$: (3.66), (3.67);

Green's function solutions

i-superscripts refer to side $\mathscr{T}^i$.

$G_j(\sigma, \xi)$: Green's functions, $j = 1, 2, 3$, (4.24);

$G^{\pm}_j(\xi)$: $j = 1$ (4.29c), $j = 2$ (4.53b);

$C^i = \mathscr{B}^i - (\zeta^i + \frac{1}{2}\xi)\, b^i$: (4.47$a$);

$\hat{b}^i, \tilde{b}^i, \tilde{b}^i_{\text{reg}}$: (4.26), (4.29$b$);

$Q^i, \tilde{I}^i, \tilde{I}^i_{\pm}$: (4.23$b$), (4.28), (4.30);

$\hat{C}^i, \tilde{C}^i$: (4.51);

$\hat{\mathscr{F}}^i_{\infty_s}, \tilde{\mathscr{F}}^i_{\infty_s}$: (4.37);

$\hat{\mathscr{E}}^i_{\infty_s}, \tilde{\mathscr{E}}^i_{\infty_s}$: (4.59).

Mainstream channel solutions

$\bar{b}_k, \bar{b}^M, \bar{A}^M$: (5.8$a$), (5.12), (5.15);

$\mathscr{B}_k = \mathscr{B} - R^{\frac{1}{2}}_2 \psi_{k+\frac{1}{2}}\, b$: (5.40$b$);

$\bar{f}_k, \bar{f}^M, \bar{h}_k, \bar{h}^M$: (5.41), (5.45), (5.48).

The superscript M is used to denote mean value over two neighbouring channels D_{k-1} and D_k (say).

References

Anuriyev, A. P. & Fishman, V. M. 1982 Magnetic field structure in the two dimensional motion of a conducting fluid. *Geomagn. Aeron.* **22**, 245–248.

Arnold, V. I. & Avez, A. 1967 *Problèms ergodiques de la mécanique classique*. Paris: Gauthier-Villars.

Arnold, V. I. & Korkina, E. I. 1983 The growth of a magnetic field in a steady incompressible flow. *Vest. Mosk. Un. Ta.* Ser. 1, *Math. Mec.* **3**, 43–46. (In Russian.)

Avellaneda, M. & Majda, A. J. 1989 Stieltjes integral representation and effective diffusivity bounds for turbulent transport. *Phys. Rev. Lett.* **62**, 753–755.

Chernikov, A. A., Sagdeev, R. Z. & Zaslavsky, G. M. 1990 Fluid webs with lagrangian chaos and intermittency. In *Topological fluid mechanics* (ed. H. K. Moffatt & A. Tsinober), pp. 45–53. Cambridge University Press.

Childress, S. 1979 Alpha-effect in flux ropes and sheets. *Phys. Earth Planet. Int.* **20**, 172–180.

Childress, S. & Soward, A. M. 1985 On the rapid generation of magnetic fields. In *Chaos in astrophysics* (ed. J. R. Buchler, J. M. Perdang & E. A. Spiegel), vol. 161, pp. 223–244. NATO ASI Series C: Mathematical and Physical Sciences. Reidel.

Childress, S. & Soward, A. M. 1989 Scalar transport and alpha-effect for a family of cat's-eye flows. *J. Fluid Mech.* **205**, 99–133.

Crisanti, A., Falcioni, M., Paladin, G. & Vulpiani, A. 1990 Anisotropic diffusion in fluids with steady periodic velocity fields. *J. Phys.* A (In the press.)

Dombre, T., Frisch, U., Greene, J. M., Hénon, M., Mehr, A. & Soward, A. M. 1986 Chaotic streamlines in the ABC flows. *J. Fluid Mech.* **167**, 353–391.

Galloway, D. J. & Frisch, U. 1984 A numerical investigation of magnetic field generation in a flow with chaotic streamlines. *Geophys. astrophys. Fluid Dyn.* **29**, 13–18.

Galloway, D. J. & Frisch, U. 1986 Dynamo action in a family of flows with chaotic streamlines. *Geophys. astrophys. Fluid Dyn.* **36**, 53–83.

Galloway, D. J., Proctor, M. R. E. & Weiss, N. O. 1978 Magnetic flux ropes and convection. *J. Fluid Mech.* **87**, 243–261.

Hénon, M. 1966 Sur la topologie des lignes de courant dans un cas particulier. *C.R. hebd. Séanc. Acad. Sci., Paris* **262**, 312–314.

Koch, D. L., Cox, R. G., Brenner, H. & Brady, J. F. 1989 The effect of order on dispersion in porous media. *J. Fluid Mech.* **200**, 173–188.

Moffatt, H. K. 1978 *Magnetic field generation in electrically conducting fluids*. Cambridge University Press.

Moffatt, H. K. & Proctor, M. R. E. 1985 Topological constraints associated with fast dynamo action. *J. Fluid Mech.* **154**, 493–507.

Perkins, F. W. & Zweibel, E. G. 1987 A high magnetic Reynolds number dynamo. *Physics Fluids* **30**, 1079–1084.

Roberts, G. O. 1972 Dynamo action of fluid motions with two-dimensional periodicity. *Phil. Trans. R. Soc. Lond.* A **271**, 411–454.

Soward, A. M. 1987 Fast dynamo action in steady flow. *J. Fluid Mech.* **180**, 267–295.

Soward, A. M. 1989 On dynamo action in a steady flow at large magnetic Reynolds number. *Geophys. astrophys. Fluid Dyn.* **49**, 3–22.

Soward, A. M. 1990 A unified approach to a class of slow dynamos. *Geophys. astrophys. Fluid Dyn.* (In the press.)

Soward, A. M. & Childress, S. 1986 Analytic theory of dynamos. *Adv. Space Res.* **6**, 7–18.

Soward, A. M. & Childress, S. 1990*a* Dynamo action at large magnetic Reynolds number in spatially periodic flow with mean motion. In *Topological fluid mechanics* (ed. H. K. Moffatt & A. Tsinober), pp. 127–137. Cambridge University Press.

Soward, A. M. & Childress, S. 1990*b* Large magnetic Reynolds number dynamo action in steady spatially periodic flows. In *Nonlinear evolution of spatio–temporal structures in dissipative continuous systems* (ed. F. H. Busse & L. Kramer). NATO ASI Series: Physical Sciences. New York: Plenum.

Vishik, M. M. 1988 On magnetic field generation by three-dimensional steady flow of conducting fluid at high magnetic Reynolds number. *Izv. Akad. Nauk SSSR, Fis. Zemli* N **3**, 3–12.

Vishik, M. M. 1989 Magnetic field generation by the motion of a highly conducting fluid. *Geophys. astrophys. Fluid Dyn.* **48**, 151–167.

Weiss, N. O. 1966 The expulsion of magnetic flux by eddies. *Proc. R. Soc. Lond.* A **293**, 310–328.

Zaslavskii, G. M., Sagdeev, R. Z. & Chernikov, A. A. 1988 Stochastic nature of streamlines in steady state flows. *Zh. eksp. teor. Fiz.* **94**, 102–115. (English transl. *Soviet Phys. JETP* **67**, 270–277 (1988).)

Zeldovich, Ya. B., Ruzmaikin, A. A., Molchanov, S. A. & Sokolov, D. D. 1984 Kinematic dynamo problem in a linear velocity field. *J. Fluid Mech.* **144**, 1–11.

Zeldovich, Ya. B., Ruzmaikin, A. A. & Sokolov, D. D. 1983 *Magnetic fields in astrophysics*. New York: Gordon and Breach.

PHILOSOPHICAL TRANSACTIONS OF THE ROYAL SOCIETY A MATHEMATICAL, PHYSICAL & ENGINEERING SCIENCES